nks

Nordic nuclear safety research

Adsorption and revaporisation studies of thin iodine oxide and CsI aerosol deposits from containment surface materials in LWRs

S. Tietze[1], M. Foreman[1], C. Ekberg[1]

T. Kärkelä[2], A. Auvinen[2], U. Tapper[2], J. Jokiniemi[2,3]

[1]Chalmers University of Technology, Göteborg, Sweden
[2]VTT Technical Research Centre of Finland, Espoo, Finland
[3]University of Eastern Finland, Kuopio, Finland

July 2013

Abstract

During a severe nuclear accident released fission and radiolysis products can react with each other to form new species which might contribute to the volatile source term. Iodine will be released from UO2 fuel mainly in form as CsI aerosol particles and elemental iodine. Elemental iodine can react in gaseous phase with ozone to form solid iodine oxide aerosol particles (IOx).

Within the AIAS-2 (Adsorption of Iodine Aerosols on Surfaces) project the interactions of IOx and CsI aerosols with common containment surface materials was investigated. Common surface materials in Swedish and Finnish LWRs are Teknopox Aqua V A paint films and metal surfaces such as Cu, Zn, Al and SS. Non-radioactive and ^{131}I labelled aerosols were produced from a KI solution and ozone with a new facility designed and built at VTT Technical Research Centre of Finland. CsI aerosols were produced from a CsI solution with the same facility. A monolayer of the aerosols was deposited on the surfaces. The deposits were analysed with microscopic and spectroscopic measurement techniques to identify the chemical form of the deposits on the surfaces to identify if a chemical conversion on the different surface materials had occured.

The revaporisation behaviour of the deposited aerosol particles from the different surface materials was studied under the influence of heat, humidity and gamma irradiation at Chalmers University of Technology, Sweden. Studies on the effects of humidity were performed using the FOMICAG facility, while heat and irradiation experiments were performed in a thermostated heating block and with a gammacell 22 with a dose rate of 14 kGy/h. The revaporisation losses were measured using a HPGe detector. The decomposition effect of the radiolysis product carbon monoxide was tested on IOx aerosols deposited on a glass fibre filter.

Iodine oxide particles were produced at 50 °C, 100 °C and 120 °C and deposited on filter samples in order to study the chemical speciation of the particles. The formation of HIO_3 was verified with Raman analysis regardless of the reaction temperature. Furthermore, elemental iodine was also observed in the measured Raman spectra. Probably, iodine oxide particles had reacted with air humidity forming iodic acid and elemental iodine.

IOx and CsI particles that were deposited on various sample surfaces were synthesized at 120°C. According to XPS analysis, it seemed that IOx particles were mainly in form of HIO_3 on the metal and on the painted surfaces.

The XPS spectrum of CsI was observed on all metal and painted samples on which CsI particles were deposited. However, the CsI particles seemed to have dissolved at least partially by air humidity. Iodine was observed at areas outside the caesium iodide deposits on metal and on painted surfaces. According to the XPS analyses, iodine was in oxidised form. The measurements indicated that

iodine may have reacted with the oxidized metal surfaces to form metal iodates. Only trace amounts of oxidized iodine were detected on the painted surfaces.

An interesting result in the XPS analysis was that a part of the acquired signal from CsI on the painted surfaces seemed to originate deeper from the structure of the paint when it was pre-treated either with heat or gamma irradiation. SEM analysis revealed that heat and gamma irradiation treatment increased the porosity of the paint. Therefore, dissolved CsI may have been transported into the matrix of the paint.

Besides copper the studied metal surfaces underwent slow reactions with the iodine of the aerosol deposits which showed in the high revaporisation rates at room temperature and elevated temperatures. On the copper and paint samples it could be shown that these surfaces react more easily with the iodine from cesium iodide deposits. From the chemically converted metal iodides only copper iodide remained on the surfaces after exposure to hot humid air and as well after immersion in boiling water. Both, non aged and fresh paint films, showed to be very reactive towards the iodine in the aerosol deposits. At lower temperatures (< 50 °C) it showed that the solvent rich paint films showed reduced revaporisation. At high temperatures when the paint starts to significantly degrade the release of iodine from the solvent rich paints increased significantly. The containment conditions or conditions of a severe nuclear accident cause the revaporisation of paint solvents and thus an uneven distribution within the paint film. Near to the surface revaporisation starts and thus an higher paint solvent concentration is found in the center of the paint profile where the iodine species migrate to and possibly are chemically converted. Thus, the paint samples that had been for a long time aged at high temperatures showed the least ability to react and retain iodine from the deposited aerosols. Most paint solvents are less water soluble than the iodine species itself. Thus, elevated temperatures and hot water are required to wash out the iodine in the paint matrix. In all paint films iodine was still detected after 4 weeks immersion in hot water (50 °C).

Key words

Severe nuclear accidents, LWR, volatile iodine source term, iodine oxide aerosols, cesium iodide, adsorption, revaporisation, containment

Adsorption and revaporisation studies of thin iodine oxide and CsI aerosol deposits from containment surface materials in LWRs

Final Report from the NKS-R AIAS activity

(Contract: AFT/NKS-R(12)98/1)

S. Tietze[1], M. Foreman[1], C. Ekberg[1]
T. Kärkelä[2], A. Auvinen[2], U. Tapper[2], J. Jokiniemi[2,3]

[1]Chalmers University of Technology, SE-41296 Göteborg, Sweden
[2]VTT Technical Research Centre of Finland, FI-02044 Espoo, Finland
[3]University of Eastern Finland, FI-70211 Kuopio, Finland

May 2013

Report's title	
Adsorption and revaporisation studies of thin iodine oxide and CsI aerosol deposits from containment surface materials in LWRs	
Customer, contact person, address	Order reference
NKS-R, Keisu Leino, FORTUM, Power Devision, P.O. Box 100, FI-00048 FORTUM, Finland	AFT/NKS-R(12)98/1
Project name	Project number/Short name
AIAS – 2: Adsorption of Iodine Aerosols on Surfaces part 2	AIAS-2
Author(s)	Pages
<u>S.Tietze</u>, <u>T.Kärkelä</u> M.Foreman, C.Ekberg, A.Auvinen, U.Tapper, J. Jokiniemi	59 +25
Keywords	Report identification code
Severe nuclear accidents, volatile iodine source term, iodine oxide aerosols, cesium iodide, sorption, revaporisation, containment	

Summary

During a severe nuclear accident a series of volatile fission products will be released from the fuel. Of major concern are volatile iodine species due to their biological toxicity. Iodine will be released mainly in form of caesium iodide and elemental iodine. Under the presence of radiolysis products such as ozone new volatile iodine species can be formed. Ozone e.g. reacts with elemental iodine to form iodine oxide aerosol particles (IOx). The interactions of these two aerosols with common surface materials in light water reactor containments (LWR) during a severe nuclear accident are not very well investigated.

An experimental set-up to expose surfaces with a monolayer of IOx or CsI aerosols was developed at VTT Technical Research Centre of Finland. One focus of the studies was on the identification of the chemical form of the deposited aerosols on metal surfaces (Al, Cu, Zn, SS 316) and Teknopox Aqua VA paint films, as well as on the revaporisation behaviour of iodine. Besides heat, gamma irradiation and humidity, the effect of CO on a possible revaporisation was investigated.

Iodine oxide particles were produced at 50 °C, 100 °C and 120 °C and deposited on filter samples in order to study the chemical speciation of the particles. The formation of HIO_3 was verified with Raman analysis regardless of the reaction temperature. Furthermore, elemental iodine was also observed in the measured Raman spectra. Probably, iodine oxide particles had reacted with air humidity forming iodic acid and elemental iodine.

IOx and CsI particles that were deposited on various sample surfaces were synthesized at 120°C. According to XPS analysis, it seemed that IOx particles were mainly in form of HIO_3 on the metal and on the painted surfaces.

The XPS spectrum of CsI was observed on all metal and painted samples on which CsI particles were deposited. However, the CsI particles seemed to have dissolved at least partially by air humidity. Iodine was observed at areas outside the caesium iodide deposits on metal and on painted surfaces. According to the XPS analyses, iodine was in oxidised form. The measurements indicated that iodine may have reacted with the oxidized metal surfaces to form metal iodates. Only trace amounts of oxidized iodine were detected on the painted surfaces.

An interesting result in the XPS analysis was that a part of the acquired signal from CsI on the painted surfaces seemed to originate deeper from the structure of the paint when it was pre-treated either with heat or gamma irradiation. SEM analysis revealed that heat and

gamma irradiation treatment increased the porosity of the paint. Therefore, dissolved CsI may have been transported into the matrix of the paint.

Both types of aerosols showed a high revaporisation rate from the surface materials already at room temperature. Significant lower amounts of iodine from the deposits were chemically converted on the metal surfaces and remained on the surfaces. Copper and the paint films showed to be more reactive with the iodine from CsI deposits. Most of the metal iodides are water soluble, only copper iodide remained even after immersion of the samples in hot water. The paint films that had been aged for a long time at 100 °C showed the least ability to chemically convert and retain iodine from the aerosol particles. Irradiated and non-treated paint films showed to consume iodine at low temperatures but at the temperatures of a severe nuclear accident (150 °C) the revaporisation significantly increased. Heat in comparison to gamma irradiation showed to be the main factor influencing the iodine revaporisation. Humidity washes a majority of the uptaken iodine out due to the water-based composition of the Teknopox Aqua VA paint. However, even after immersing the paint films for 1 month in hot water still I-131 could be detected in the paint films indicating reactions with the resin. Most of the iodine is washed out of long-time heat-treated paint films where most of the mobile paint ingredients have been evaporated.

Confidentiality	Public

Göteborg, 17.05.2013

Christian Ekberg,
Professor,
Project Leader

Contact address

Chalmers University of Technology, Kemivägen 4, SE-41296 Göteborg, Sweden
VTT Technical Research Centre of Finland, Biologinkuja 7, FI-02044 VTT, Espoo, Finland

Preface

The AIAS-2 project is a continuation of the AIAS-1 project. AIAS-1 focussed mainly on the identification of the composition of IOx aerosols formed at different temperatures and the change of composition when reacting with surface materials, as well as on the revaporisation behaviour of the particles from these surfaces. Within AIAS-1 the deposits were of rather thick nature and thus showed a mainly substrate independent revaporisation behaviour. Within AIAS-2 the thickness of the deposit was reduced to a monolayer to study the surface-aerosol interactions.

Iodine oxide aerosols, as well as CsI aerosols were deposited on common LWR containment surface materials in Swedish and Finnish nuclear power plants. The investigated surface materials were Al, Cu, Zn, stainless steel (SS 316) and Teknopox Aqua VA epoxy paint films, which were aged with heat and irradiation.

New methods for the IOx and CsI particle production were developed and a new particle deposition facility was designed and built at VTT Technical Research Centre of Finland for AIAS-2 project. Non-radioactive aerosols were produced and analysed by microscopic and spectroscopic means (SEM-EDX, XPS, RAMAN) at VTT.

As well the ^{131}I labelled aerosols were produced at VTT in order to study the revaporisation behaviour of ^{131}I species under severe accident containment conditions. The studied parameters were gamma radiation, humidity and temperature effects. Studies on the revaporisation behaviour were performed at the Nuclear Chemistry department of the Chalmers University of Technology in Göteborg, Sweden.

Table of contents

1   Introduction

During a severe nuclear accident in a nuclear power plant (NPP), iodine will be released as volatile CsI aerosols and elemental iodine from damaged fuel. In the containment gas phase elemental iodine can react with radiolysis products, such as ozone. As a result, iodine oxide aerosol particles can be formed [1, 2]. Both types of aerosols are rather small in diameter and can either remain in the gas phase of the containment or deposit on the various surfaces of the containment. Typical containment materials in Swedish and Finnish light water reactors are Teknopox Aqua VA epoxy paint, stainless steel, aluminium, copper and zinc. The deposited particles may react with the surfaces, change its properties and possibly form new inorganic and organic iodine species. The deposits may act as new sources of volatile iodine species which could be re-released into the gas phase of the containment and contribute to the volatile iodine source term. Therefore, it is important to further investigate the behaviour and properties of iodine containing aerosols.

2   Goals

The aim of this study was to generate monolayer deposits of non-radioactive and radioactive (labelled with ^{131}I) CsI and IOx aerosols on various containment surface materials with a new facility, designed and built at VTT. Another aim was to identify the chemical speciation of the deposits on different surface materials (Al, Cu, Zn, SS, Teknopox Aqua VA epoxy paint). The deposited particles as well as the surfaces themselves were analysed with several microscopic and spectroscopic measurement techniques (SEM-EDX, XPS, RAMAN).

The revaporisation and distribution behaviour of the iodine species released from the deposits in presence of humidity in a LWR containment like environment was studied in a small-scale model of a Swedish BWR containment (FOMICAG facility) using NaI detectors. The revaporisation in dry areas of the containment was studied with a temperature controlled heating block and a gamma cell with a dose rate of 14 kGy/h. The change of ^{131}I activity from the deposits on the surfaces was measured with a HPGe detector and an autoradiograph. Furthermore the effect of CO release from organic materials in the containment on the deposition of IOx aerosols was investigated.

3 Background

3.1 Release of iodine from fuel

During normal operation in a nuclear power plant the fission products representing 99 % of the radioactivity remain in the fuel rods and are just a minor part of the radiation dose exposed to workers.

In case of a meltdown of the core the iodine inventory will be released from the fuel and become airborne. Most of the iodine will be present in form of caesium iodide aerosol particles ($CsI(s)$) and only few percentage as $I_2(g)$ [3]. $CsI(s)$ can dissolve in the water phase or steam and dissociate into iodide ions and and caesium hydroxide corresponding to the following reactions:

$$CsI + H_2O \rightarrow CsOH + HI \rightarrow CsOH + H^+ + I^- \tag{1}$$
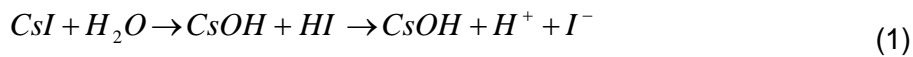
Gaseous elemental iodine can as well hydrolyse in water or steam or react in gaseous phase with radiolysis products such as ozone to form iodine oxide aerosols (see 3.2).

Both, iodine oxide aerosols and cesium iodide aerosols, could alternatively condense and undergo interactions with the containment surface materials and may form new iodine species of less volatility which would reduce the volatile source term. Under the conditions of a severe nuclear accident the condensed aerosols might be decomposed and regenerate elemental iodine which could be potentially released in case of a containment failure.

3.2 Formation of IOx aerosols

In the containment atmosphere gaseous iodine is exposed to air radiolysis products, such as ozone, as well as to the radiation - such as alpha, beta, gamma and X-ray - itself. This may lead to oxidation of gaseous iodine and subsequent formation of iodine containing aerosol particles.

The formation of iodine oxide aerosol particles from gaseous elemental iodine and ozone has been reported in the literature [1, 2]. In these experiments, ozone has been generated by passing air or O_2 through a corona discharge.

The oxidation of iodine occurs in several steps. Vikis *et al.* [1] found two feasible reaction routes in the temperature range of 293-370 K:

$$I_2 + O_3 \rightarrow IO + I + O_2 \tag{2}$$
$$I_2 + O_3 \rightarrow IO + IO_2 \tag{3}$$

By successive oxidation of the I, IO and IO_2 primary products, the final product I_4O_9 is formed with ozone:

$$I + O_3 \rightarrow IO + O_2 \tag{4}$$
$$IO + O_3 \rightarrow IO_2 + O_2, \text{ etc.} \tag{5}$$

The formed solid I_4O_9 showed no visible changes when it was stored for several days in a dry atmosphere. When exposed to ambient air, the samples changed colour from yellow to brown within a few hours. The oxide (I_4O_9) has been reported to be dark yellow in colour [4].

It is reported that when the sample was heated up to ~400 K (*circa* 130 °C), I_4O_9 decomposed and I_2O_5 was formed. The sample underwent a mass loss when heated further to ~570 K due to decomposition of I_2O_5 to gaseous I_2 and O_2 and the mass loss was enhanced when temperature was further increased [1].

HIO_3 (iodic acid) can be formed from I_2O_5 (or I_4O_9) when being exposed to water or humid air according to the following equation [5]:

$$I_2O_5 + H_2O \rightarrow 2\ HIO_3 \tag{6}$$

Dehydration (heating) of HIO_3 regenerates I_2O_5 [5]:

$$3\ HIO_3 \rightarrow I_2O_5 \cdot HIO_3 + H_2O \tag{7}$$

The properties of different solid iodine-oxide compounds are presented in Table 1 [4]. The colour of solid iodine oxide particles are yellow or dark yellow for I_2O_4 and I_4O_9 respectively. The decomposition temperature of these iodine oxides is rather low (≤ 100 °C). Both I_2O_4 and I_4O_9 decompose to I_2O_5 and I_2 upon heating. In water both species decompose to HIO_3 and I_2. Solid elemental iodine is blue-black in colour and it is purple as gas. HIO_3 is a white solid, but it is very soluble in water. Dehydration of HIO_3 leads to a formation of white crystalline I_2O_5, which has a high melting point of approximately 300 °C.

Table 1: The properties of solid iodine compounds [4].

Compound	Appearance in the solid state	Melting or decomposition temperature	Solubility in water	Other comments
I_2, iodine	blue-black crystals	113.7 °C	slightly soluble	purple gas
I_2O_4, iodine tetroxide	yellow solid	100 °C (Decomp.)	decomp. to HIO_3 + I_2	-
I_2O_5, iodine pentoxide	white crystalline solid	~300 °C	soluble	-
I_4O_9, iodine nonaoxide	dark yellow solid	75 °C (Decomp.)	decomp. to HIO_3 + I_2	-
HIO_3, iodic acid	white solid	110 °C	very soluble	-

4   Experimental

4.1   Production of thin layer deposits of IOx and CsI aerosols

New methods for the IOx and CsI particle production were developed and a new particle deposition facility was designed and built at VTT for this study. The main principle of the particle production process was as follows. Iodine containing particles – IOx or CsI - were produced from a precursor solution with an atomizer (TSI 3076) at the inlet of the new deposition facility. A reservoir bottle containing KI or CsI water solution was connected with a tube to the atomizer. In some tests the solution was labelled with ^{131}I (250 MBq – 500 MBq). Air flow (3 l/min, NTP conditions: 0 °C, 101325 Pa) was directed through an orifice of the atomizer to form a high-velocity jet. Solution was drawn from the reservoir bottle into the atomizing section through the connecting tube and was then atomized by the jet. Large droplets were removed by impaction on the wall opposite the jet and excess liquid was drained back into the reservoir bottle.

Fine droplets were carried by the gas flow into the deposition facility heated to 120 °C. Within the facility the flow was at first diluted with hot air (120 °C, dilution ratio 1:14) and the droplets were dried. Upon drying of the droplets solid CsI particles were formed. During the production of iodine oxide particles, gaseous ozone was produced from air with an additional ozone generator (OZV-8). When iodine and ozone containing flows were mixed, the formation of IOx particles took place. After the formation of particles the flow was diluted with cold air (20 °C, dilution ratio 1:3). All gas flows were controlled with mass flow controllers (Brooks 5851S). The average diameter of particles produced with this method was less than ~100 nm.

Aerosol samples were produced at 50 °C, 100 °C and 120 °C and collected on a filter paper.

4.2   Exposure of the surface materials with IOx and CsI aerosols

The surface samples to be exposed with particles (size of a sample 15 mm x 15 mm x 0.25-1 mm) were placed in a custom made single stage low pressure impactor at the end of the exposure line. The impactor was designed and built at VTT for this study. In order to deposit the particles, the total flow rate inside the deposition facility had to be increased to ~100 l/min (NTP). Therefore, a porous tube diluter was attached in line before the impactor of the facility. Since the production rate of particles by the atomization process was very stable, the amount of particles on the samples was controlled by adjusting the sampling time. This method enabled the production of a mono-layer deposit of iodine containing particles on the samples. It was also possible to produce similar deposits on several samples at the same time, e.g. on 12 to 24 samples in this study. Some samples were prepared with particles labelled with ^{131}I. The amount of radioactivity deposited on the samples could be adjusted easily by controlling the activity of the precursor solution.

4.3 Preparation of samples for surface analyses

The details of the surface analysed samples are presented in Tables 2a and 2b. The total number of samples was 36. The first set of samples was produced in October 2012. The IOx and CsI particles were deposited on stainless steel (SS 316), aluminium, copper and zinc surfaces. In addition, some IOx particles produced at 50 °C, 100 °C and 120 °C were collected also on Teflon™ filter (Millipore Mitex®).

The second set of samples was produced in February 2013. The IOx and CsI particles were deposited on Teknopox Aqua V A paint. The paint (TEKNOPOX Aqua V A) was the same as that used in some Finnish and Swedish NPP containments. The paint samples were pretreated as follows: no treatment (fresh paint), heat treated (heated for 2 years at 100 °C), short gamma irradiation (radiation dose 100 kGy), long gamma irradiation (radiation dose 10 MGy). All samples were stored in a desiccator over silica gel at 5 °C for 2 weeks before the analysis.

Table 2a. Sample list for SEM-EDX, XPS and Raman measurements.

Sample	Substrate of particle deposition	Particle formation T [°C]	IOx or CsI	Production date	Analysis Techniques
1	filter (Mitex®)	50	IOx	10/2012	RAMAN
2	filter (Mitex®)	100	IOx	10/2012	RAMAN
3	filter (Mitex®)	120	IOx	10/2012	RAMAN
4	filter (Mitex®)	no particles	no particles	10/2012	RAMAN
5A, 5B	stainless steel (316)	120	IOx	10/2012	5A) SEM, EDX 5B) XPS
6A, 6B	Aluminium	120	IOx	10/2012	6A) SEM, EDX 6B) XPS
7A, 7B	Copper	120	IOx	10/2012	7A) SEM, EDX 7B) XPS
8A, 8B	Zinc	120	IOx	10/2012	8A) SEM, EDX 8B) XPS
9A, 9B	stainless steel (316)	120	CsI	11/2012	9A) SEM, EDX 9B) XPS
10A, 10B	Aluminium	120	CsI	11/2012	10A) SEM, EDX 10B) XPS
11A, 11B	Copper	120	CsI	11/2012	11A) SEM, EDX 11B) XPS
12A, 12B	Zinc	120	CsI	11/2012	12A) SEM, EDX 12B) XPS

Table 2b. Sample list for SEM-EDX, XPS and Raman measurements.

Sample	Substrate of particle deposition	Particle formation T [°C]	IOx or CsI	Production date	Analysis Techniques
13A, 13B	paint, no treatment	120	IOx	02/2013	13A) SEM, EDX 13B) XPS
14A, 14B	paint, heat treated	120	IOx	02/2013	14A) SEM, EDX 14B) XPS
15A, 15B	paint, short gamma irradiation	120	IOx	02/2013	15A) SEM, EDX 15B) XPS
16A, 16B	paint, long gamma irradiation	120	IOx	02/2013	16A) SEM, EDX 16B) XPS
17A, 17B	paint, no treatment	120	CsI	02/2013	17A) SEM, EDX 17B) XPS
18A, 18B	paint, heat treated	120	CsI	02/2013	18A) SEM, EDX 18B) XPS
19A, 19B	paint, short gamma irradiation	120	CsI	02/2013	19A) SEM, EDX 19B) XPS
20A, 20B	paint, long gamma irradiation	120	CsI	02/2013	20A) SEM, EDX 20B) XPS

4.4 Analysis techniques for IOx and CsI particles in gas phase and on surfaces

A Scanning Mobility Particle Sizer (SMPS) was used for the analysis of number size distribution of the produced particles. The SMPS consisted of two units: a Differential Mobility Analyser (DMA, TSI 3080 electrostatic classifier with TSI 3081/TSI 3085 DMAs) and a Condensation Particle Counter (CPC, TSI 3775). The DMA size classifies the particles based on their electrical mobility in the size range 0.01-1 μm and the CPC calculates the amount of particles in a gas flow up to 10^7 particles/cm^3.

The mass concentration of the produced particles in the gas flow was measured online with a Tapered Element Oscillating Microbalance (TEOM, ThermoScientific 1400a). TEOM can detect a very low mass concentration of particles which have been transported onto its filter. TEOM calculates the particle mass from the decrease in the oscillation frequency of a glass tube connected to the filter.

The IOx and CsI particle deposits on the surfaces of the samples were analysed with several surface analysis techniques: RAMAN spectroscopy, X-ray photoelectron spectroscopy (XPS) and Scanning Electron Microscopy (SEM) coupled with Energy dispersive X-ray analysis (EDX).

In order to determine the chemical form of deposited iodine, Raman spectroscopy was conducted for samples 1 to 4 (see Tables 2A and 2B) at University of Eastern Finland (Kuopio) by PhD Anna Lähde. The used spectroscope was a Senterra 200LX (Bruker Optics GmbH, Ettlingen, Germany). The wavelength of the laser (for excitation) was 785 nm (red laser) and its power was 10 mW. The wavenumbers studied ranged either from 82 to 1538 cm^{-1} with 3 cm^{-1} resolution or from 127 to 3800 cm^{-1} with 9 cm^{-1} resolution. The filter samples were analysed 2 weeks after preparation of the sample.

X-ray photoelectron spectroscopy (XPS) was applied to determine the elemental composition on the surface of the samples 5B to 20 B (see Tables 2A and 2B). Some indication of the iodine chemistry could also be found, since the binding energy of electrons depends on the chemical state. The XPS analysis was conducted at Aalto University (Espoo) by the PhDs Leena-Sisko Johansson and Joseph M Campbell. Surface chemical compositions of the samples were investigated with XPS, using a Kratos Analytical AXIS 165 or a Kratos AXIS Ultra electron spectrometer with monochromatic Al Kα irradiation at 100 W (X-ray tube voltage 12.5 kV, anode current 8 mA) and charge neutralization. The samples were pre-evacuated in the instrument fore-chamber overnight, in order to stabilize the vacuum conditions. The analysis area in all experiments was less than 1 mm^2, the analysis depth was less than 10 nm and the electron take-off angle was 90°. The analysis was conducted at 3 to 4 different locations per sample. The XPS analysis was conducted after 2 weeks of storage period.

The SEM analysis of the samples 5A to 20A (see Tables 2A and 2B) was conducted at VTT (Espoo) by PhD Unto Tapper in order to study the morphology of the deposit layer. The first samples were studied with a LEO, 982 Gemini FEG-SEM. During the project the SEM was replaced with a Zeiss, Merlin® FEG-SEM, which was used for the later samples. Both SEMs were equipped with an EDX micro analyser (NORAN Pioneer Si(Li) X-ray detector). The EDX spot analysis was carried out to determine the elemental composition of the samples. The concentration of elements in the EDX analysis was detected by measuring the intensity of their characteristic K-α and L-α X-ray emission. The painted samples were coated with platinum in order to prevent the accumulation of electrical charges on the surface during the SEM analysis. The SEM-EDX analysis was started after 2 weeks of storage period and it was completed after 3 weeks.

4.5 Study of the ^{131}I distribution on the substrate by radioactive means

Samples with radioactive deposited aerosols were studied using a HPGe detector and autoradiography. Measurements with the HPGe detector allow to determine the total amount of ^{131}I sorbed on the surfaces. The autoradiograph shows a mapping of the distribution of ^{131}I nuclides on the entire surface as well as an indication of the quantitative distribution.

The samples received from VTT did not show any visible deposit of the aerosols on the samples in comparison to samples produced within AIAS-1 (see Figure 1). Thus, autoradiography allowed to locate the point exposure on the sample and the spreading of the activity on the surfaces.
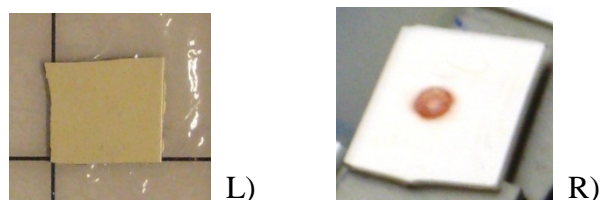

Figure 1: L.) Paint surface with thin deposit R.) Sample with thick deposit of IOx deposits

Metal and Teknopox Aqua VA paint films of different age were exposed to the iodine aerosols. The studied metal surfaces were Al, Cu, Zn and SS. The studied paint films were fresh (non-heat treated and non-pre-irradiated) (**N**), samples heated for 2 year at 100 °C (**H**), samples being exposed to intensive gamma irradiation (10 MGy) (**I**) and samples which were short time irradiated (100 kGy) and short time heated at 50 °C (1 week) before being irradiated (**H/I**).

4.6 Studied conditions in the revaporisation studies

The main parameters that determine the gas phase conditions of a severe accident in a boiling water reactor are the temperature, humidity and the intensity of the radiation field. To investigate the complexity of these conditions in different parts of the containment 3 main experiments regarding the desorption behaviour of ^{131}I deposited as aerosol particles in gaseous phase have been performed:

1. Desorption in humid air in a temperature range between room temperature and 250 °C gas phase temperature. (see 4.7)
2. Desorption in dry parts of the containment at room temperature (21.5 ± 1 °C; max. storage and transportation temperature), 50 °C (gamma cell temperature) and 150 °C (average containment temperature in a BWR when venting of the containment is initiated). (see 4.8)
3. Desorption under dry conditions under the influence of a continuous gamma radiation field with a dose rate of 14 kGy/h from a Co-60 source. The gamma cell sample chamber temperature was 50 °C. (see 4.9)

Furthermore the desorption behaviour of the deposits in contact with water as model for a hot steam water film on the paint surfaces in real reactor scenarios has been investigated by inserting the samples into distilled water with/without heating.

4.7 Measurement of the revaporisation of ^{131}I from iodine aerosol deposits

The revaporisation losses from the sample surfaces have been investigated using a HPGe detector. The ^{131}I activity was measured using the gamma emisson of 365 keV rays. The paint sample exposure chambers were during the experiments equipped with a > 99.9 % Cu spiral. Cu wire is known to be reactive towards elemental iodine but close to inert for the reaction with organic iodides such as methyl iodide. The studied epoxy paint was Teknopox Aqua VA paint which has been chemically examined at Chalmers [6]. It is known that the paint contains ingredients which are reactive towards iodine species. Thus it was expected that under the presence of irradiation and heat chemically reacted ^{131}I from the IOx could be converted into organic iodides.

4.8 Desorption studies on iodine aerosols in humid air

The desorption behaviour of IOx and CsI exposed surfaces in humid air has been studied using the **FOMICAG** facility (= **F**acility set-up for **O**n-line **M**easurements of the **I**odine **C**oncentration in an **A**queous and a **G**as phase) at Chalmers (see Figure 2) [7].
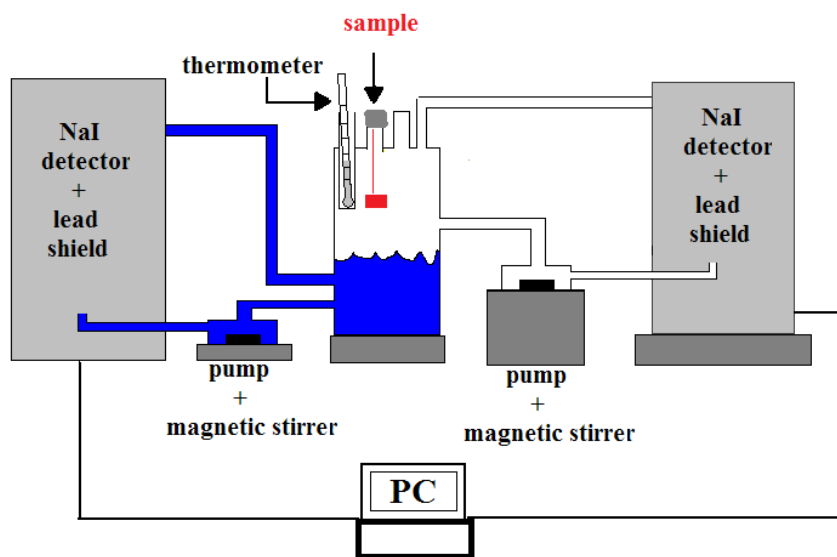

Figure 2: Schematic of the FOMICAG set-up (Chalmers, [7])

The experimental set-up is a lab-scale model of a BWR containment with the relative proportions of the Swedish BWR Oskarshamn 3 ((aq)/(g) = 0.71/0.29) [7]. The centre of the facility is a vessel representing a water pool with lid through which samples can be introduced to the gas phase and aqueous system. The vessel is connected with pipes to one aqueous and one gaseous phase loop. The phases are circulated by two centrifugal pumps to ensure mass transfer and a magnetic stirrer in the central vessel. The system is heated by a heating plate located under the central vessel and heating tapes placed around all surfaces. To reduce heat losses to the environment the tapes are covered with insulation material. The temperature of the aqueous phase is monitored with a thermometer inserted through one of the openings in the lid and thermo couples are placed on the lid and on the lid surfaces. In each of the loops, gaseous and aqueous, a NaI detector is placed and the change of the ^{131}I concentration in aqueous and gaseous phase is measured on-line.

15

For the experiments the vessel was filled up to one-third with double distilled water. The gas phase was normal air. The samples have been placed through one of the openings in the lid with a glass hook into the gas phase. The temperature has been raised in a ramp between room temperature (21.5 ± 1 °C) and 250 °C.

4.9   Desorption studies on iodine aerosols in dry air

The desorption of IOx aerosols under the storage conditions (21.5 ± 1 °C, dry conditions) has been monitored for the samples between arrival time at Chalmers and usage in the experiments with a HPGe detector.

The desorption behaviour of ^{131}I of deposited aerosols caused by temperature effects has been investigated heating the samples separately in miniature gas chambers of 20 ml volume filled with air. The chambers in which paint films have been studied contained additionally a copper spiral. Copper is known to be reactive towards elemental iodine. Thus, measuring the Cu wire allowed to conclude if ^{131}I is released from the painted surface in form of elemental iodine or organic iodides. The chambers have been heated and thermo stated in a aluminium block at the studied temperature and after defined time intervals the samples and copper wires have been examined using a HPGe detector.

The desorption effects at 50 °C had been monitored since samples being exposed to gamma irradiation have been irradiated in a gamma source with a sample chamber inner temperature of 50 °C. Furthermore, the desorption behaviour of ^{131}I has been investigated at 150 °C based on the reference temperature in severe accident research for BWR reactors. In Swedish BWR reactors the venting of the containment is initiated when the average containment temperature reaches 150 °C and exceeds a pressure of 5-6 bars [8].

4.10   Desorption studies on iodine aerosols under the influence of gamma irradition

The desorption behaviour of ^{131}I from deposited aerosols caused by a high gamma dose rate of 14 kGy/h has been investigated irradiating the samples separately in miniature gas chambers of 20 ml volume filled with air. The sample chamber temperature in the gamma cell during the irradiation was app. 50 °C. Analogous to the heat treated samples the samples were examined using HPGe measurement technique. The samples have been pre-heated for app. 24 h at the irradiation cell temperature to evaluate the temperature effect.

The ability of metal samples (Cu, Al, Zn, SS) and fresh and artificially aged paint films of the epoxy paint Teknopox Aqua V A to bind ^{131}I from the aerosols chemically to the substrate has been compared.

16

4.11   Solubility of iodine aerosols on water covered surfaces

The desorption behaviour of ^{131}I of deposited aerosols on surfaces covered with a water film have been simulated by inserting the samples into double distilled water. Both types of aerosols are known to be water soluble. Reacted with the surfaces a reduced solubility has been assumed to be caused by the formation of new, less water soluble iodine species.

4.12   The effect of CO on IOx aerosol decomposition

A glass fibre filter was exposed to IOx aerosols produced at 120 °C. The filter was placed in a syringe filter and volume fractions of air and carbon monoxide were passed through the filter. The amount of revaporised ^{131}I was measured with a HPGe detector on the filter, as well as in a 1 M sodium thiosulfate solution in which the gas stream was trapped.

5   Results

I.   Deposit and surface characterisation

5.1   Properties of IOx and CsI particles in a gas phase

When the construction of particle production and deposition facility was completed and all the parameters for its operation were optimized (e.g. temperature, pressure, flow rates, concentration of precursor solutions), the properties of produced particles were analysed with SMPS.

The number size distribution of particles in gas phase was measured at the inlet of the impactor. The count median diameter (CMD) of IOx particles was ~28 nm, Figure 3. The distribution was quite narrow and the corresponding geometric standard deviation (GSD) was only 1.4. This means that 95 % of the produced particles had a diameter in a range from 14 nm to 55 nm. The total number concentration of particles (N_{tot}) was rather high, $2.18*10^7$ particles/cm^3.
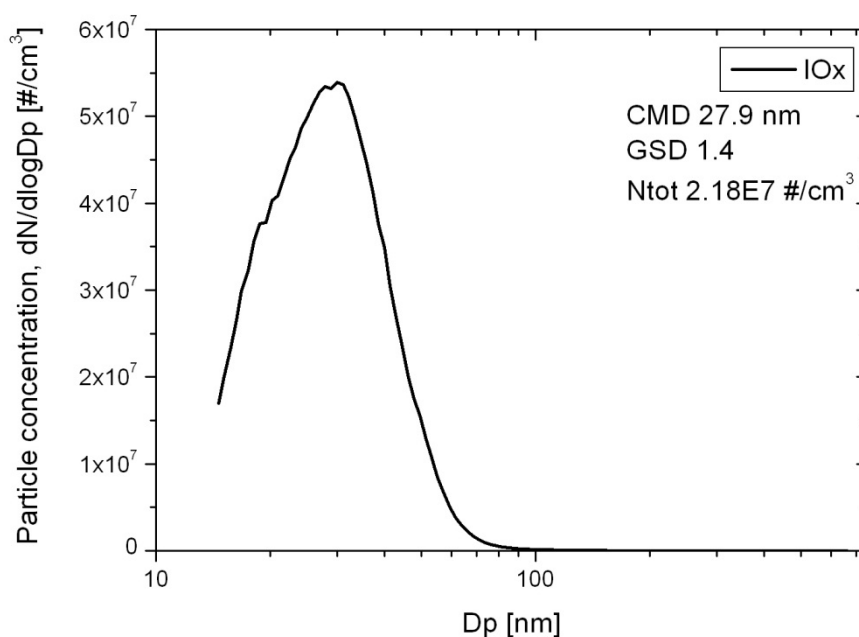

Figure 3. A typical number size distribution of the produced IOx particles in gas phase. The size distribution of the particles was analysed with SMPS.

The stability of the particle production was followed on-line as well. This kind of process is very sensitive to any kind of changes in the facility (e.g. temperature, flow rate). On the other hand, it is very easy to adjust the properties of particles - such as diameter, mass and number concentration - if there is a need for that. The stability of the measured CMD, GSD and N_{tot} values over a 24 minutes period of IOx particle production is presented in Figure 4. As it can be seen, the production of particles remained rather stable - the count median diameter of particles was almost constant. The total number concentration of particles varied slightly. The mass concentration of particles in the gas phase was monitored with TEOM. It remained very stable during the facility testing with the average mass concentration of ~ 1100 µg/m^3.

18
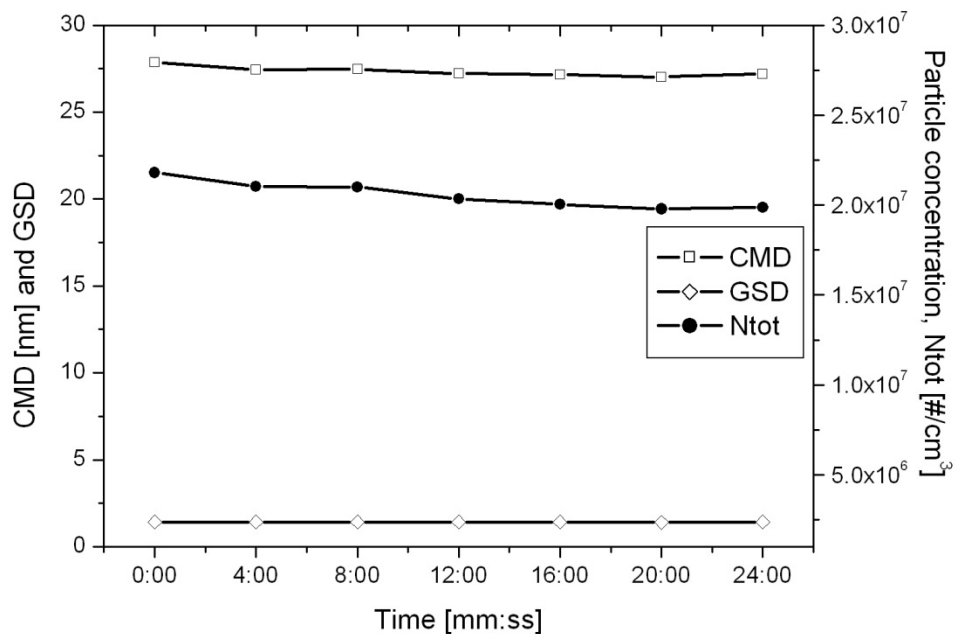
Figure 4. The CMD, GSD and N$_{tot}$ values measured online over a 24 minutes period of IOx particle production.

The produced CsI particles were analysed with SMPS similarly, Figure 5. The CMD of CsI particle number size distribution was a bit larger than for IOx particles, 41 nm. Furthermore, the distribution was wider as well (GSD 1.6). Most particles (95 %) had a diameter in a range from 16 nm to 105 nm. With the current set-up, the total number concentration in the gas phase was only $3.77*10^5$ particles/cm^3.
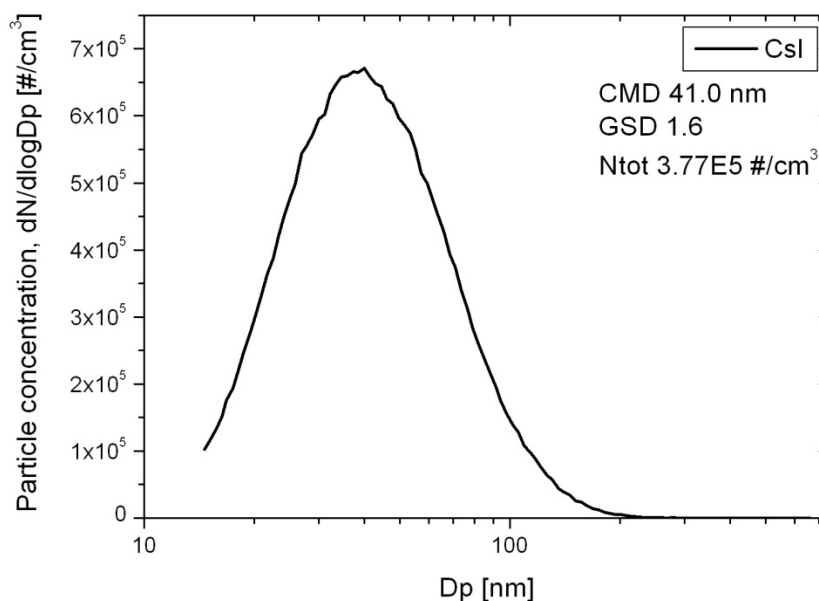

Figure 5. A typical number size distribution of the produced CsI particles in the gas phase. The size distribution of the particles was analysed with SMPS.

The stability of the measured CMD, GSD and N_{tot} values over a 12 minutes period of CsI particle production is presented in Figure 6. The production of particles was rather stable; all the observed parameters remained practically unchanged. After 10 minutes of testing, the dilution flow was decreased slightly and as an outcome the number concentration and the count median diameter of the particles increased. The mass concentration of CsI particles in gas phase was significantly lower, 200 µg/m^3, when compared with IOx particle production.
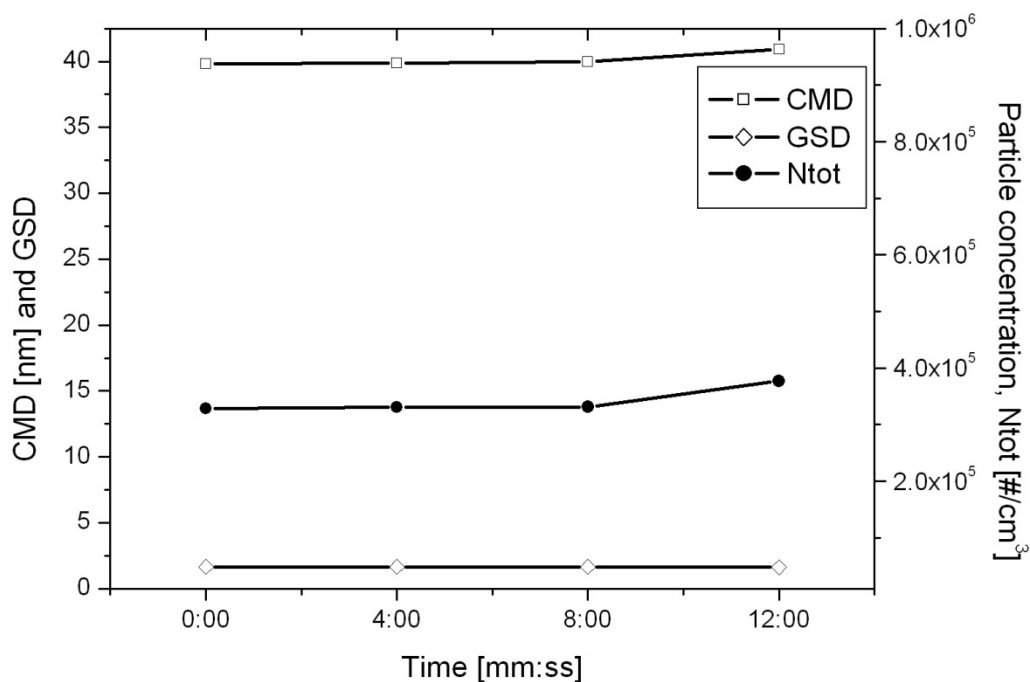

Figure 6. The CMD, GSD and N_{tot} values measured online over a 12 minutes period of CsI particle production.

5.2 Properties of IOx and CsI particles deposits on a copper surface

As a part of the facility testing, IOx and CsI particles were deposited on a copper surface in order to analyse their size and distribution. The analysis was conducted with two different SEMs. The SEM micrographs of IOx and CsI particles on copper surface are presented in Figures 7 and 8. It can be seen, that the deposited IOx particles were smaller in diameter compared to CsI particles. This was also verified with SMPS analysis of particles in the gas phase (previous chapter 5.1). The particles were distributed quite evenly on the deposit area. It seemed that the particles were not overlapping each other and the deposit was mono-layer. However, some large particles, which have already been agglomerated in the gas phase, were observed on the surfaces.

As a result of the facility testing, the production of thin layer deposit was verified. In the previous AIAS-1 project the deposit layer was thick and therefore it was more difficult to observe the chemical reactions taking place in the boundary layer of particles and the studied surface materials.
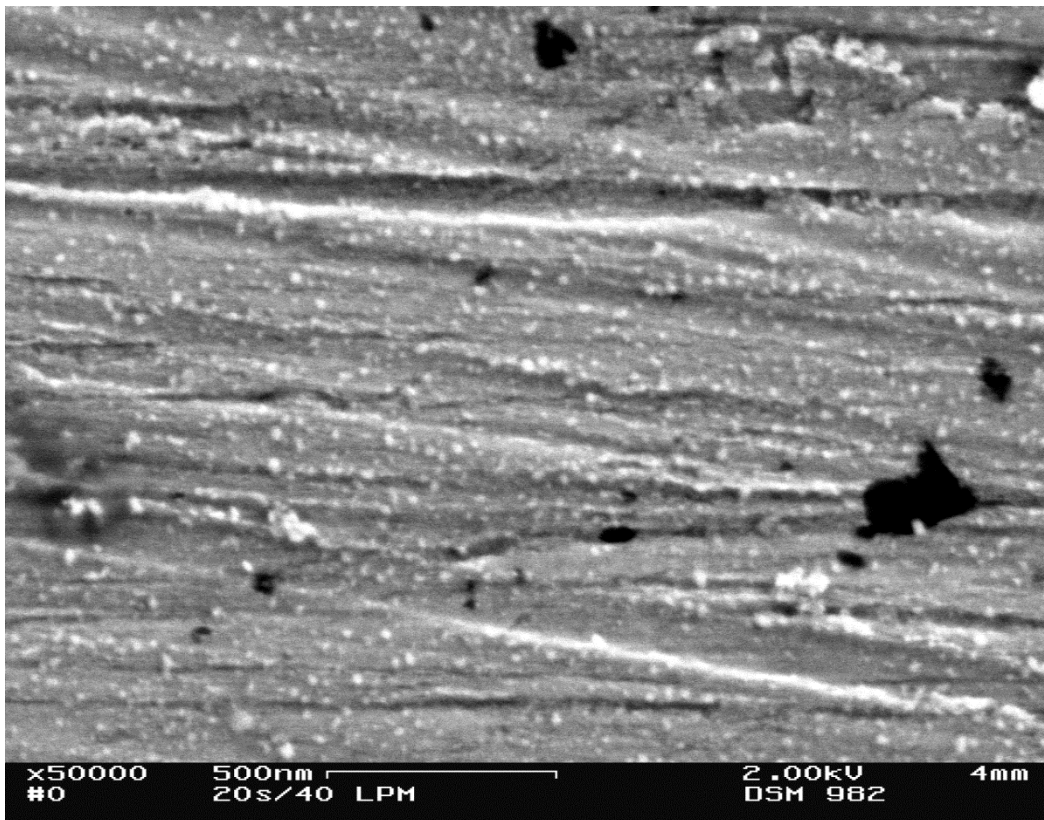
**Figure 7. A SEM (LEO, 982 Gemini) micrograph of IOx particle deposit on copper surface.**
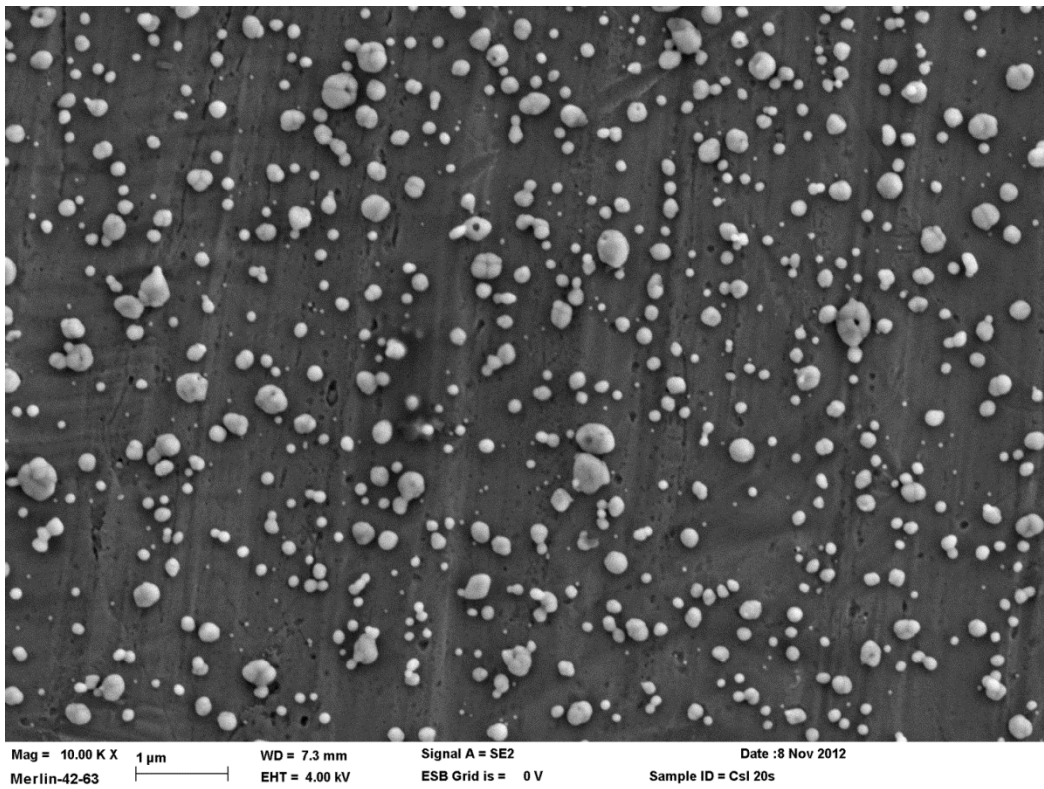
Figure 8. A SEM (Zeiss, Merlin® FEG-SEM) micrograph of CsI particle deposit on copper surface.

5.3 Raman analysis of IOx particles collected on a filter

The measured Raman spectra of IOx particles produced at 50 °C, 100 °C and 120 °C and then collected on a plane Teflon™ filter (Mitex™) - samples 1, 2 and 3 respectively - are presented in Figure 9. The reference Raman spectrum of a clean filter (sample 4) is presented in the figure as well. The spectral data are presented in Appendix B, Table B1. The duration of the particle sampling on the filters was 1 hour at each temperature. The measured Raman spectrum of particles produced at 50 °C ranged from 100 cm^{-1} to 4000 cm^{-1}. Due to noise in the analysis of particle samples produced at 100 °C and 120 °C, the Raman spectra were only recorded in a range from 400 cm^{-1} to 3600 cm^{-1}.
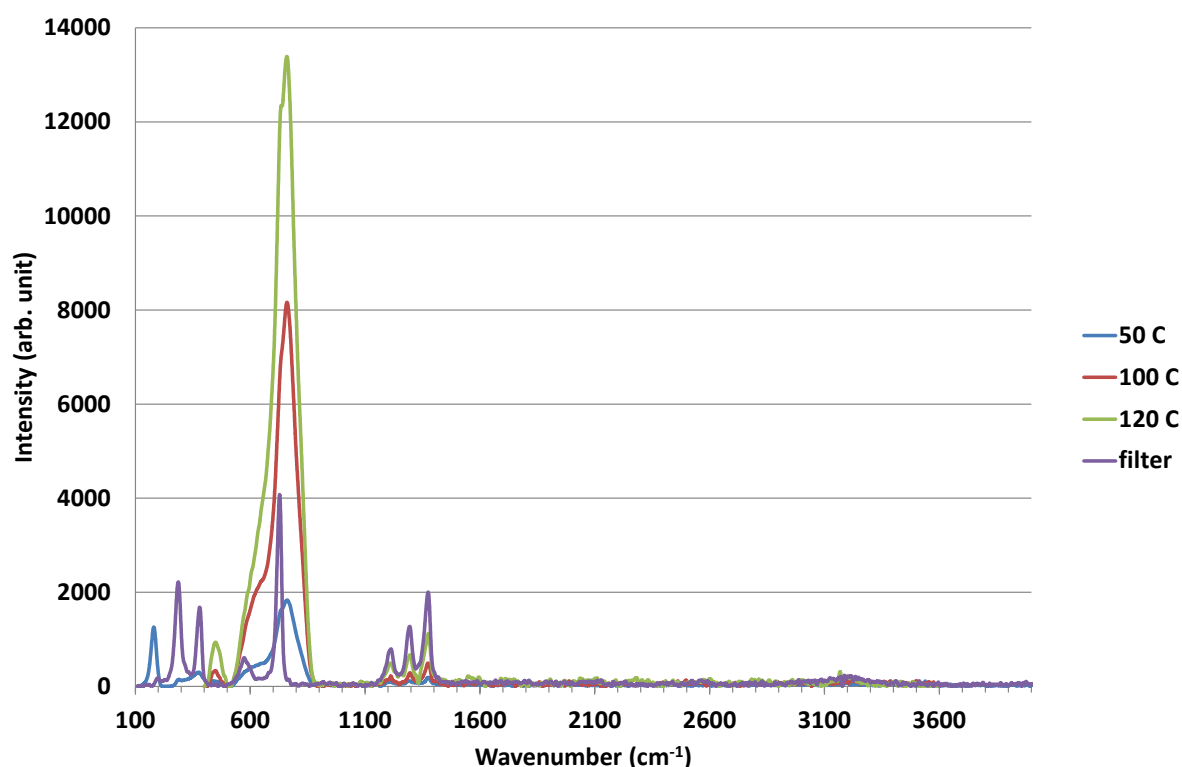

Figure 9. Raman spectra (wavenumbers 100-4000 cm^{-1}) of IOx particles collected on a Teflon™ filter. Particles were produced at 50 °C, 100 °C and 120 °C. The reference Raman spectrum of clean filter is presented as well.

The measured Raman spectra of IOx particles on the filters were similar regardless of the particle production temperature. The measured spectra corresponded to the Raman spectrum of deliquesce HIO_3 presented in Appendix A, Figures A1 and A2. There was also a very weak signal at 3100-3400 cm^{-1}. That is probably the wide OH stretch band associated with water (~3400 cm^{-1}) [9]. Since the intensity of its Raman spectra was low, it verifies that the concentration of water on the samples was also low. The clearly visible band at ~188 cm^{-1} (50 °C spectrum) is most likely originating from iodine molecules (I_2) [10, 11] which were adsorbed on HIO_3. Elemental iodine and iodic acid (HIO_3) are formed when I_2O_4 reacts with water (e.g. humid air). Therefore, the IOx particles on the filter sample were originally likely I_2O_4 or a mixture of I_2O_4 and I_2O_5.

The bands at 1100 cm to 1400 cm^{-1} were visible in every Raman spectra measured. These bands originated from Teflon™ (PTFE) which was the filter material used. Since the layer of

22

IOx particles was thin, the strongest signals penetrated through the particle layer and they were also recorded. The complete spectrum of clean Teflon^{TM} filter is presented in Figure 9. It corresponds to the Raman spectrum of PTFE measured previously by Mihály *et al.* [12], presented in Appendix B.

5.4 XPS analysis of IOx and CsI particle deposits

The binding energy of electrons in the IOx and CsI deposits on paint, stainless steel, copper, aluminium and zinc samples was analysed with XPS. The analysis results are discussed in the following chapters.

5.4.1 XPS analysis of IOx deposits on metal surfaces

The XPS spectra of the binding energy of electrons in the centre and on the edge of the IOx deposits on stainless steel, aluminium, copper and zinc (samples 5B to 8B respectively) are presented in Appendix C. The XPS spectra of the surfaces without iodine deposits are presented as well. The corresponding elemental concentrations are presented in Appendix D. The binding energy of IOx deposit (spin orbit I $3d_{5/2}$) was high on all surfaces (peaks at approx. 623 eV). It means that iodine was oxidised. A small fraction of iodine was in a low oxidation state on the steel and aluminium surfaces, which is evident as a shoulder in the spectra at a smaller energy (peaks at approx. 621 eV).

A significant difference in the oxygen binding energy (spin orbit O 1s) between the IOx deposit area and the area without deposit was detected. On all the samples – except for Zn - oxygen had two binding energies (peaks at approx. 531 eV and 533 eV) at IOx deposit area. At areas without iodine, oxygen had only the high energy peak. These results also indicate that iodine was oxidized on the studied surfaces.

Accurate speciation of iodine oxides is not possible from the XPS results alone as the devices used in the analysis have a resolution of ~1 eV. The difference in the iodine binding energy between different iodine oxide species can be as small as 0.1 eV, see Table 3. However, the XPS analysis results of oxygen and iodine suggest that iodine on the surfaces was mostly in form of iodic acid (HIO_3).

Table 3: Binding energies of I 3d$_{5/2}$ and O 1s [13].

I 3d$_{5/2}$ binding energy		O 1s binding energy	
	eV		eV
I$_2$	619.9	metal oxides	approx. 528-531
I$_2$O$_5$	623.3	CuO	529.6
HIO$_3$	623.1	Cu$_2$O	530.3
H$_5$IO$_6$	623.0	HIO$_3$	530.6
CuI	619.0	I$_2$O$_5$	529.9
ZnI$_2$	619.8		
NiI$_2$	619.0		
CsI	618.2		
NaI	618.6		
NaIO$_3$	623.5		
NaIO$_4$	624.0		
KI	618.8		
CH$_3$I	620.8		

5.4.2   XPS analysis of CsI deposits on metal surfaces

The XPS spectra of the binding energy of electrons in the centre and on the edge of the CsI deposits on stainless steel, aluminium, copper and zinc (samples 9B to 12B respectively) are presented in Appendix E. Furthermore, the spectra optimized on iodine and on caesium are also presented. The corresponding elemental concentrations are presented in Appendix F. Iodine had two binding energies (spin orbit I 3d$_{5/2}$) at CsI deposit area on all surfaces (peaks at approx. 618 eV and 623-624 eV). The intensity of lower energy peak of iodine increased when the XPS analysis was optimized on Cs. Therefore, it most likely corresponded to the binding energy of iodine in CsI (618.2 eV [13]). At other locations, the intensity of low energy peak, corresponding to CsI, was weak or it was not observed at all. However, the high energy peak of iodine was observed at all locations. It seemed that iodine had separated from the CsI deposit, probably due to reaction with air humidity, and transported on the sample surface.

A significant difference in the oxygen binding energy (spin orbit O 1s) between the area of CsI deposits optimized either on caesium or on iodine was detected. On all the samples oxygen had two binding energies (peaks at approx. 529-530 eV and 531-532 eV). At areas optimized with Cs, the binding energy of oxygen was higher and iodine was bound mainly to caesium. The lower binding energy of oxygen was particularly observed at areas optimized on iodine. It means that iodine was oxidised. It may be that iodine separated from CsI deposit had reacted with the oxidized metal surfaces and formed metal iodates. The reference binding energies for these compounds were not found in a short literature review. However,

24

the binding energy value of the characteristic I $3d_{5/2}$ peak for an iodine atom implying iodide (619.3 – 619.7 eV), iodate (623.5-624 eV) and for organic molecules (620-621.4 eV) have already been determined [14, 15, 16, 17]. Generally, the binding energies of metal iodides are close to 619 eV (spin orbit I $3d_{5/2}$), e.g. NaI 618.6 eV [13]. For the metal iodates the binding energies are higher, due to higher degree of oxidation, and they are close to 623 eV, e.g. $NaIO_3$ 623.5 eV and $NaIO_4$ 624 eV [13, 18]. Therefore, the observed high binding energy of iodine (623-624 eV) on the samples could be resulting from the formation of metal iodates.

5.4.3   XPS analysis of IOx deposits on paint surfaces

The XPS spectra of the binding energy of electrons in the centre and on the edge of the IOx deposits on paint (samples 13B to 16B) are presented in Appendix G. The corresponding elemental concentrations are presented in Appendix H. There were several different treatment procedures for the painted samples before the deposition of particles. The pre-treatments were as follows: no treatment, heat treatment, a short gamma irradiation and heat treatment, and a long gamma irradiation (see chapter 4.5). The binding energy of IOx deposit (spin orbit I $3d_{5/2}$) was again high on all surfaces (peaks at approx. 623-624 eV). It means that iodine was oxidised. A small fraction of iodine was in a low oxidation state, which is evident as a shoulder in the spectra at a smaller energy (peaks at approx. 621 eV).

As on the studied metal surfaces, a difference in the oxygen binding energy (spin orbit O 1s) between the IOx deposits and area without a deposit was detected. On all samples oxygen had two binding energies (peaks at approx. 531 eV and 533 eV) at the area with IOx deposit. At areas outside of the deposits, the binding energy of oxygen had a single peak, which located at 533 eV. These results indicate that iodine was oxidized on the studied surfaces. Most likely, iodine was in form of iodic acid (HIO_3) on the painted surfaces regardless of the pre-treatment of the surface.

5.4.4   XPS analysis of CsI deposits on paint surfaces

The XPS spectra of the binding energy of electrons in the centre and on the edge of the CsI deposits on paint (samples 17B to 20B) are presented in Appendix I. The corresponding elemental concentrations are presented in Appendix H. There were several different treatment procedures for the painted samples. The pre-treatments were as follows: no treatment, heat treatment, a short gamma irradiation and heat treatment, and a long gamma irradiation (see chapter 4.5). Iodine had two binding energies (spin orbit I $3d_{5/2}$) at the area with CsI deposits on all surfaces (peaks at approx. 618 eV and 623-624 eV). The intensity of lower energy peak was high in the centre of the deposits where also Cs was observed. This verified that the deposits contained CsI particles (618.2 eV [13]). At other locations, the intensity of iodine binding energy corresponding to CsI was low or it was not observed at all. However, the high binding energy peak of iodine was observed at all locations, although its intensity was extremely low. It seemed that a small fraction of iodine had separated from the CsI deposit on the painted surface as well. The high binding energy of iodine suggests that iodine was in oxidised form.

An interesting result was that a part of the acquired signals of caesium and iodine seemed to be coming deeper from the structure of the paint. That could be concluded from the shape of XPS binding energy spectra. Apparently, CsI dissolved on the surfaces due to air humidity

25

and transported into the structure of paint. This phenomenon was noticed on surfaces which were pre-treated with heat or gamma irradiation.

5.4.5   Other observations on surfaces analysed with XPS

As it was discussed in chapter 5.2, the deposit layers were very thin on the samples and single particles could clearly be observed on the surfaces. Therefore, the sample substrate materials were also visible under the deposits and their XPS spectra were recorded as well.

According to the XPS spectra of CsI and IOx deposits on copper, iodine may have reacted with the copper surface. Even though the formation of copper iodide was not observed in the spectra, it may have formed as was verified in the previous AIAS-1 project. However, the data suggest that the formation of copper iodate was more likely in these experiments. The formation of HIO_3 was also very likely in case of IOx particles. Furthermore, a part of the iodine signal seemed to be originating deeper from the copper surface. This would support the suggestion on the reaction of iodine with copper.

All metal and paint samples contained rather high fractions of carbon (C) and silicon (Si) impurities. Some surface contamination has likely taken place during the handling and storage of the samples in the laboratory or these elements could be present due to the use of silicone pump oils in vacuum pumps. Overall, it seemed that the contamination had taken place before particles were deposited on the samples. Nitrogen was observed on all samples.

On metal and on painted surfaces, the intensities of the binding energy signals of carbon (C, spin orbit 1s) at approx. 286 eV and 289 eV increased, when the concentration of iodine with low binding energy, approx. 621 eV, increased. At the same time, the binding energies of carbon seemed to differ slightly from the XPS spectra without iodine. It is possible that iodine has formed a compound with carbon, either with the surface contamination or with organic compounds of paint (e.g. the binding energy of iodine in CH_3I is 620.8 eV [13] - spin orbit I $3d_{5/2}$).

Sodium and chlorine were observed on the painted samples. These elements could be coming from the handling of samples or from the air as the laboratory was located next to sea shore. However, the atomic concentration of chlorine seemed to increase when the painted surface was shortly pre-treated with gamma irradiation before the deposition of particles. Longer exposure to irradiation increased the atomic concentration of calcium. The origin of calcium is not known. Some traces of potassium were also observed on painted surfaces. It originated probably from the production of IOx particles and the glass substrate of painted samples.

5.5   SEM-EDX analysis of IOx and CsI deposits

IOx and CsI particle deposits on metal and paint surfaces were also studied with SEM-EDX method. The particles deposited on the surfaces were extremely small in diameter and the aim was to prepare as thin layer of particle deposit as possible (meaning a mono-layer in practice). Therefore, it was rather challenging to locate the area of deposit on the samples with SEM-EDX. Another problem was that both IOx and CsI particles are sensitive to air humidity. It was impossible to avoid any contact with air during the handling of samples. For the EDX analysis, the main difficulty was that for caesium and iodine the K-α and L-α X-ray emission energies are rather close to each other. In addition, the X-ray emissions for

titanium, calcium and barium were also overlapping with iodine and caesium. This causes difficulties in separating the signals from each other when the mass concentration of particle deposit is very low and the background signal level of the substrates is high. The painted samples were coated with platinum (Pt) in order to avoid the accumulation of electrical charge during SEM-EDX analysis.

5.5.1 SEM analysis of metal and paint surfaces

Metal and paint surfaces, which were to be exposed with particles in this study, were examined with SEM. SEM micrographs of stainless steel (SS 316), aluminium, copper and zinc surfaces without particle deposits are presented in Figure 10. When the surfaces were compared, some obvious differences were observed. The grain boundaries of stainless steel were very wide and the surface was irregular. The surfaces of aluminium and copper samples were generally smooth with shallow grooves. The most irregular surface structure was found on zinc.
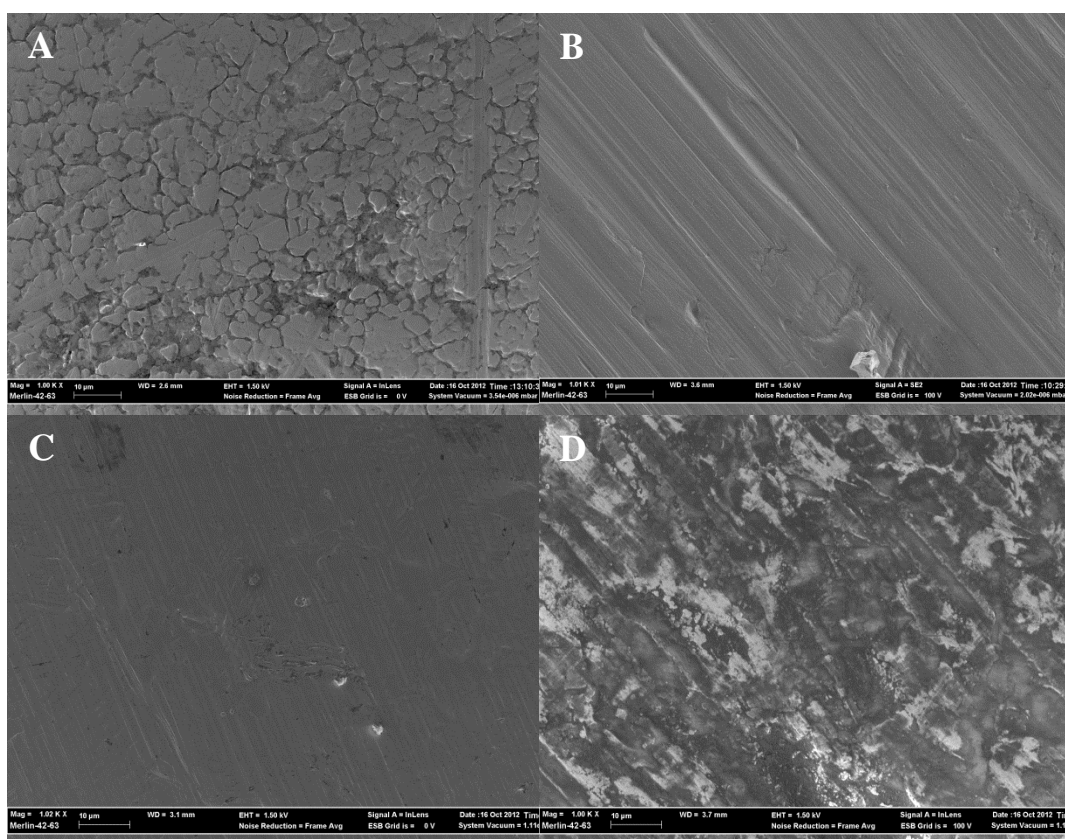

Figure 10. SEM micrographs of a) stainless steel (SS 316), b) aluminium, c) copper and d) zinc surfaces without particle deposit.

SEM micrographs of the pre-treated painted surfaces (no treatment, heat treatment, short gamma irradiation and heat treatment, long gamma irradiation – see chapter 4.5) without particle deposits are presented in Figure 11. Different kinds of areas were found on painted surfaces. Generally, the surfaces studied were smooth. But when studied more in detail, a small scale roughness caused by the filler materials within the paint could be observed. On one hand, the exposure to heat and/or gamma irradiation seemed to decrease the small scale roughness, but on the other hand it also increased the larger scale roughness and porosity of the surfaces.
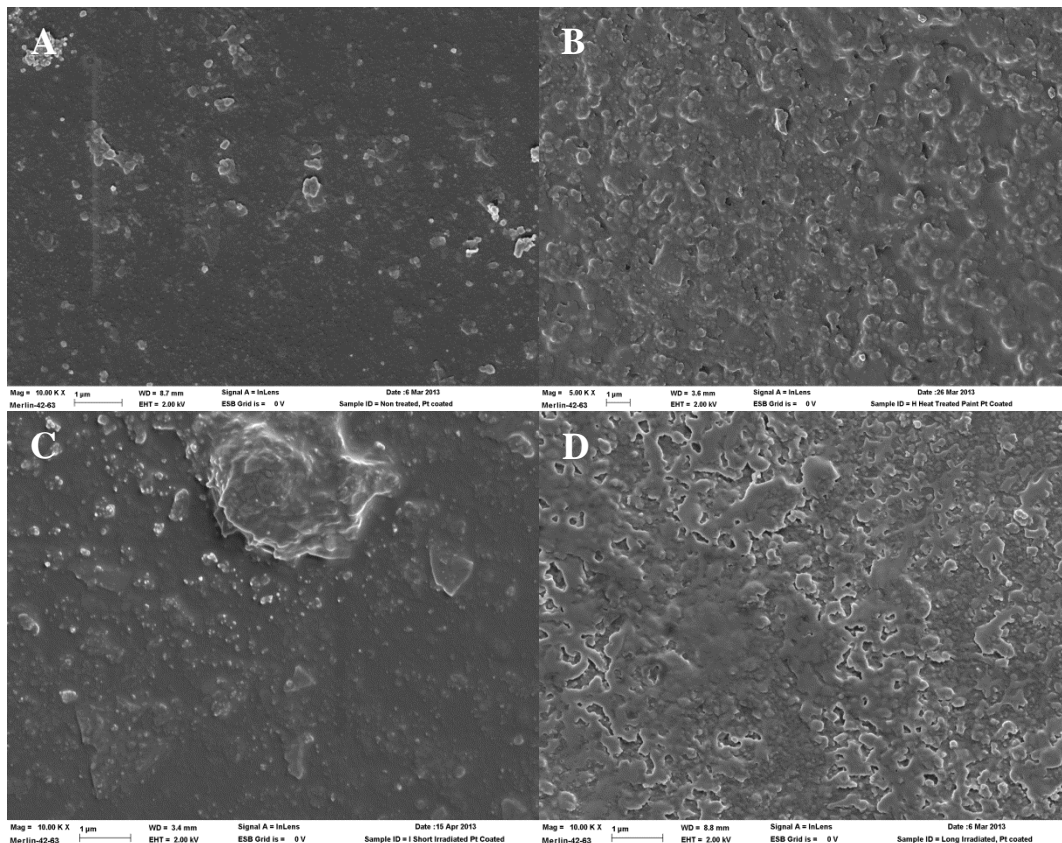
Figure 11. SEM micrographs of the pre-treated paint surfaces without particle deposits: a) no treatment, b) heat treatment, c) short gamma irradiation and heat treatment and d) long gamma irradiation.

5.5.2　SEM-EDX analysis of IOx deposits on metal surfaces

SEM micrographs of IOx deposits on stainless steel (SS 316), aluminium, copper and zinc surfaces (samples 5A to 8A respectively) with EDX spot analysis locations are presented in Figure 11. The corresponding EDX spectra are presented in Figures 12 to 15. Since IOx particles are very soluble in water, they tend to react with the humidity in air. This reaction is very fast as it was verified in the previous AIAS-1 project. A very good example of dissolved IOx particles can be seen on the aluminium surface in Figure 11. That pool-like area of deposit is several micrometres wide and it contains iodine according to the EDX spectrum. Iodine was not observed outside the deposit area. The original IOx particles deposited on the sample were ranging from 14 nm to 55 nm in diameter.

On the irregular surfaces, e.g. stainless steel and zinc, dissolved IOx particles could move through the grooves and cuts. On zinc surface only small traces of iodine could be seen in the EDX analysis. On stainless steel surface no iodine was found at all. IOx particles were dissolved also on copper surface. An interesting observation was that a strong signal of iodine was acquired from a solid particle on the copper surface (Figure 14, spot 1). The signal of copper was also strong and it was impossible to separate whether it resulted from the particle or from the background signal of copper substrate. Furthermore, the signal of oxygen in the EDX spectrum was strong at the same location. It is very likely that iodine from the dissolved IOx deposit has reacted with copper and formed copper iodate.

28
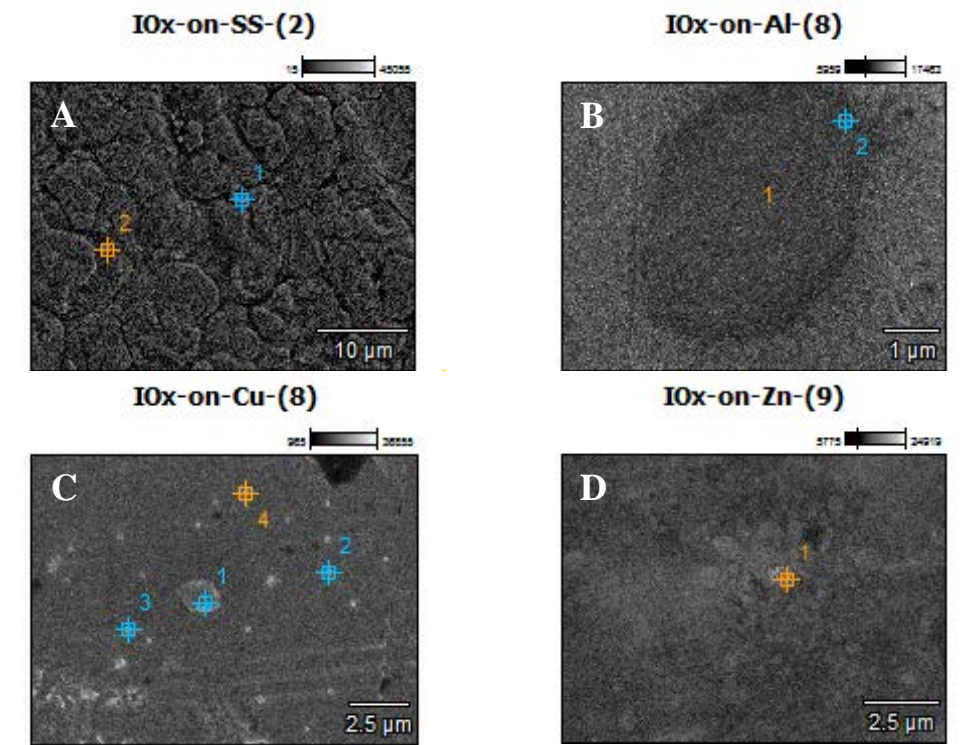
Figure 11. SEM micrographs of IOx deposits on a) stainless steel, b) aluminium, c) copper and d) zinc. The EDX spot analysis locations on the samples are marked in the micrographs.
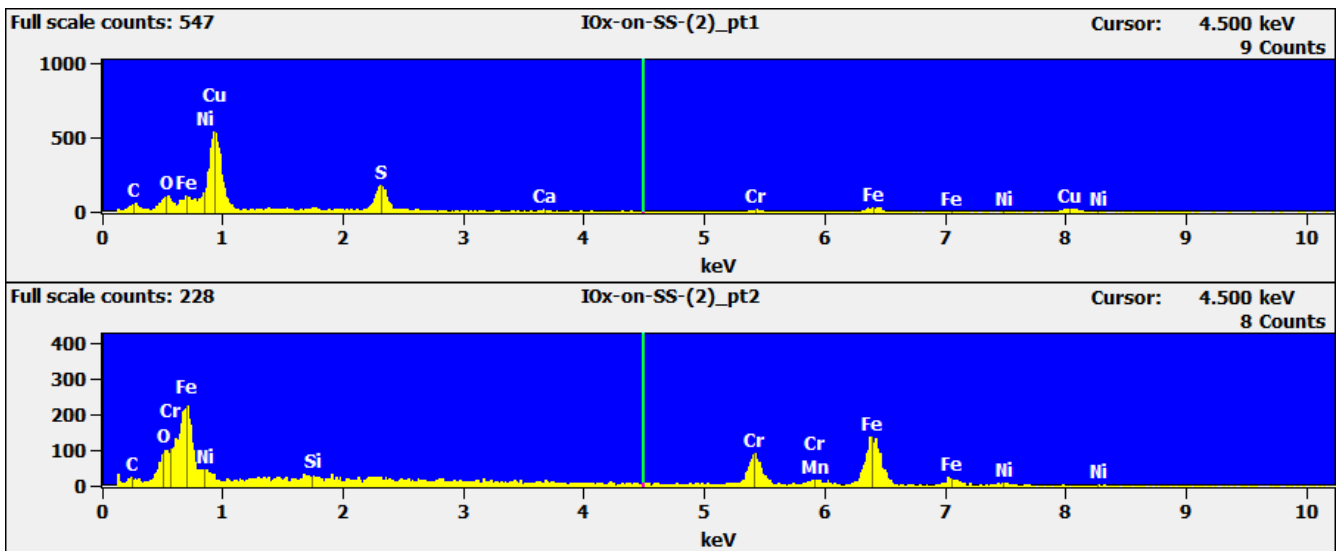
Figure 12. The EDX spectra of two locations on a stainless steel surface (see Figure 11a). Spot 1 is located on the surface of the sample. Spot 2 is on a grain boundary area.
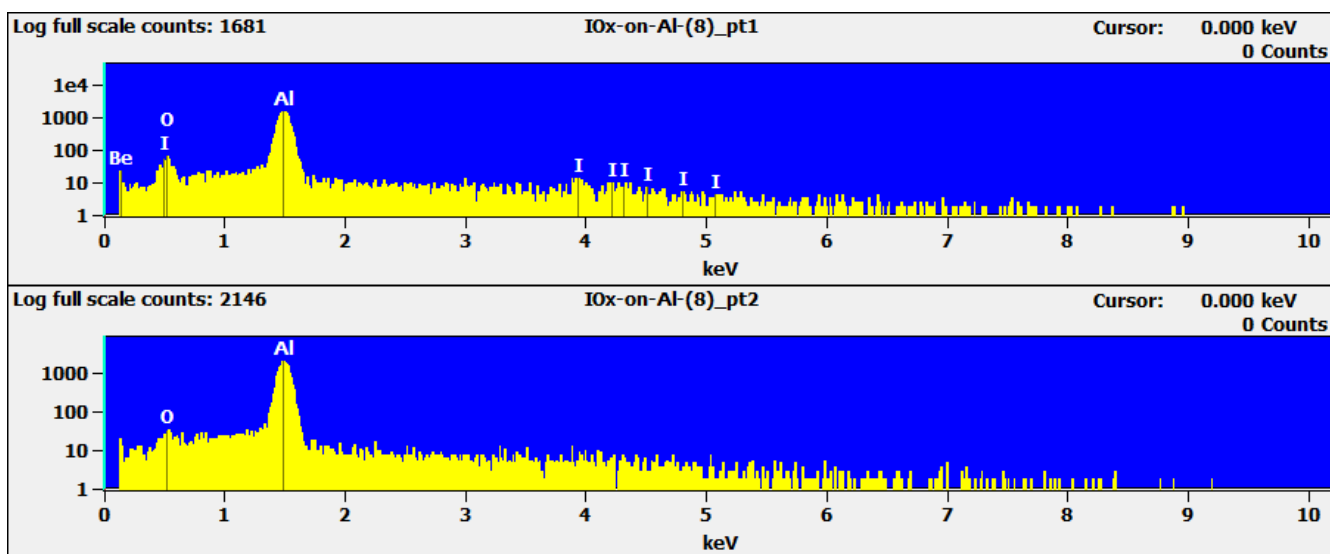
Figure 13. The EDX spectra of two locations on an aluminium surface (see Figure 11b). Spot 1 is located on a dissolved deposit containing iodine. Spot 2 is on the edge of deposit.
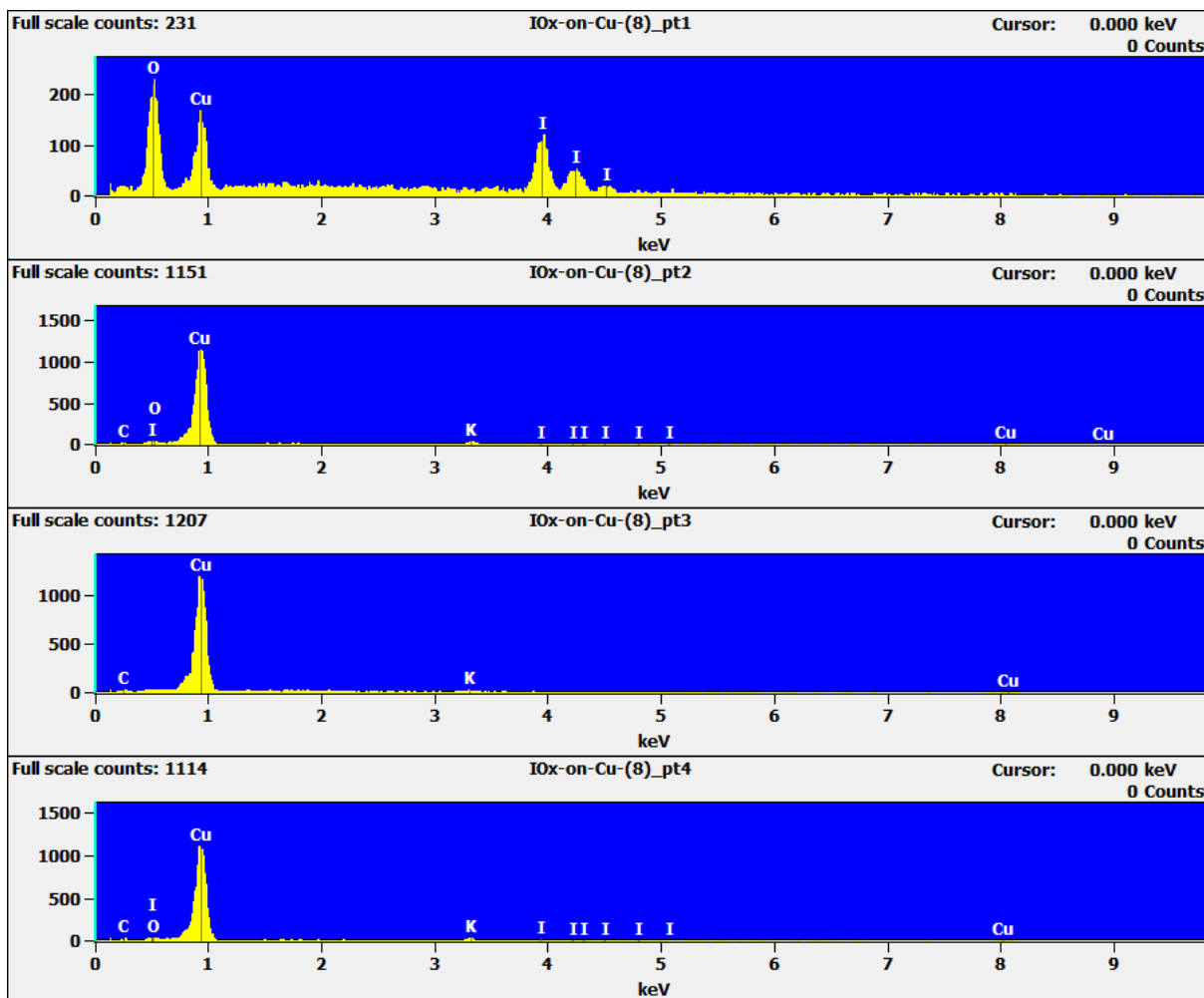
Figure 14. The EDX spectra of four locations on a copper surface (see Figure 11c). Spot 1 is located on a solid deposit containing iodine. Spots 2 to 4 are located next to the solid deposit.
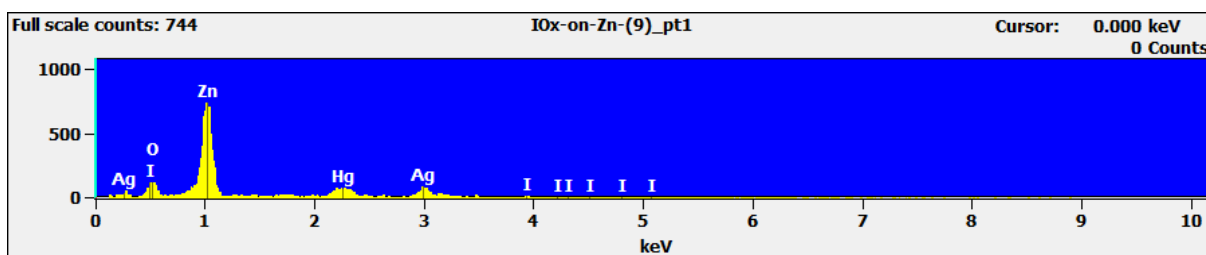
Figure 15. The EDX spectra of one location on a zinc surface (see Figure 11d). Spot 1 is located on the surface containing trace amounts of iodine.

5.5.3   SEM-EDX analysis of CsI deposits on metal surfaces

SEM micrographs of CsI deposits on stainless steel (SS 316), aluminium, copper and zinc surfaces (samples 9A to 12 A respectively) with EDX spot analysis locations are presented in Figure 16. The corresponding EDX spectra are presented in Figures 17 to 20. Even though CsI is water soluble, the particles were much more stable and therefore easier to observe on the surface than IOx particles. On stainless steel, aluminium and zinc surfaces the particles clearly contained both caesium and iodine. However, on copper surface EDX analysis did not reveal either caesium or iodine. The reason for this is not known.
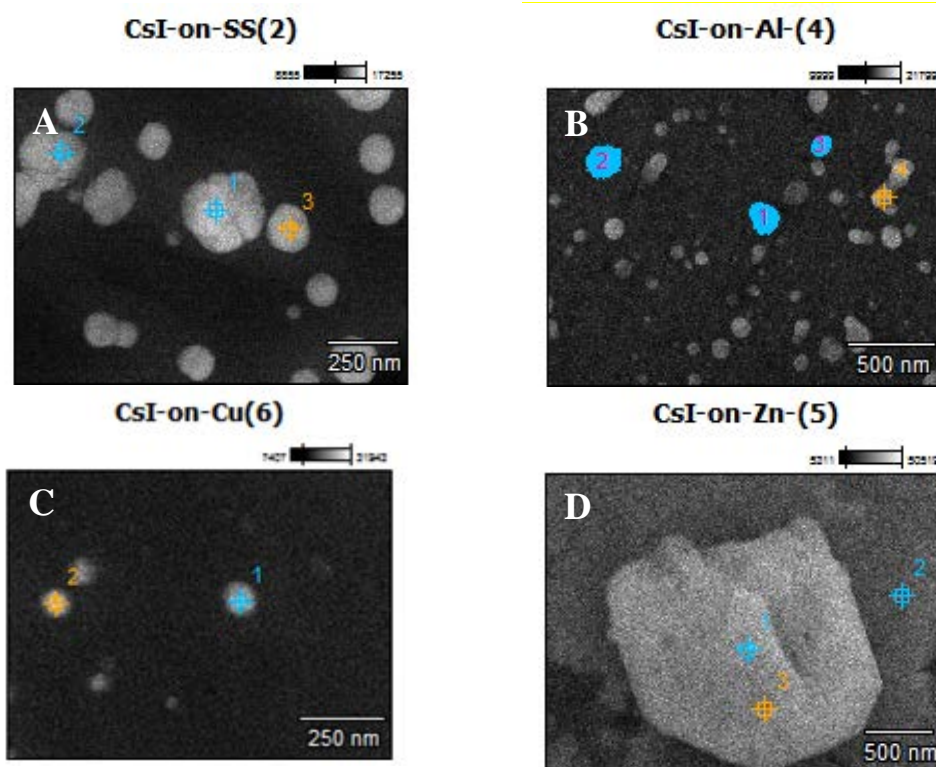
Figure 16. SEM micrographs of CsI deposits on a) stainless steel, b) aluminium, c) copper and d) zinc. The EDX spot analysis locations on the samples are marked in the micrographs.
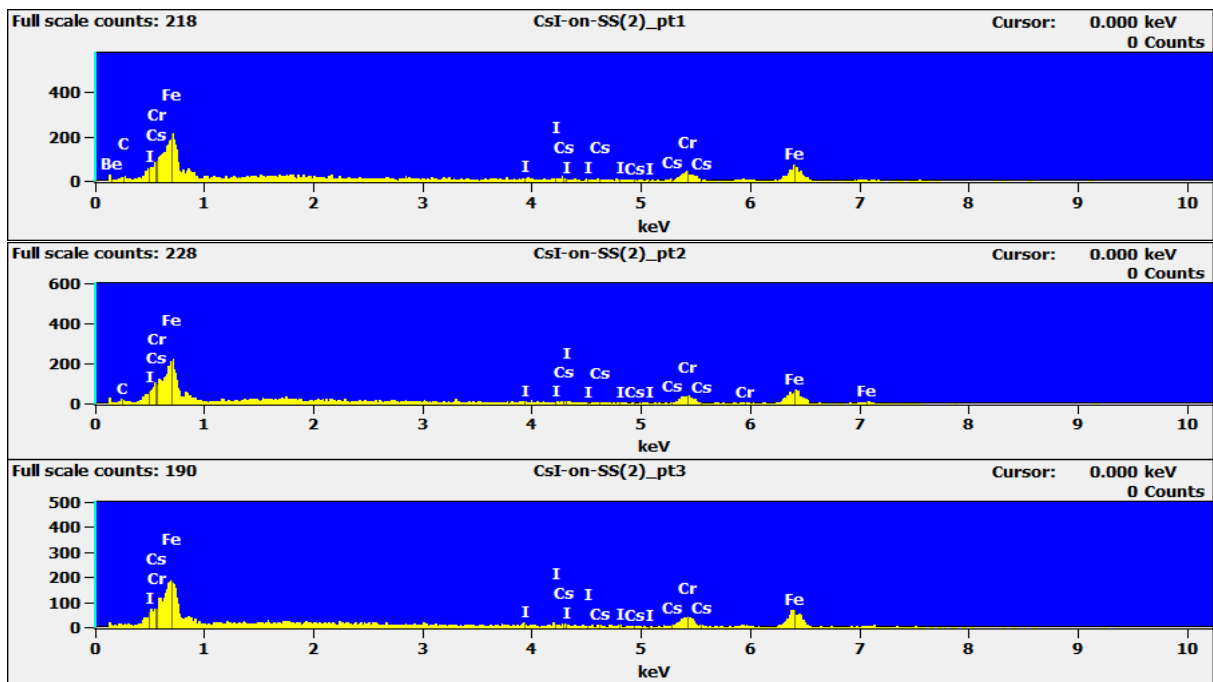
Figure 17. The EDX spectra of three locations on a stainless steel surface (see Figure 16a). Spots 1 to 3 are located on CsI particles.
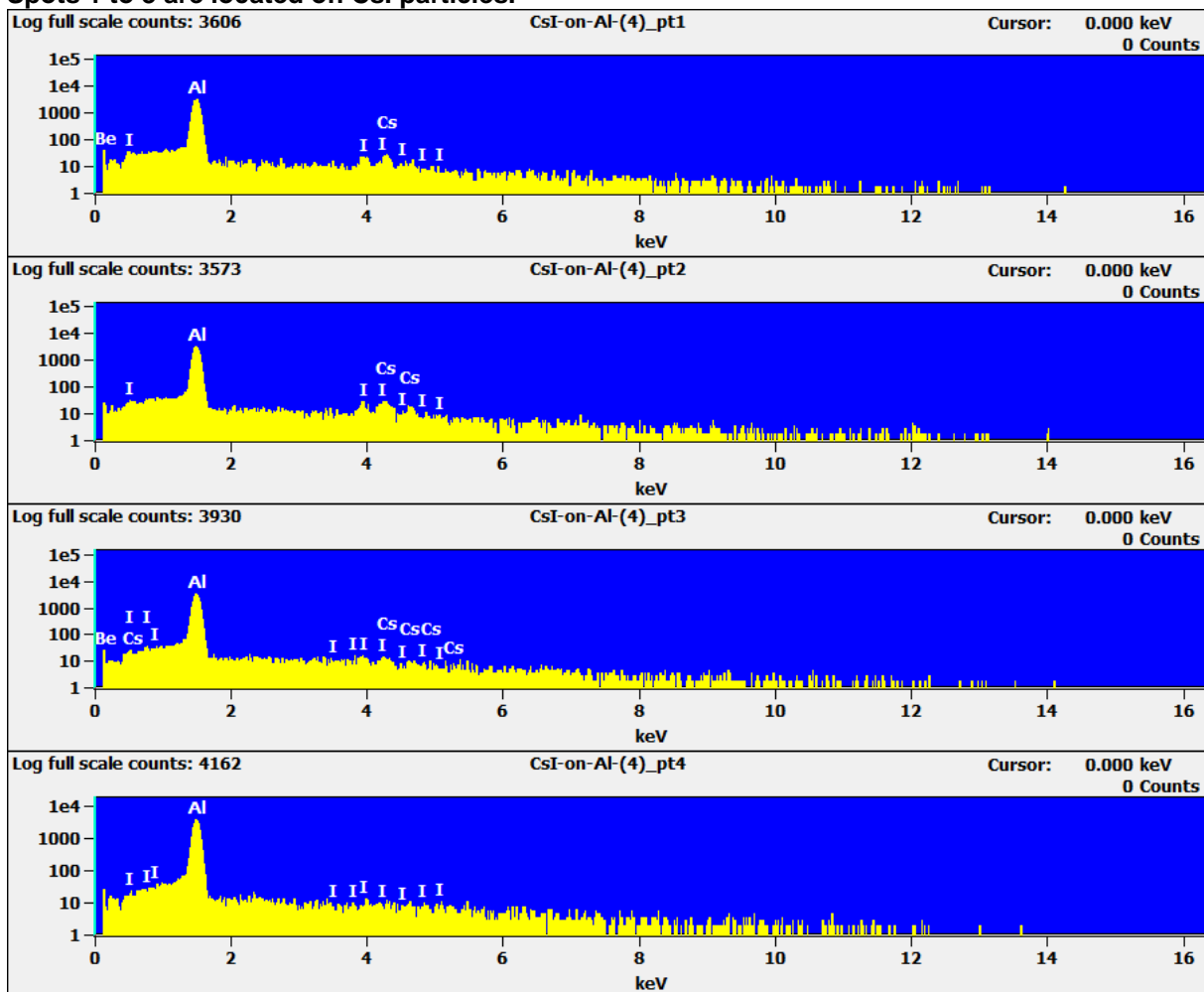
Figure 18. The EDX spectra of four locations on an aluminium surface (see Figure 16b). Spots 1 to 4 are located on CsI particles.
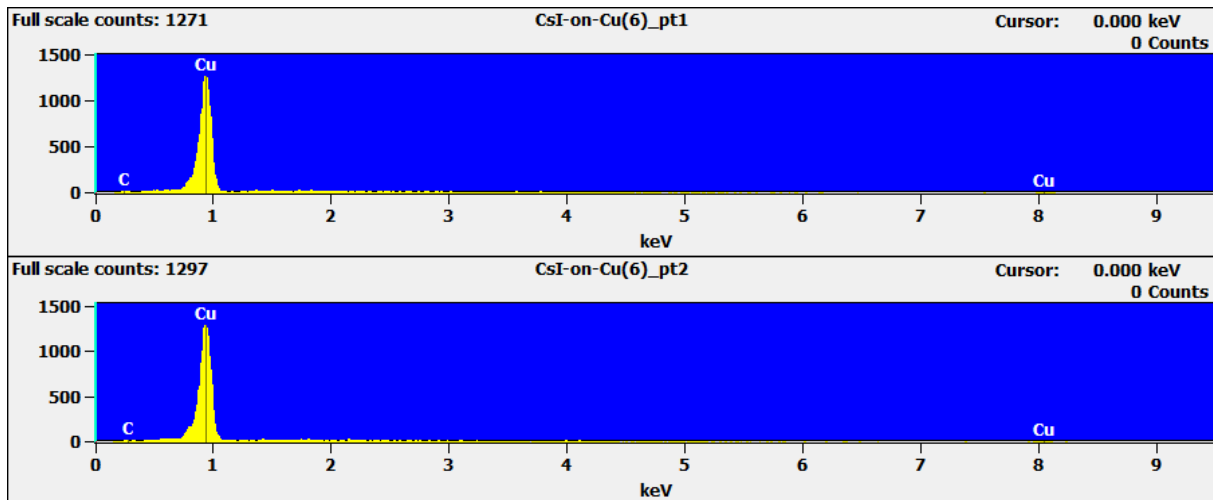
Figure 19. The EDX spectra of two locations on a copper surface (see Figure 16c). Spots 1 and 2 are located on CsI particles.
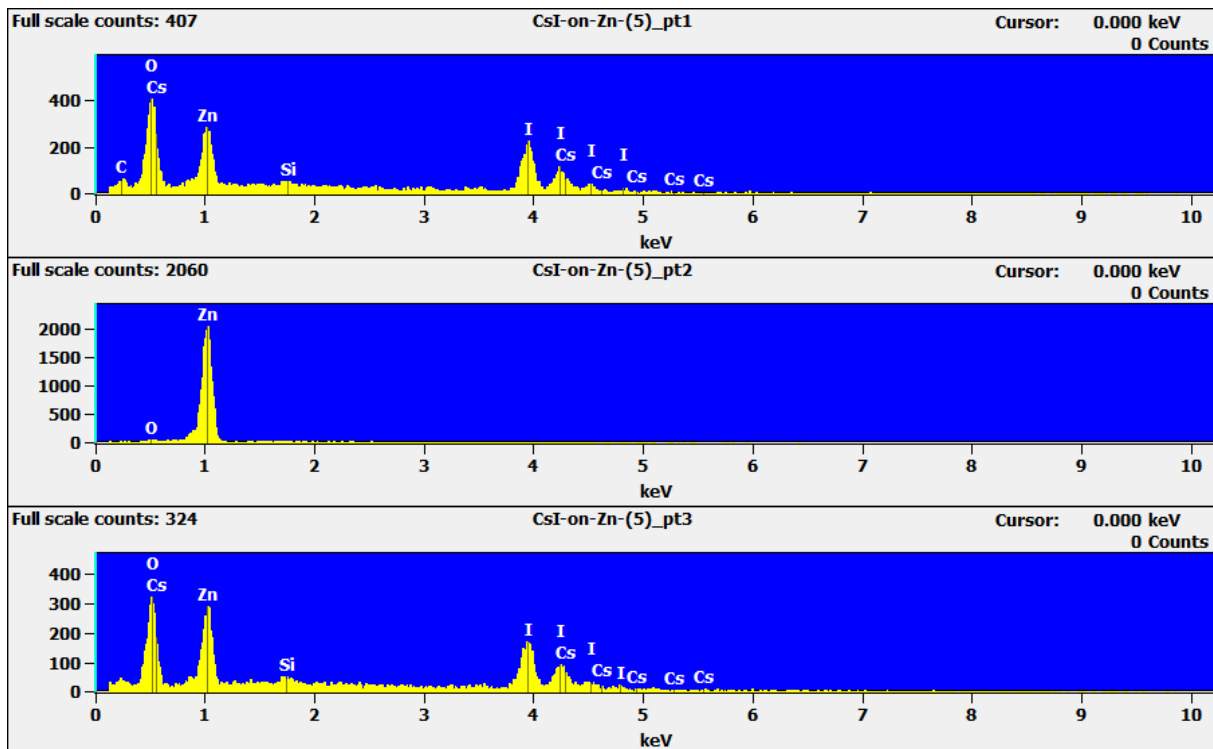
Figure 20. The EDX spectra of three locations on a zinc surface (see Figure 16d). Spots 1 and 3 are located on a CsI particle. Spot 2 is located on the zinc surface next to the CsI particle.

5.5.4 SEM-EDX analysis of IOx deposits on paint surfaces

SEM micrographs of IOx deposits on paint surfaces (samples 13A to 16A) which were pre-treated in different ways (no treatment, heat treatment, short gamma irradiation and heat treatment, long gamma irradiation – see chapter 4.5) are presented in Figure 21 together with the locations of EDX spot analysis. The corresponding EDX spectra are presented in Figures 22 to 25. It is very likely that the IOx particle deposits were dissolved by air humidity and spread on the surfaces before the SEM-EDX analysis. Therefore, iodine was observed here and there on the samples regardless of the pre-treatment procedure.
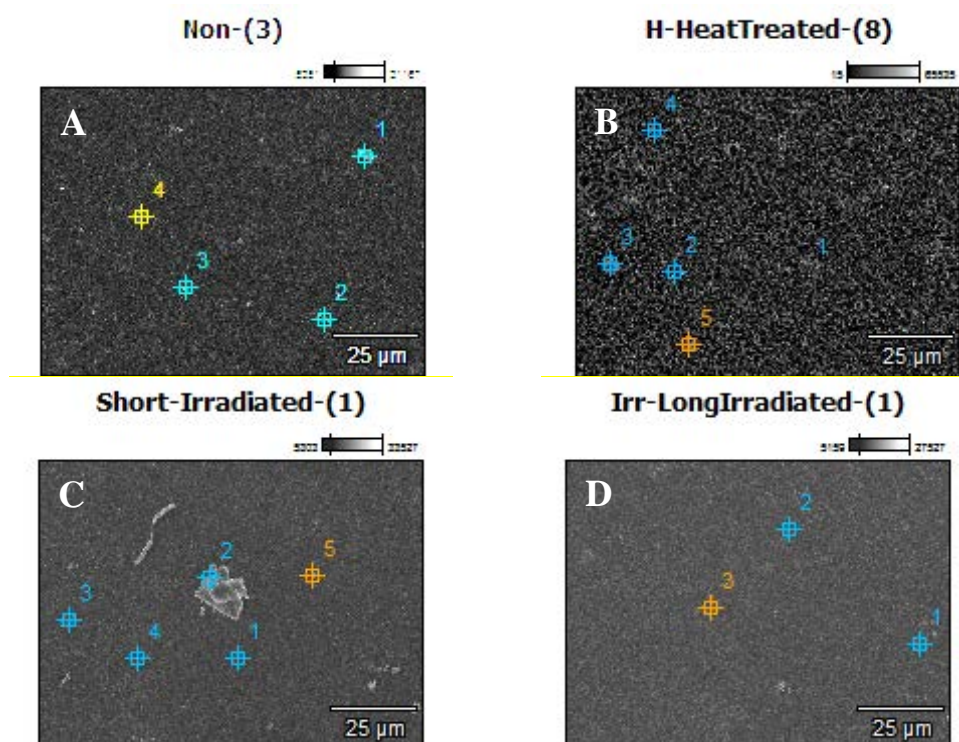
Figure 21. SEM micrographs of IOx deposits on painted surfaces which were pre-treated as follows a) no treatment, b) heat treatment, c) short gamma irradiation and heat treatment and d) long gamma irradiation. The EDX spot analysis locations on the samples are marked in the micrographs.
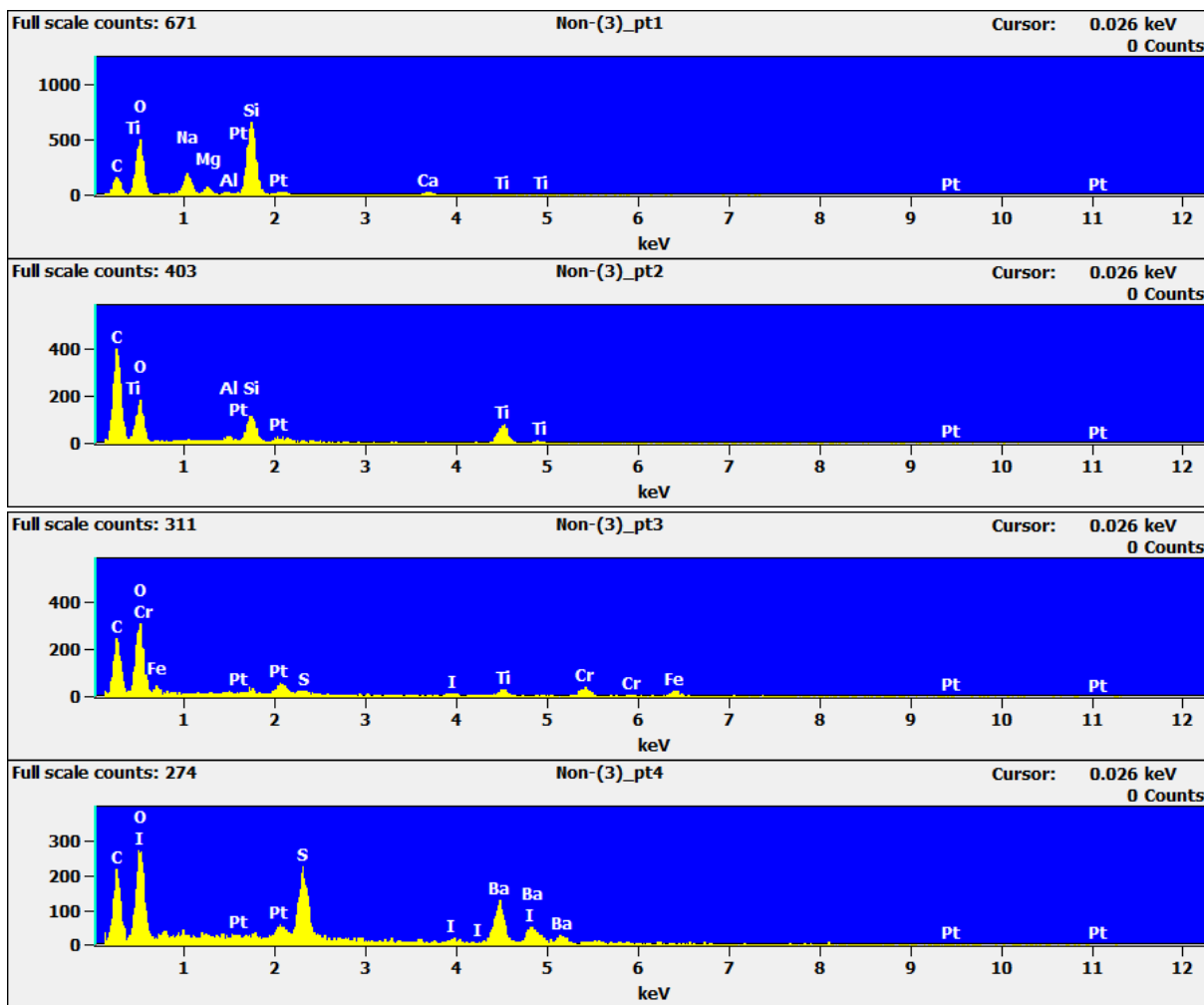
Figure 22. The EDX spectra of four locations on a non-treated paint surface (see Figure 21a). Spots are located on the area of IOx particle deposit.
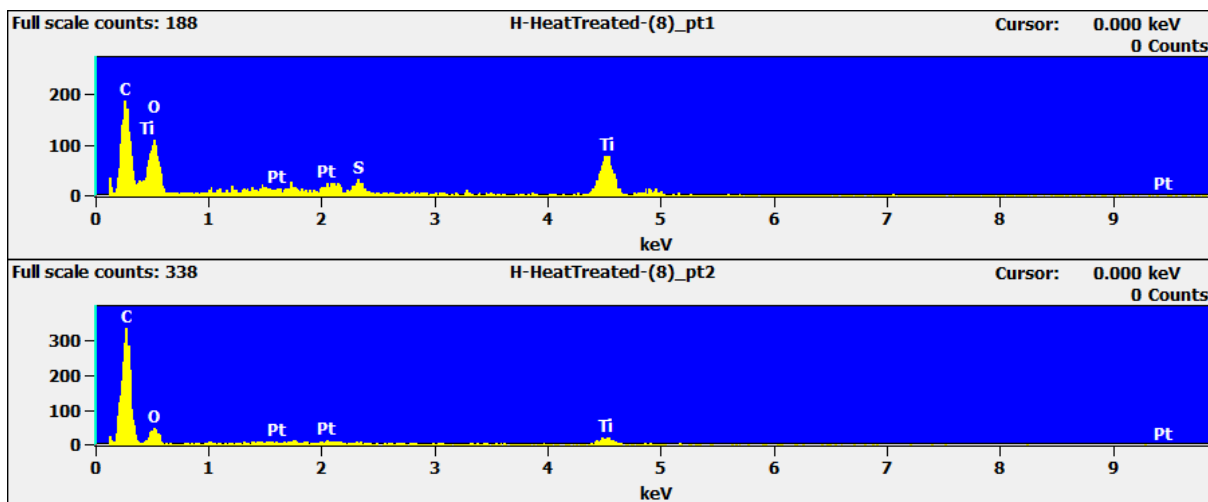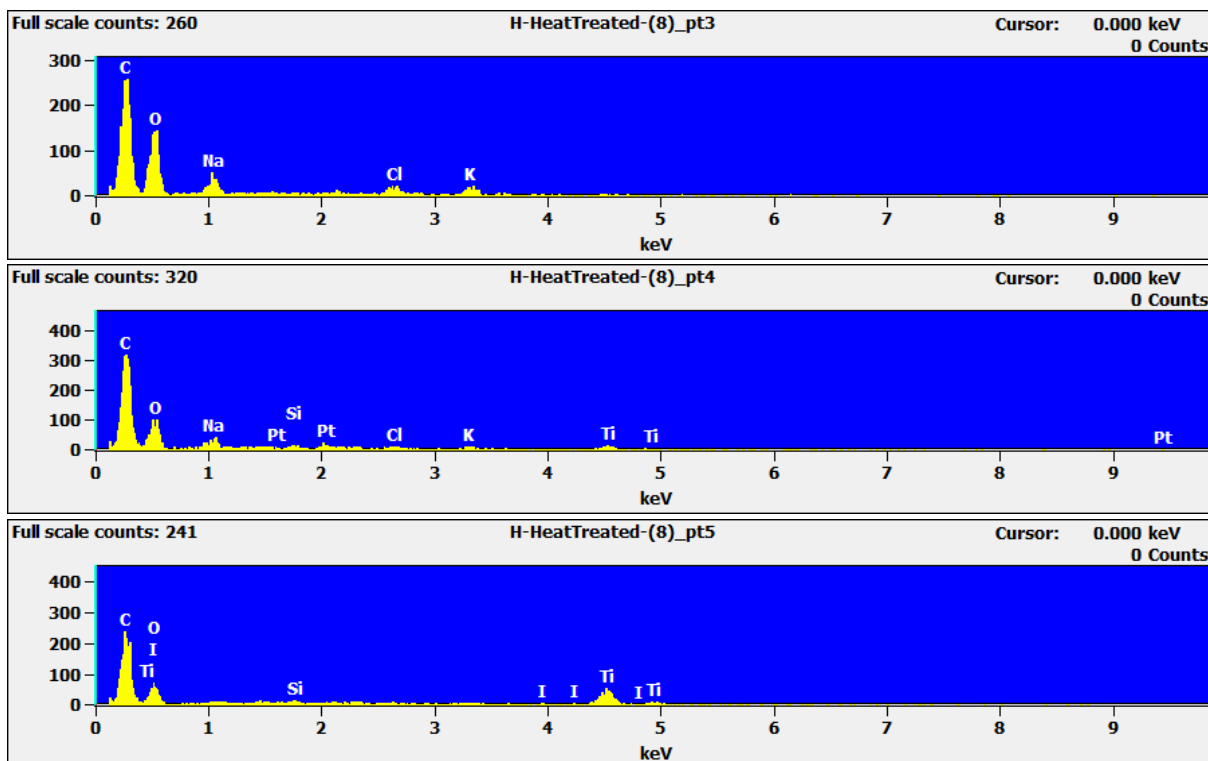
Figure 23. The EDX spectra of five locations on a heat treated paint surface (see Figure 21b). Spots are located on the area of IOx particle deposit.
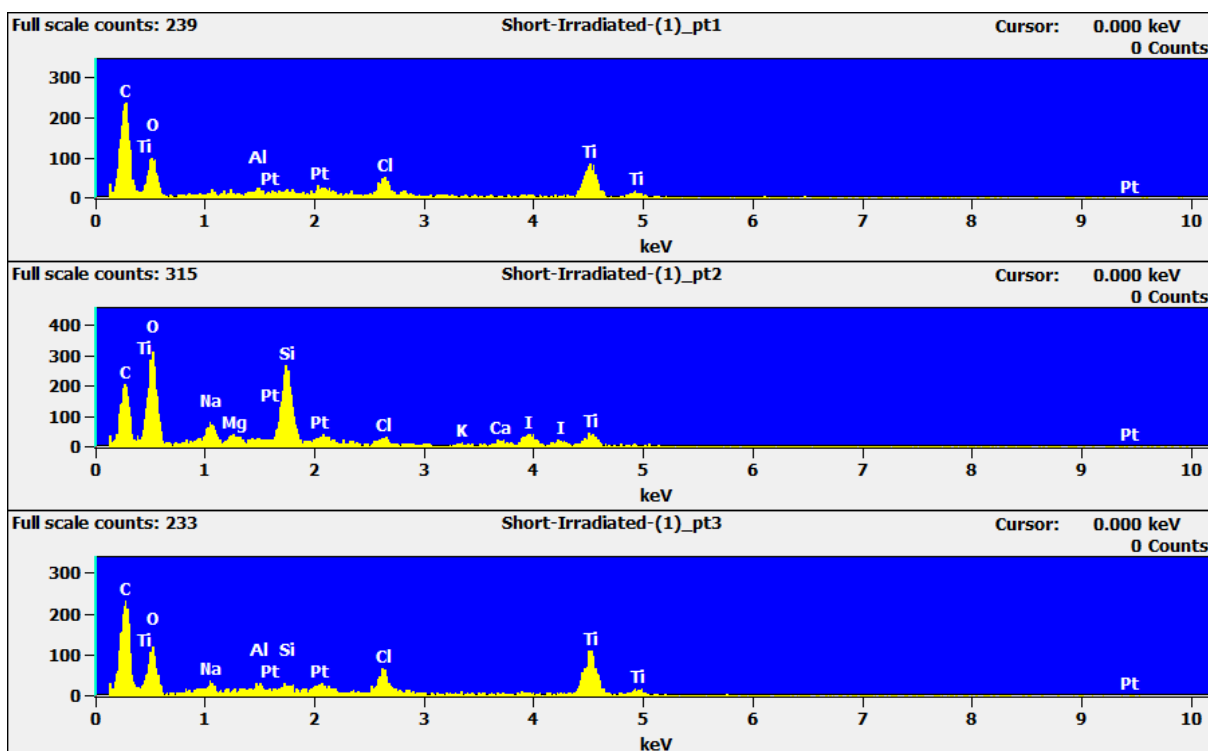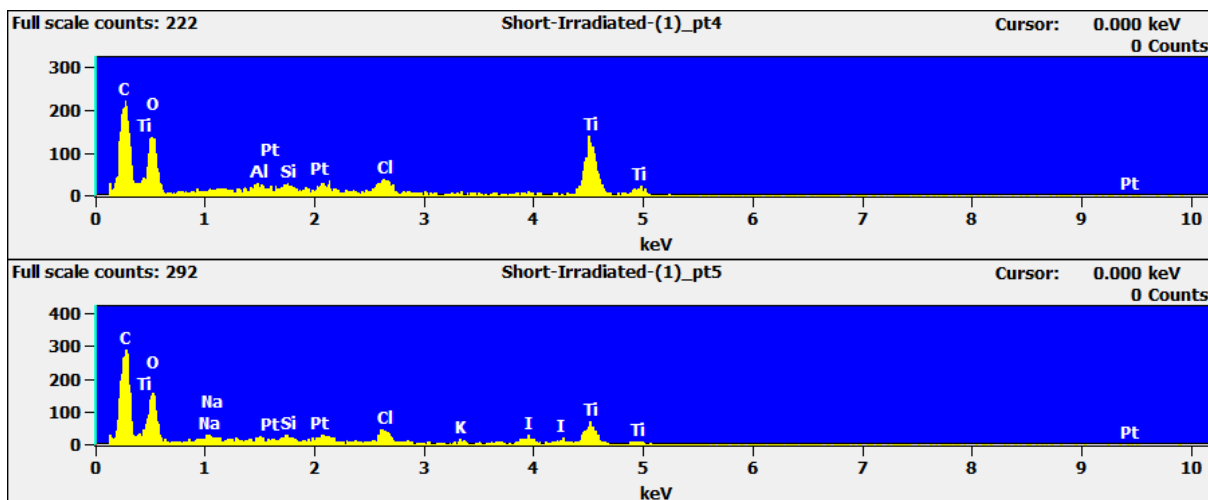
Figure 24. The EDX spectra of five locations on a paint surface which was pre-treated with short-term gamma irradiation and heat treatment (see Figure 21c). Spots are located on the area of IOx particle deposit.
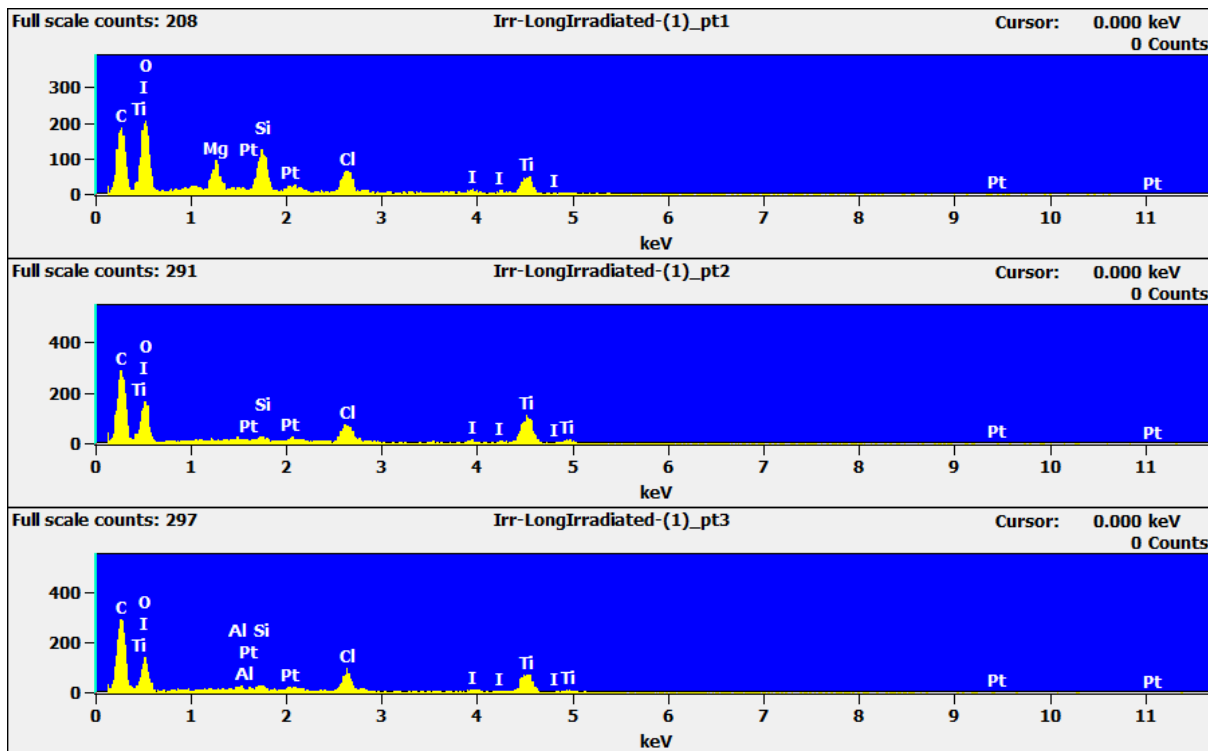
Figure 25. The EDX spectra of three locations on a paint surface which was pre-treated with long-term gamma irradiation (see Figure 21d). Spots are located on the area of IOx particle deposit.

5.5.5 SEM-EDX analysis of CsI deposits on paint surfaces

SEM micrographs of CsI deposits on paint surfaces (samples 17A to 20A) which were pre-treated in different ways (no treatment, heat treatment, short gamma irradiation and heat treatment, long gamma irradiation – see chapter 4.5) are presented in Figure 26 together with the locations EDX spot analysis. The corresponding EDX spectra are presented in Figures 27 to 30. Solid CsI particles were not observed on the studied surfaces regardless of the pre-treatment of surface. It seems that on the painted surfaces also CsI particles were dissolved in water (humidity of air) and spread outside the deposition area, since iodine and caesium were observed only in some EDX spot analyses (surface with no treatment and shortly gamma irradiated and heat treated surface).
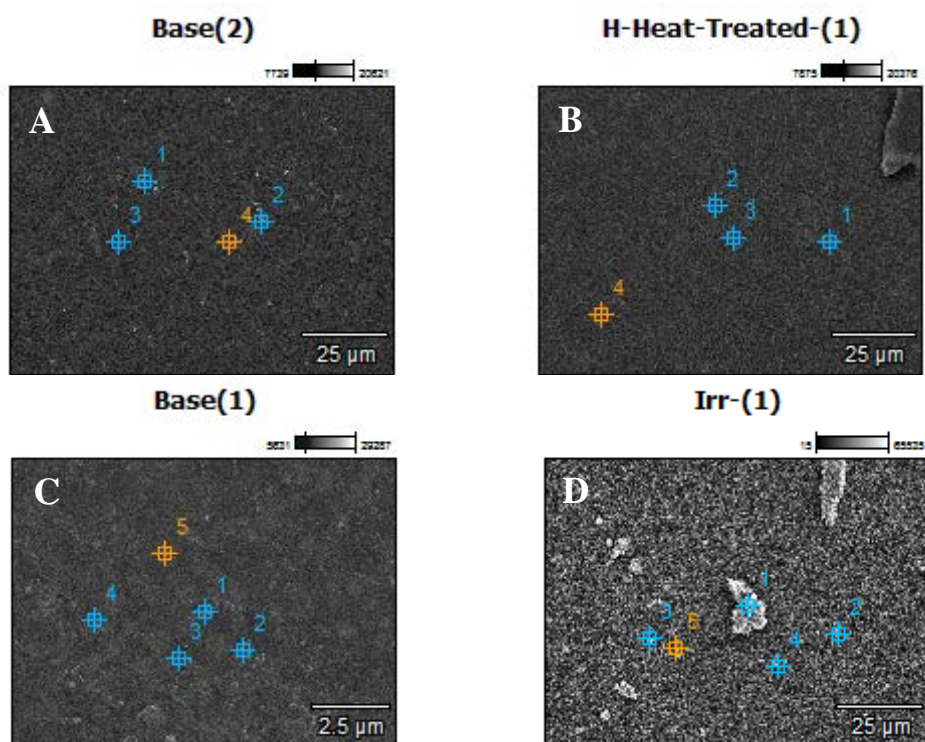

Figure 26. SEM micrographs of CsI deposits on painted surfaces which were pre-treated as follows a) no treatment, b) heat treatment, c) short gamma irradiation and heat treatment and d) long gamma irradiation. The EDX spot analysis locations on the samples are marked in the micrographs.
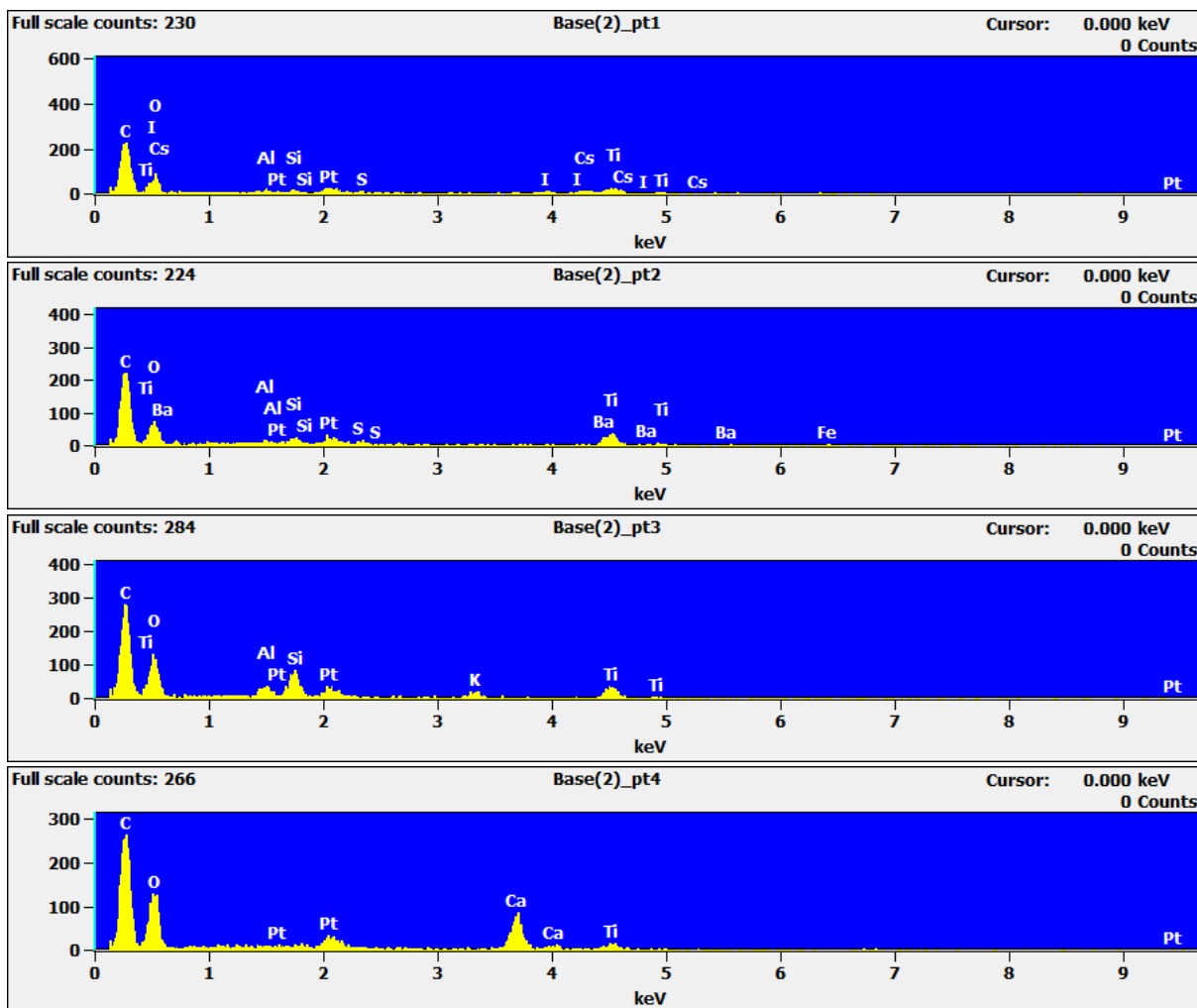
Figure 27. The EDX spectra of four locations on a non-treated paint surface (see Figure 26a). Spots are located on the area of CsI particle deposit.
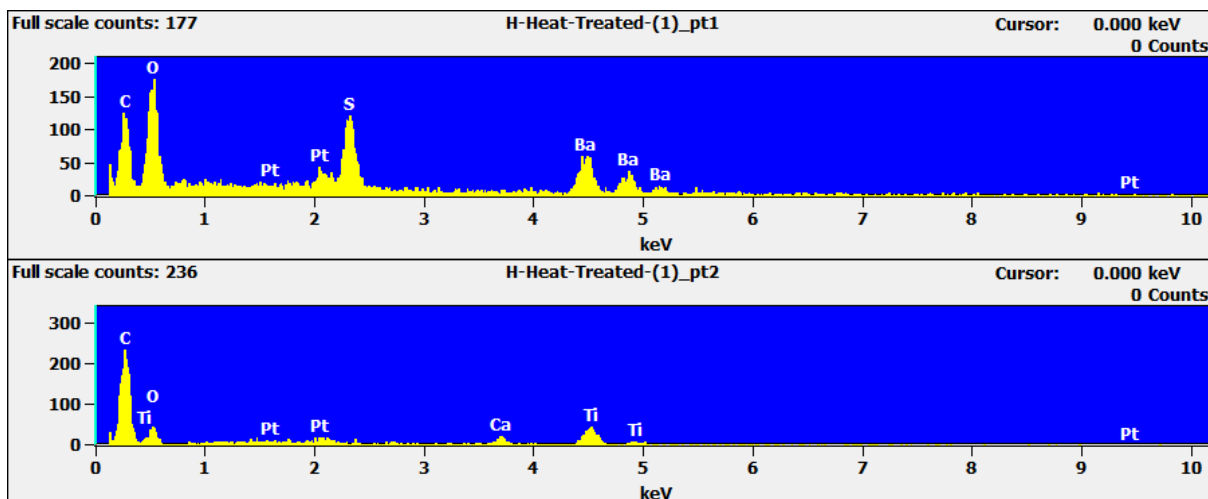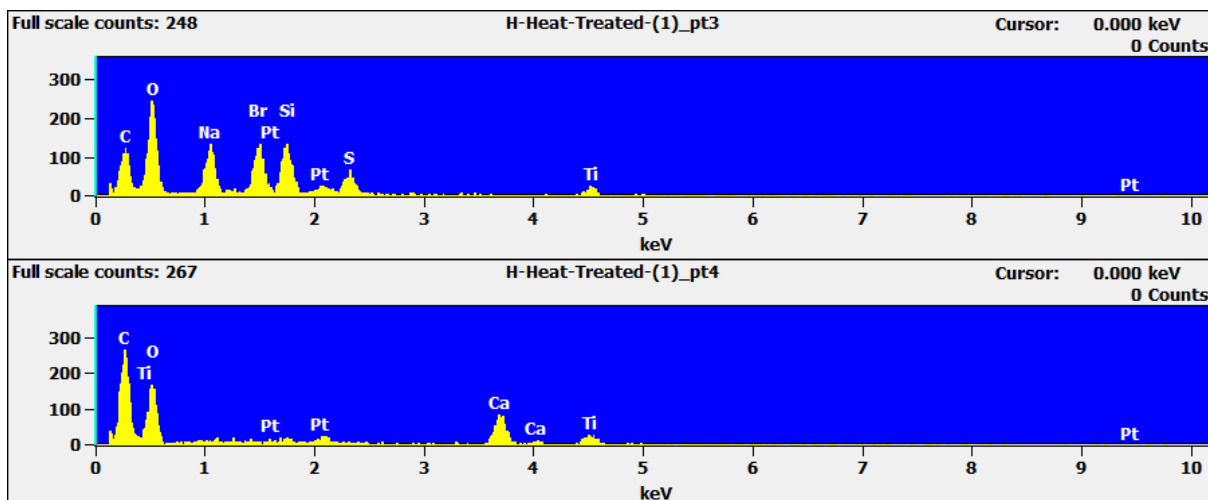
**Figure 28. The EDX spectra of four locations on a heat treated paint surface (see Figure 26b). Spots are located on the area of CsI particle deposit.**
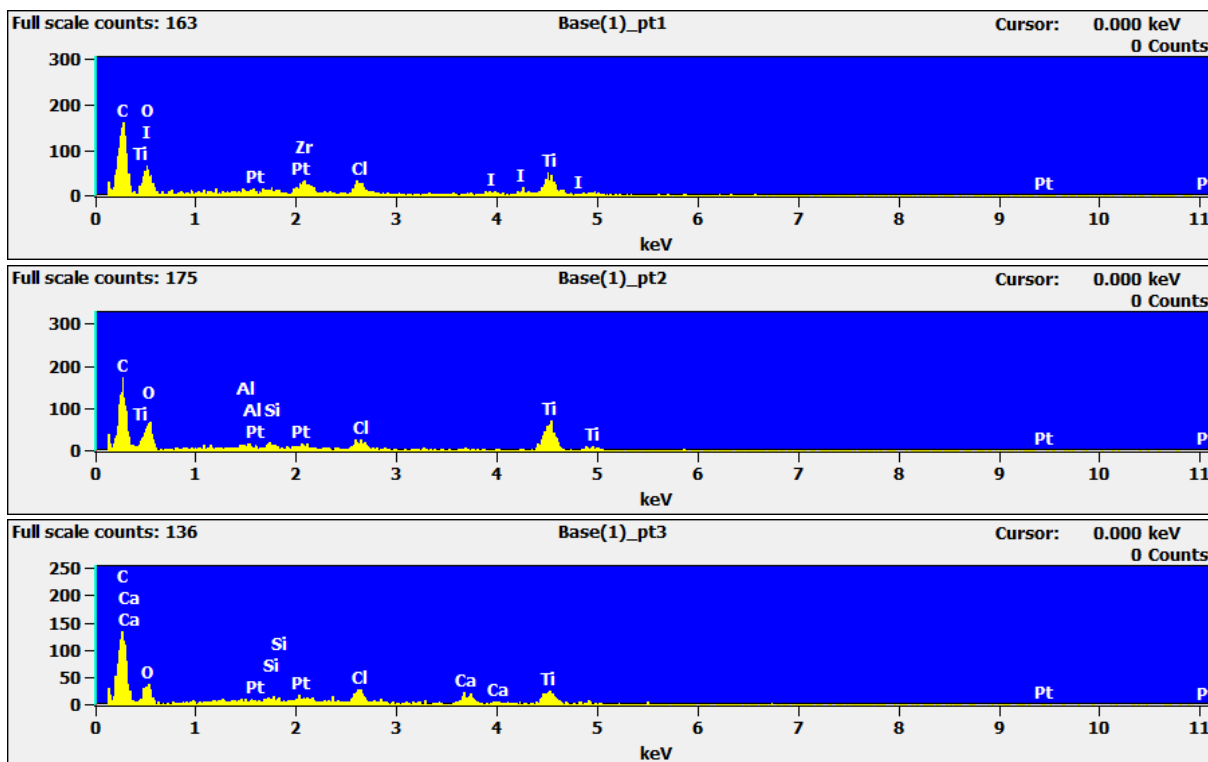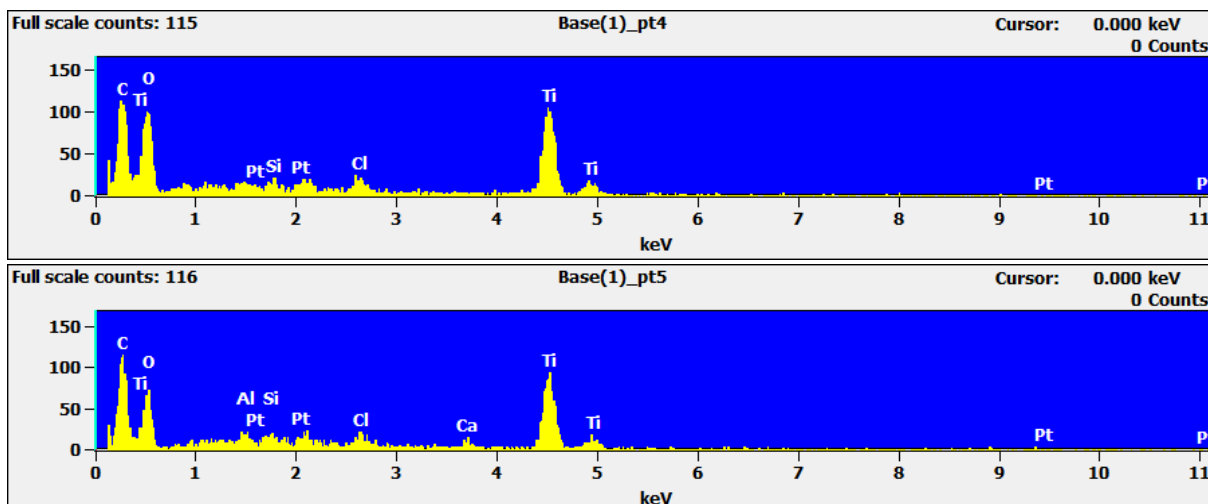
Figure 29. The EDX spectra of five locations on a paint surface which was pre-treated with short-term gamma irradiation and heat treatment (see Figure 26c). Spots are located on the area of CsI particle deposit.
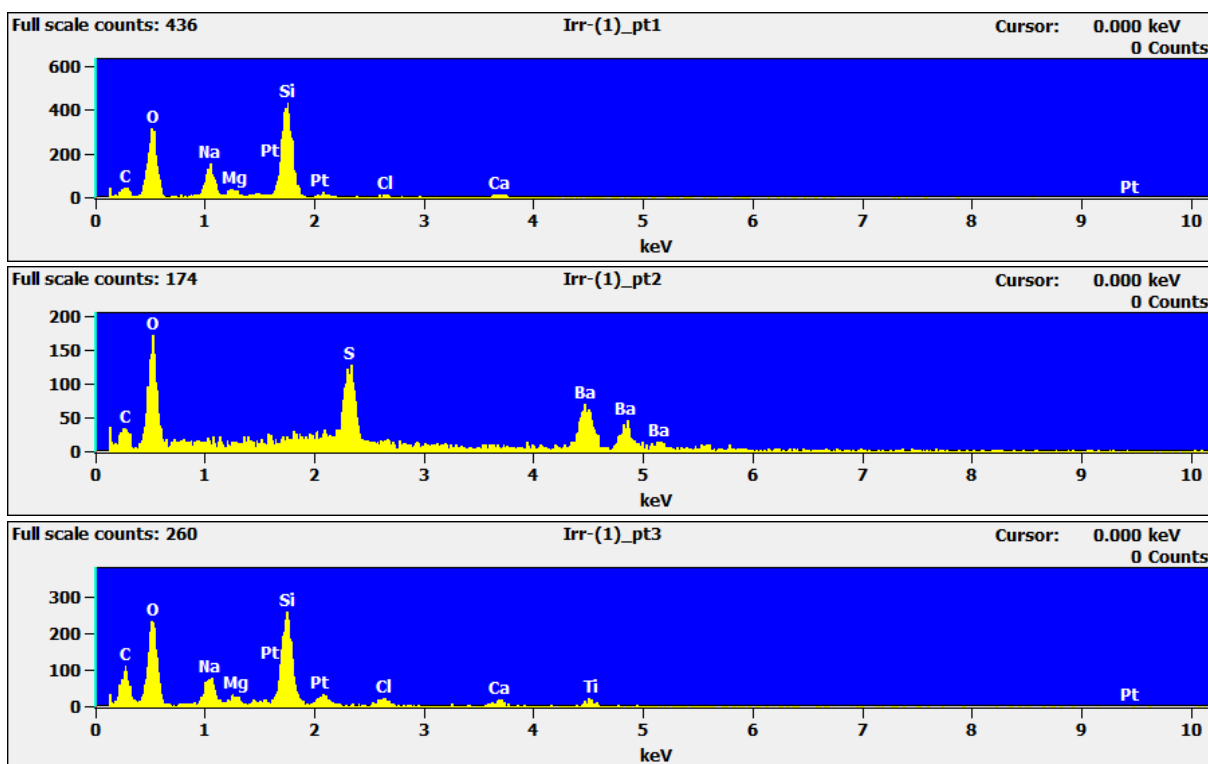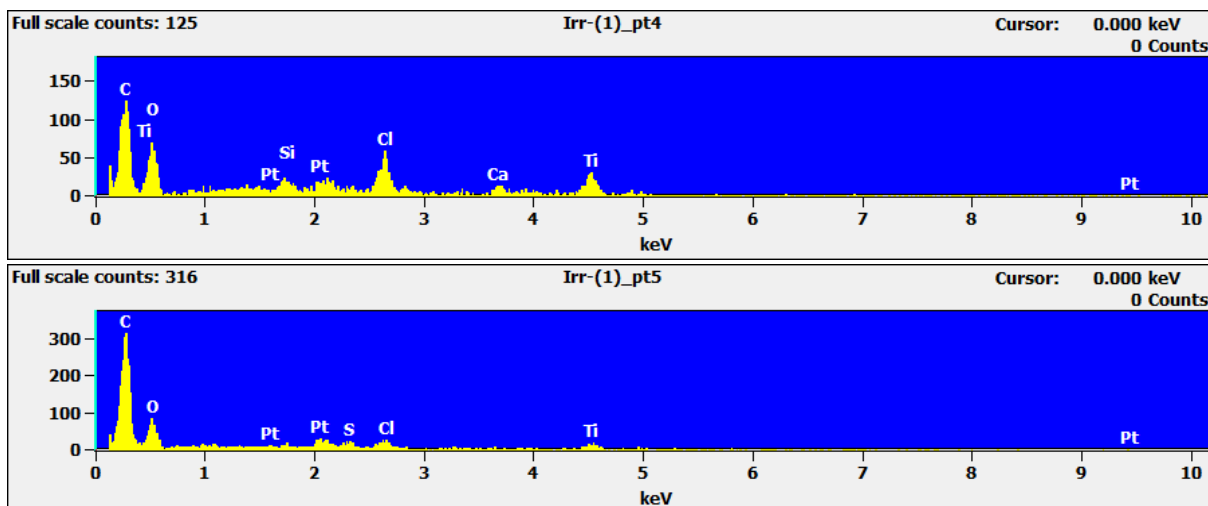
Figure 30. The EDX spectra of five locations on a paint surface which was pre-treated with long-term gamma irradiation (see Figure 26d). Spots are located on the area of CsI particle deposit.

II. Revaporisation studies

5.6 Distribution of the aerosols on the substrates after deposition

Within measurements with the autoradiograph in AIAS-1 it had been shown that the exposure was point-wise and in form of a thick multi-layer. The IOx deposits were visible by eye as a white-yellowish deposit on metal samples and up to brown ones on the paint samples. Exposure to heat, gamma irradiation and humidity caused the outer layer of the deposit to revaporise. The original main deposit was at any time visible. With the mono-layer exposure a non-visible and more even deposit was possible to realise. However, in both cases for both aerosols the iodine moved into the depths of the paint samples with time. With increasing treatment time the released amount of inorganic elemental iodine decreased while the detected activity of iodine on the sample surface and the total iodine activity decreased confirming a migration of the iodine in the depths of the paint film and chemical reactions of the iodine in the aeosol deposits with the organic paint solvents [6,19]. This is likely since even after a long time exposure to gamma irradiation an additional immersion of the samples in water/steam caused a further loss of activity from the paint. Extraction of the aqueous phase with octane showed that the majority of the iodine was found in the organic phase. This can be due to iodinated, water soluble benzyl alcohol. The activity on the surface was much lower after different treatment steps and higher exposure times of the measurement plate were necessary. Areas with a thicker deposit did not dilute out to an changed distribution (see Figure 31). The iodine migrated and revaporised evenly over the surface.
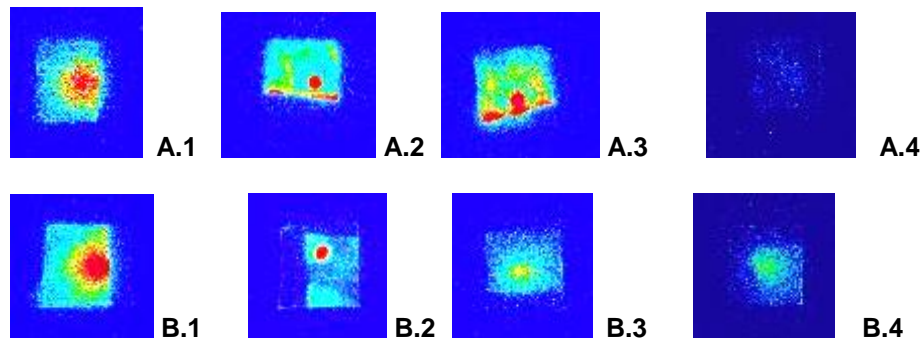
Figure 31: Distribution of I-131 on a paint surface before and after exposure to e.g. gamma irradiation
A.1 – IOx-Metal, A.2 – CsI-Metal, A.3 – Irr/heat IOx/CsI-Metal, A.4 – Steam/water IOx/CsI-Metal
B.1 – IOx-Paint, B.2 – CsI-Paint, B.3 – Irr/heat IOx/CsI-Paint, B.4 – Steam/water IOx/CsI-Paint

5.7 Revaporisation of CsI aerosols and IOx aerosols from metal and paint surfaces at room temperature (RT)

Tests on the volatility of the IOx and CsI aerosols under room temperature conditions (21.5 ± 1 °C) showed that both IOx and CsI aerosols revaporise from the substrates already at room temperature which is assumed to be physisorbed and not chemically converted iodine from the deposits.

The revaporisation rate of iodine from IOx deposits from the long time heat treated paint sample was highest in comparison to the non-aged sample (see Figure 32). The sample which was pre-treated shortly with heat and irradiation showed a similar revaporisation rate as the low irradiated sample.
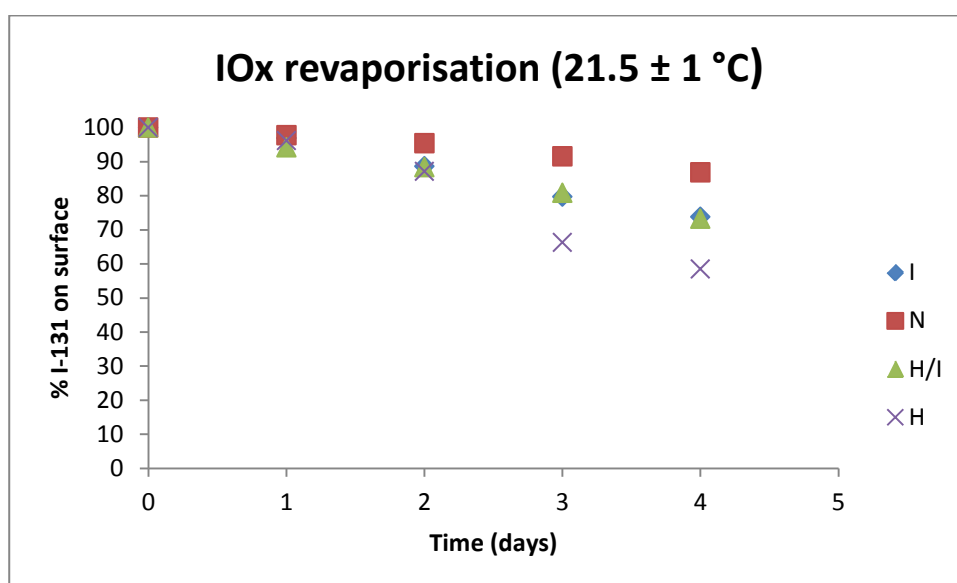
Figure 32: Revaporisation of ^{131}I from IOx deposits from paint substrates at RT

The revaporisation of IOx aersols from the metal surfaces was slowest from Cu and Zn, while the larger but similar losses were measured from Al and SS surfaces (see Figure 33).
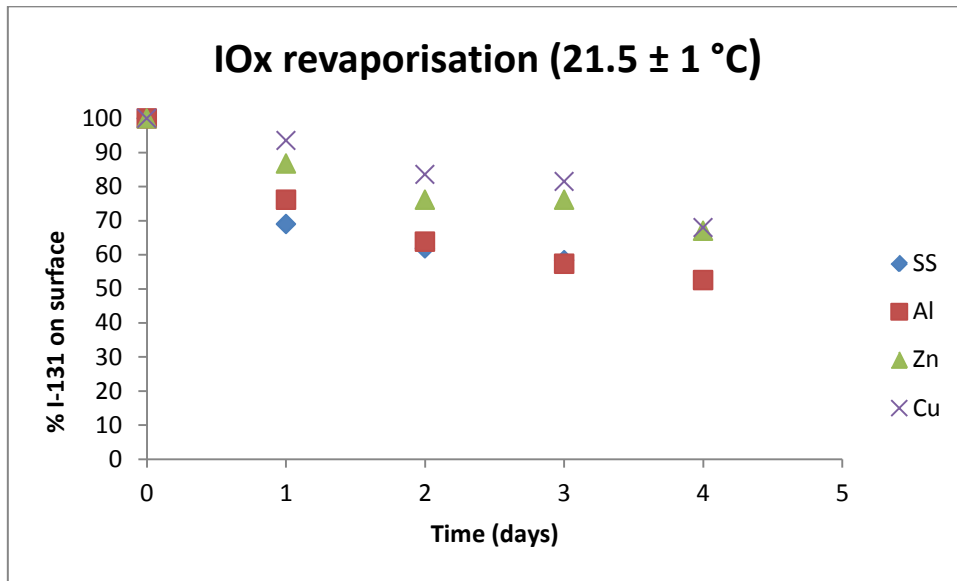
Figure 33: Revaporisation of ^{131}I from IOx deposits on metal substrates at RT

The revaporisation of CsI aerosols from the metal surfaces was similar on all substrates. The same tendencies as for the IOx revaporisation apply. From Cu and Zn the iodine release is lower while from SS it is higher (see Figure 34).
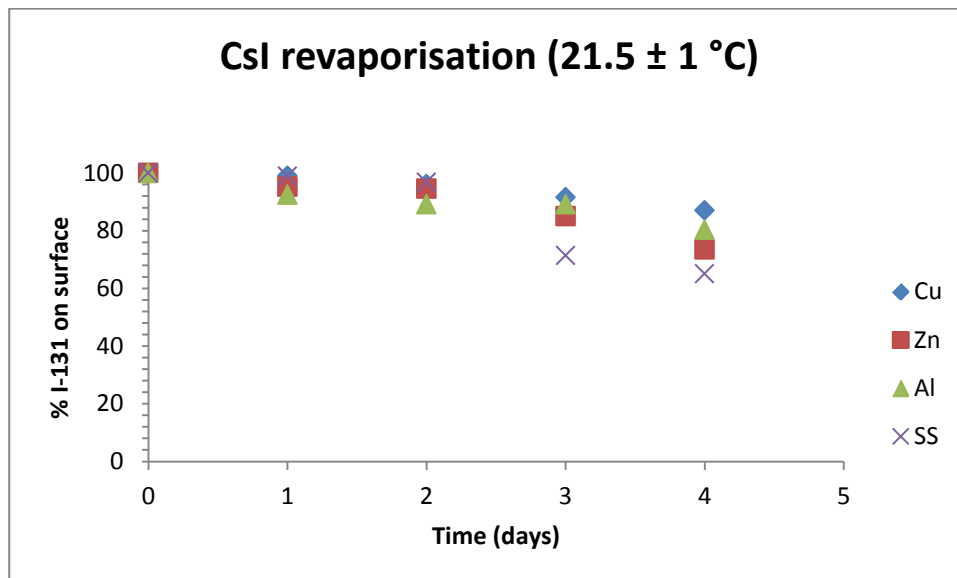
Figure 34: Revaporisation of ^{131}I from CsI deposits on metal substrates at RT

On the paint surfaces a slightly higher revaporisation was detected on the long time heat treated sample in comparison to the other aged samples (see Figure 35). The chemical uptake of the iodine into the paint seems to be faster in the non-aged paint.
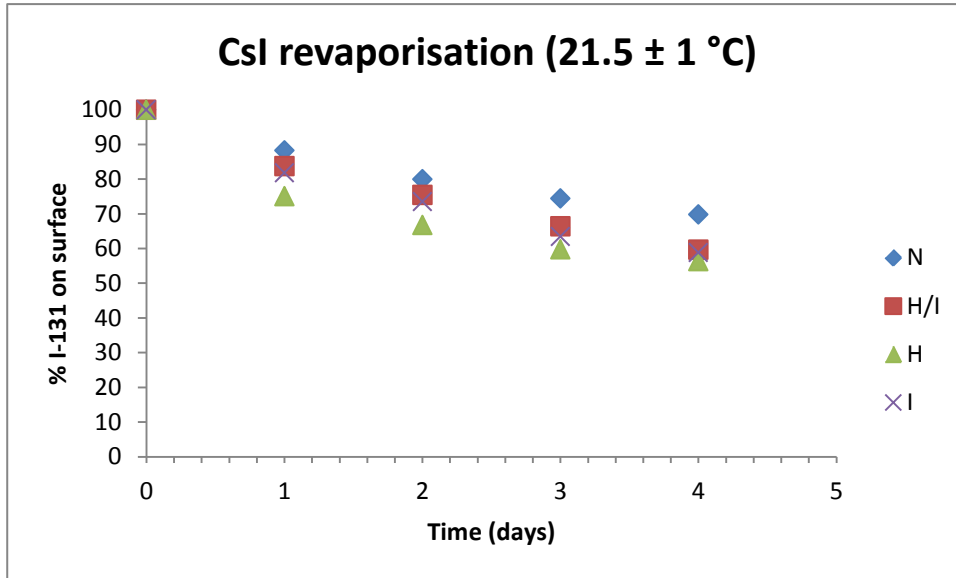
Figure 35: Revaporisation of ^{131}I from CsI deposits on paint substrates at RT

5.8 Revaporisation of CsI aerosols and IOx aerosols from metal and paint surfaces at 50 °C

The revaporisation of iodine from deposited IOx aerosols was highest from SS and lowest from Cu (see Figure 36). The same result was found for CsI deposits (see Figure 37). The revaporisation of the aerosols on the metals was found to be similar.
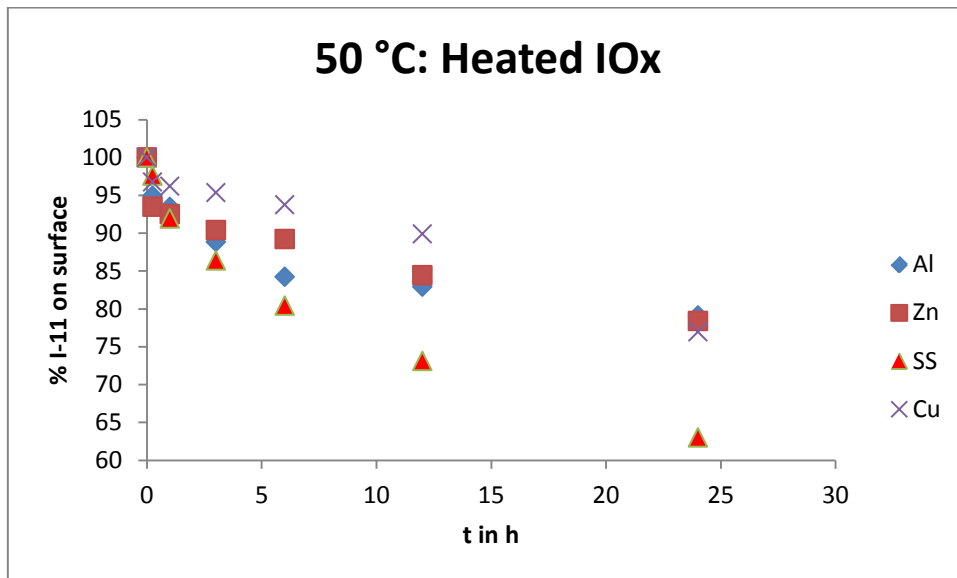
Figure 36: Revaporisation of ^{131}I from IOx deposits on metal substrates at 50 °C
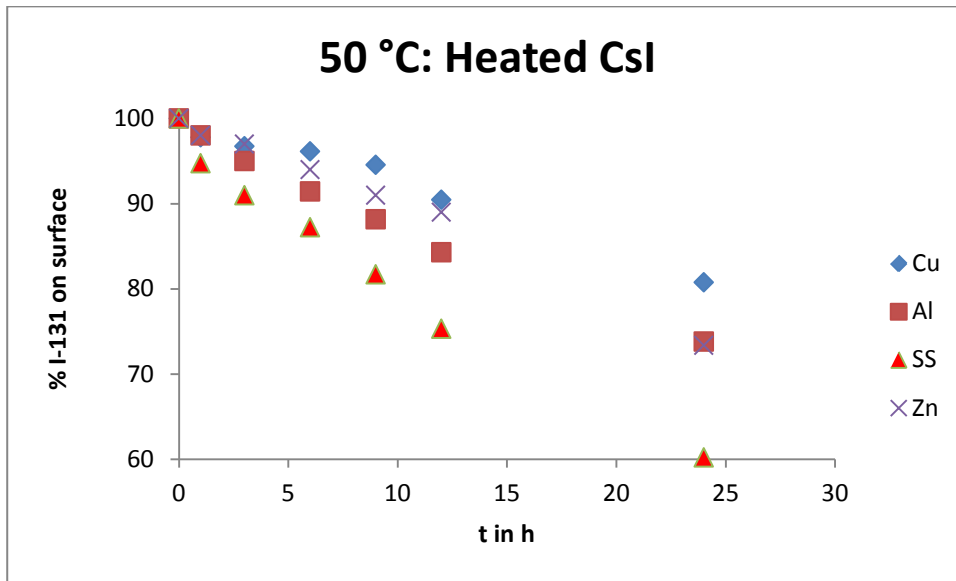
Figure 37: Revaporisation of ^{131}I from CsI deposits on metal substrates at 50 °C

From the paint surfaces exposed to IOx and CsI the release was highest from the heat treated paint film (see Figure 38). The increased temperature caused an increased release from the non-aged paint film due to vaporisation of paint solvents which are most likely to react with the iodine [6, 19]. The revaporisation was higher on CsI exposed samples than on IOx exposed ones. The CsI long-time pre-irradiated samples showed similar high re-release as the long-time heat-treated samples (see Figure 39).
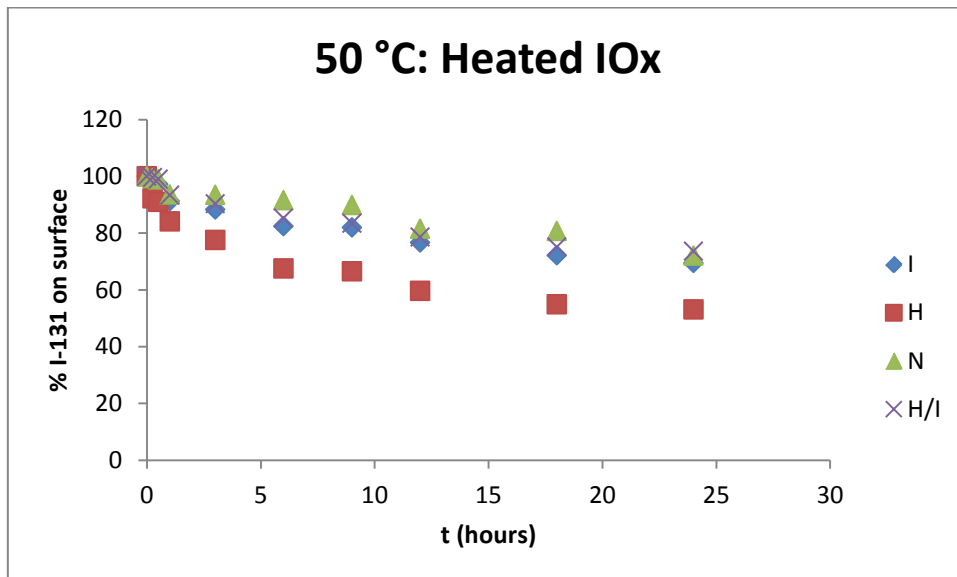
Figure 38: Revaporisation of ^{131}I from IOx deposits on paint substrates at 50 °C
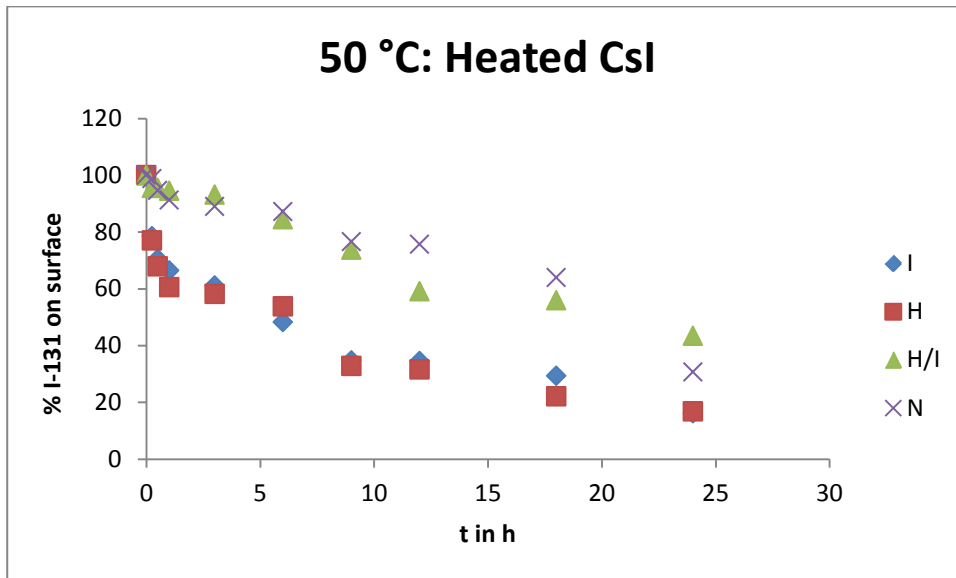
Figure 39: Revaporisation of ^{131}I from CsI deposits on paint substrates at 50 °C

5.9 Revaporisation of CsI aerosols and IOx aerosols from metal and paint surfaces at 150 °C

While it is difficult to distinguish significant differences in the revaporisation rate of IOx aerosols at 150 °C (see Figure 40), for the revaporisation of the CsI aerosols it is clearly visible that the revaporisation is lowest from the Cu surface (see Figure 41). This suggests that Cu reacted chemically more with the iodine from CsI than from the IOx aerosols.
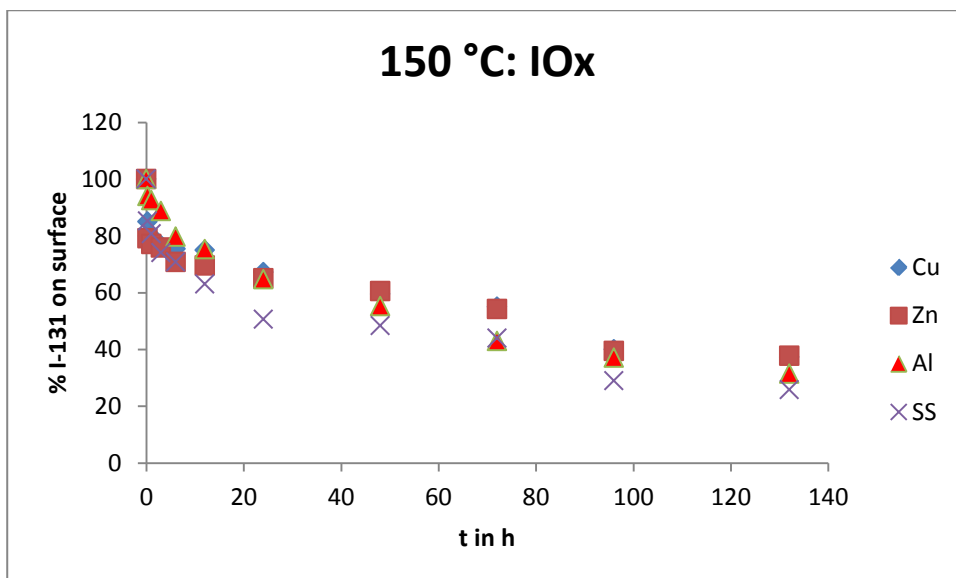
Figure 40: Revaporisation of ^{131}I from IOx deposits on metal substrates at 150 °C
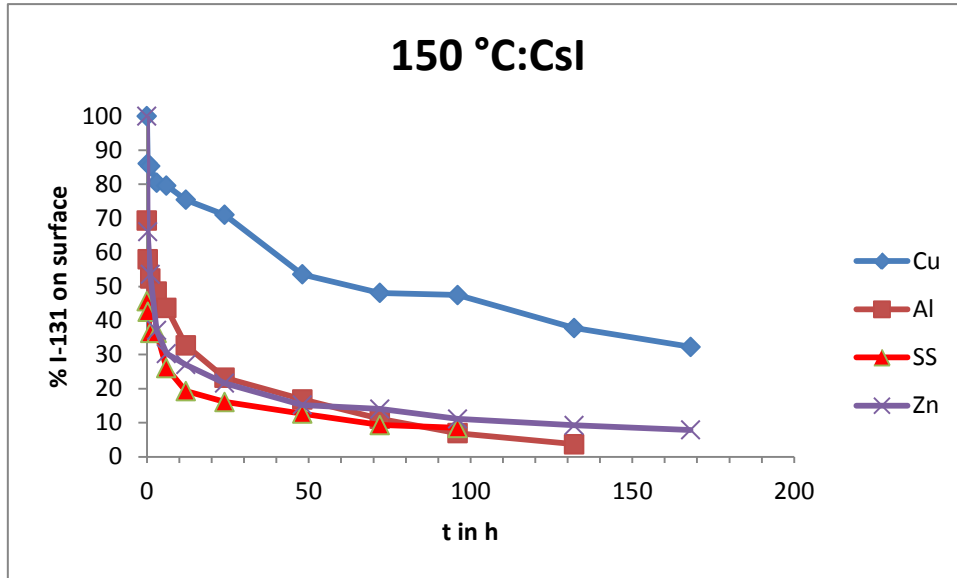
Figure 41: Revaporisation of ^{131}I from CsI deposits on metal substrates at 150 °C

On the paint samples the revaporisation behaviour of the differently pre-treated paint films varies less (see Figure 42, Figure 43). A much higher release from the short time heat and irradiation and non-treated samples occurs. Due to the time gap of several days between production and treatment of the samples after exposure iodine migrated in the depth of the paint films and had time to as well chemically react with paint ingredients. At rather low temperatures the vapour pressure of the mainly paint solvents in which the iodine species are most likely to be found is rather low, while at elevated temperatures closer to the boiling points of the longer chained paint solvents such as benzyl alcohol the revaporisation is much higher and thus as well the release of iodine wheather it is chemically converted or not. This could also be confirmed with the more strong smell of released organic materials at this temperature. More of the I-131 of original IOx was released than of CsI suggesting a higher reactivity of the iodine from the CsI particles.
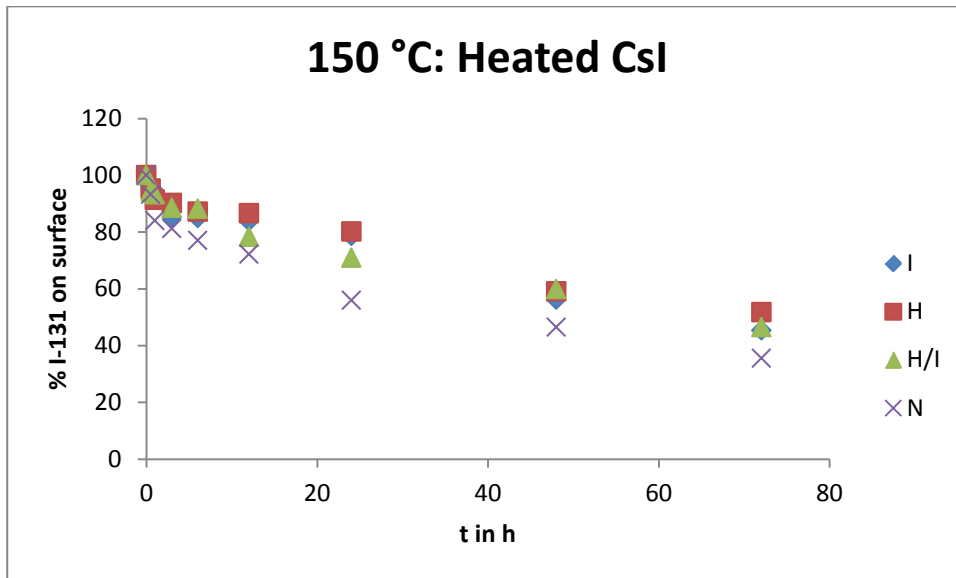
Figure 42: Revaporisation of ^{131}I from CsI deposits from paint films at 150 °C
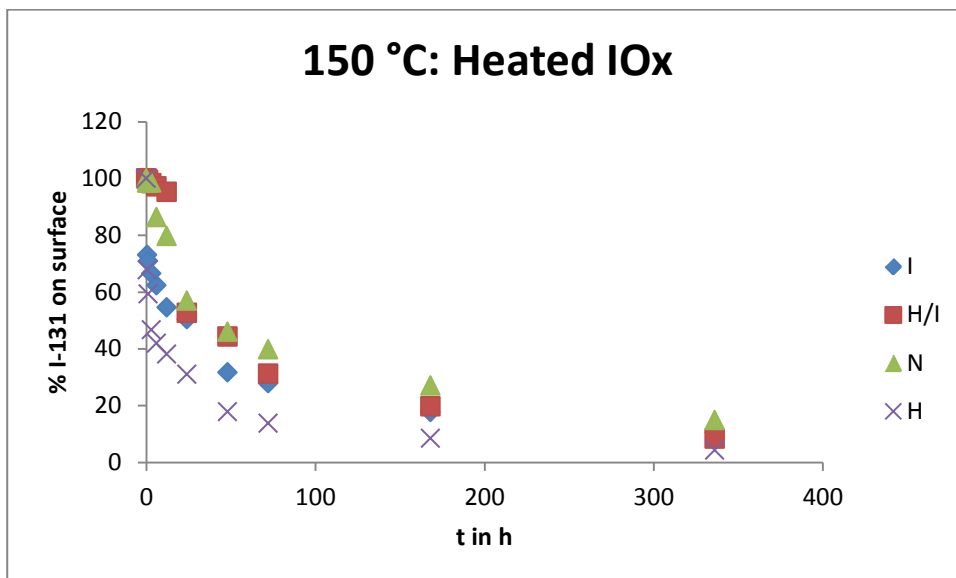
Figure 43: Revaporisation of ^{131}I from IOx deposits from paint films at 150 °C

5.10 Revaporisation of CsI aerosols and IOx aerosols induced by gamma irradiation (50 °C)

The revaporisation studies under gamma irradiation from the metal surfaces show the same result as the temperature studies. While the revaporisation behaviour of Zn and Al is similar, the revaporisation on SS is highest, the revaporisation is significant lower on the Cu surface (see Figure 44).
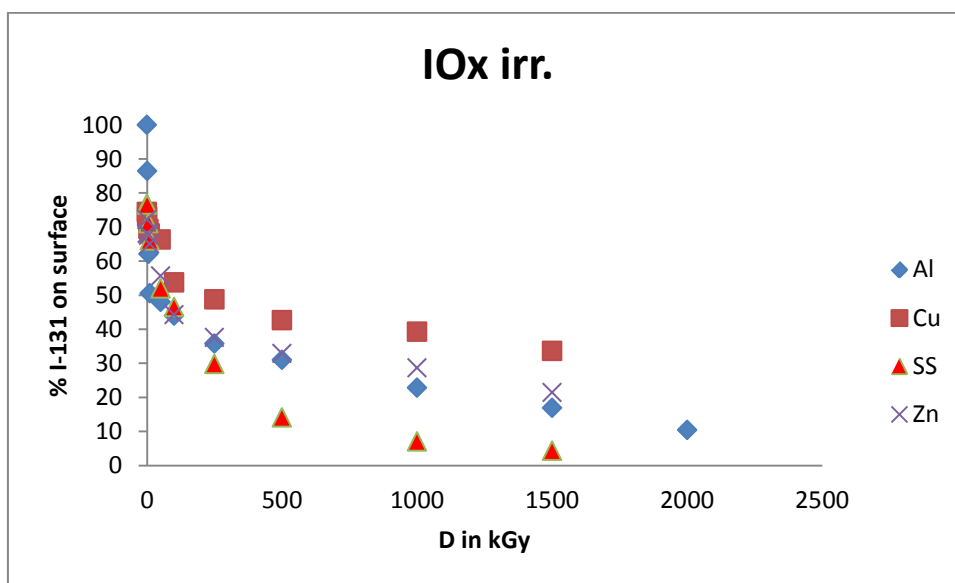
Figure 44: Revaporisation of ^{131}I from IOx deposits on metal substrates under gamma irradiation with a dose rate of 14 kGy/h (50 °C)

The differences in the revaporisation behavior in presence of gamma radiation for Al, Cu and SS become less while the amount of sorbed iodine on the Cu surfaces is significant higher indicating a significant formation of copper iodide (see Figure 45).
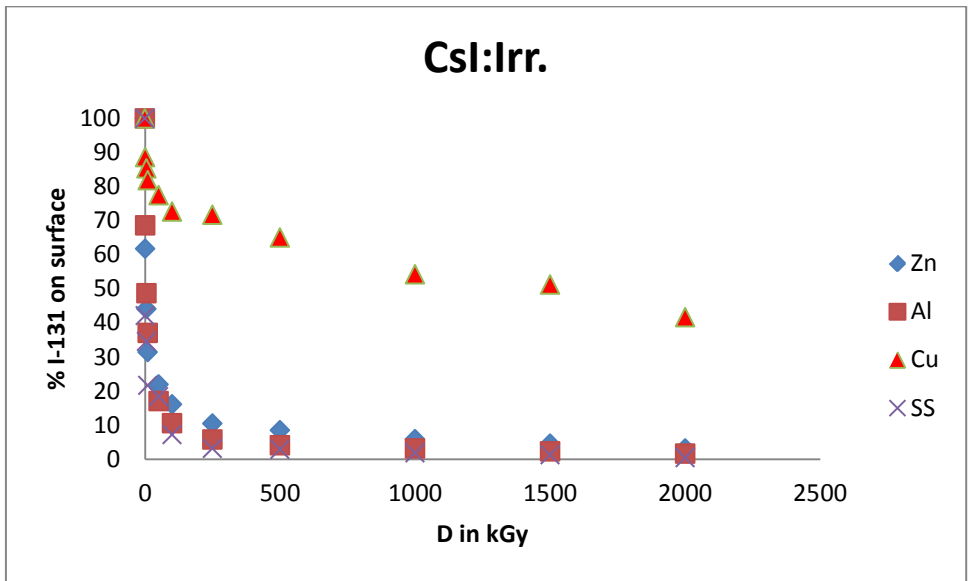
Figure 45: Revaporisation of ^{131}**I from CsI deposits on metal substrates under gamma irradiation with a dose rate of 14 kGy/h (50 °C)**

From the paint samples the revaporisation of IOx was significant lower from the fresh paint film (see Figure 46) and was highest from the heat treated samples.
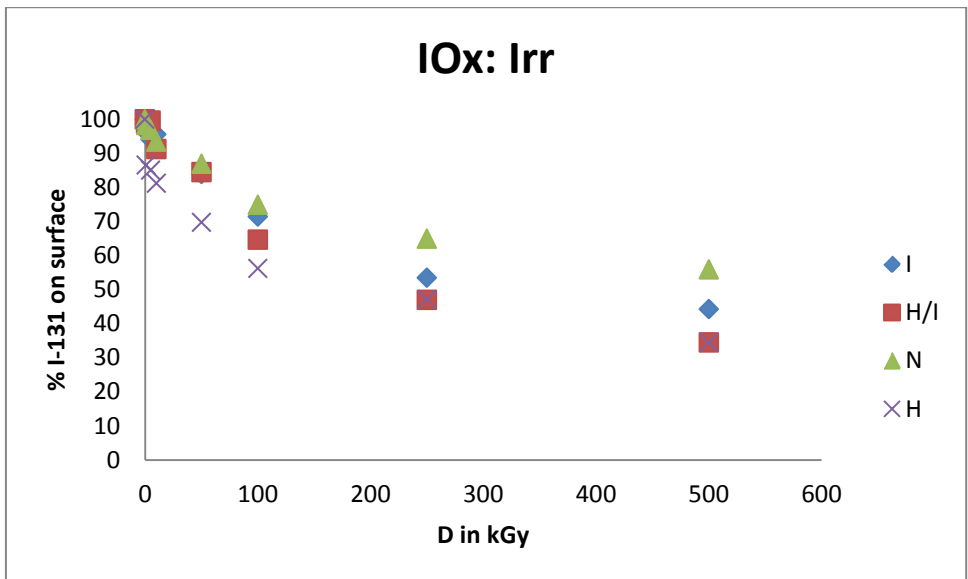
Figure 46: Revaporisation of ^{131}**I from IOx deposits on paint substrates under gamma irradiation with a dose rate of 14 kGy/h (50 °C)**

The differences between the differently aged paint films in the revaporisation are smaller for CsI deposits (see Figure 47). However, the long-time heat treated paint film showed to be less able to chemically sorb iodine.
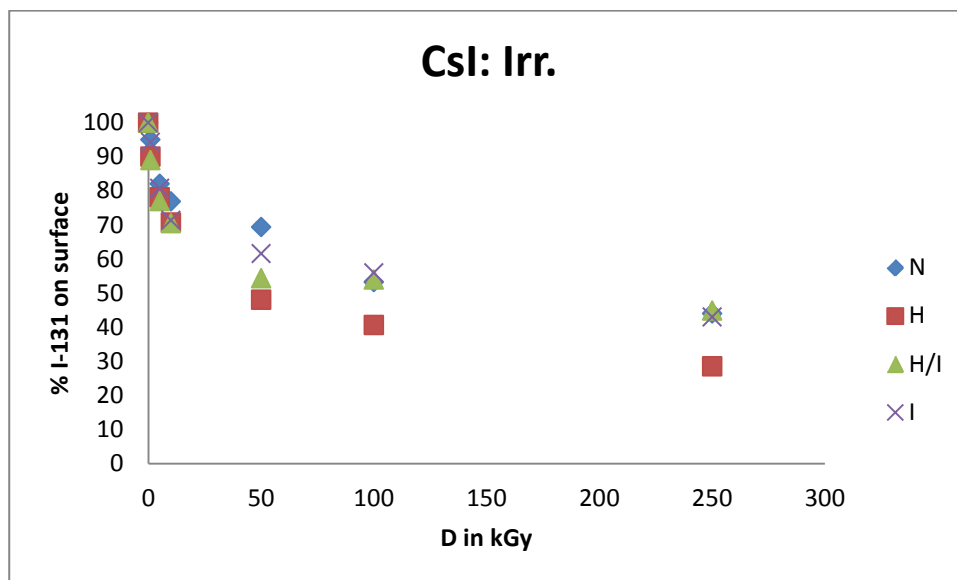
Figure 47: Revaporisation of ^{131}I from Cs deposits on paint substrates under gamma irradiation with a dose rate of 14 kGy/h (50 °C)

5.11 Desorption studies on IOx and CsI aerosols in humid air and water

Most of the ^{131}I activity on the surfaces of the to the accident conditions exposed metal surfaces washed off immediately in contact with cold water. Some remaining activity washed off within 5 min in 50 °C water from zinc surfaces. On copper surfaces the majority of the activity remained even after 24 h (app. 30 % less) heating the aqueous phase to about 50 °C and later on until boiling indicating the chemical bond of iodine as cupper iodide.

Other than on the metal surfaces from the paint films far lower amounts of the activity washed off in hot humid air and water indicating the migration of the species in the depths of the paint films and chemically conversion into less water-soluble iodine species. While up to 62 - 88 % were washed off in steam, about 5 - 25 % additional activity were washed out by direct immersion of the paint films into water. The maximum wash out was 97 % for the long time heat treated paint which contained the lowest amount of organic solvents and thus has the lowest retain ability for iodine species.

Solvent extraction of the leaching water of exposed paint films that had been heat treated and irradiation treated is in form of organic iodides. Even after 4 weeks of leaching still I-131 could be detected in the paint film.

5.12   Decomposition of IOx aerosols with CO

The revaporisation rate from a Teflon filter with IOx aerosols deposited on was significantly increased when exposing the filter to CO (see Figure 48).
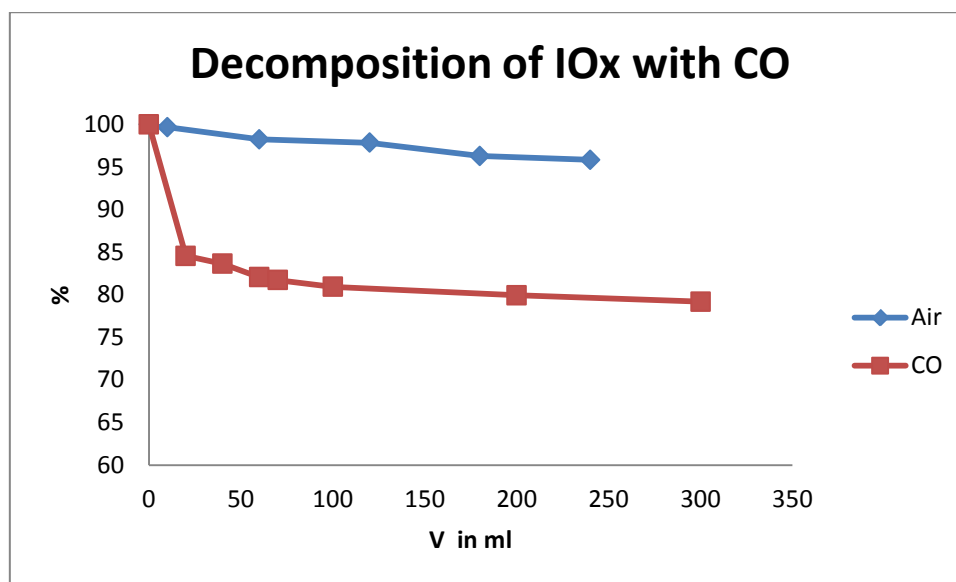
Figure 48: Revaporisation of ^{131}I from IOx deposits under air and carbon monoxide flow

The oxidation of carbon monoxide into carbon dioxide by iodine pentoxide (I_2O_5) is known to form elemental iodine (see Reaction 8) which will contribute to the volatile iodine source term [20].

$$I_2O_5(s) + 5CO(g) \rightarrow I_2(g) + 5CO_2(g) \tag{8}$$
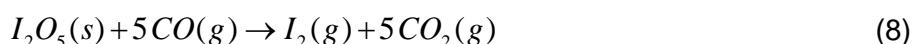
It is likely that the deposited iodine-oxide species are oxidised in a similar way.

6   Summary and conclusions

The interactions of iodine oxide and caesium iodide aerosols with the surfaces of a LWR NPP containment during a severe accident are not much reported in the literature. Particles deposited on various surfaces may act as a source of volatile iodine, which may be release back into the containment atmosphere and contribute to the volatile iodine source term. The focus of the study was on the analysis of IOx and CsI particle properties on various surfaces and the revaporisation behaviour of those under severe accident conditions. IOx and CsI particles were deposited on Teknopox Aqua V A paint films of different aged state and metal surfaces such as stainless steel, aluminium, copper and zinc.

6.1 Deposit and surface characterisation

During a severe accident iodine is assumed to be mostly transported into the containment in form of aerosol particles, such as caesium iodide, and only a few percentages as gaseous iodine. CsI can dissolve in the water phase or steam and dissociate into iodide and hydrogen ions and caesium hydroxide. Iodine oxide particles are formed in a reaction of gaseous iodine and ozone. The speciation of IOx particles depends on the reaction temperature. The chemical forms of I_2O_4 and I_4O_9 are dominating at dry conditions when the reaction temperature is below 100°C. At higher temperatures up to ~300 °C, I_2O_5 particles are formed and both other oxides decompose to I_2O_5. When I_2O_4 and I_4O_9 particles react with humidity they form HIO_3 and I_2. After exposure to humid air, I_2O_5 is rapidly converted to its partially hydrated form $I_2O_5 \bullet HIO_3$, also defined as HI_3O_8. On the other hand, the same product is formed when HIO_3 is partially dehydrated. The decomposition reaction, observed in AIAS-1 project, was faster than reported in the literature and is assumed to be caused by a smaller diameter of the iodine oxide particles.

New methods to produce IOx and CsI particles were developed and a new particle deposition facility was designed and built at VTT. The generation of iodine containing aerosol particles was very stable with this facility. Thus, the mass concentration of particles to be deposited on samples could be adjusted easily. The analysis of particle deposits with SEM verified that the samples had less than mono-layer coverage of particles as was the aim in sample preparation.

Iodine oxide particles were produced at 50 °C, 100 °C and 120 °C and deposited on filter samples in order to study the particle speciation. The formation of HIO_3 was verified with Raman analysis regardless of the reaction temperature. Furthermore, elemental iodine was also observed in the measured Raman spectra. Probably, iodine oxide particles have reacted with humid air forming iodic acid and elemental iodine.

IOx particles that were deposited on various sample surfaces were synthesized at 120°C. According to XPS analysis, it seemed that IOx particles were mainly in form of HIO_3 on metal and on painted surfaces. No solid particles were detected on the samples with SEM. Further analysis with SEM-EDX indicated that IOx particles had dissolved on the examined surfaces probably due to air humidity. This observation agrees well with the formation of HIO_3. A very small fraction of iodine was also in a low oxidation state on all surfaces. It is possible that a fraction of iodine had formed a compound with carbon, either with the surface contamination or with organic compounds of paint

The XPS spectrum of CsI was observed on all metal and painted samples on which CsI particles were deposited. Solid CsI particles were observed on the studied metal surfaces with SEM. However, on painted samples no CsI particles were observed. It is very likely that the particles on painted samples were mostly dissolved. Some CsI was most likely dissolved also on metal surfaces as iodine was observed outside the area with caesium iodide deposit. According to XPS analyses, this iodine may have reacted with the oxidized metal surfaces to form metal iodates. Only traces of oxidised iodine were detected on painted surfaces.

An interesting result in the XPS analysis was that a part of the acquired signal from CsI on the painted surfaces seemed to originate deeper from the structure of the paint, when it was pre-treated either with heat or gamma irradiation. SEM analysis revealed that heat and gamma irradiation treatment increased the porosity of the paint. Therefore, dissolved CsI may have been transported into the matrix of the paint.

6.2 Revaporisation studies

The revaporisation studies showed that the iodine from both IOx and CsI aerosols binds stronger on copper and zinc surfaces than on Al and SS surfaces. The affinity to zinc seems to be slightly higher than to Al and SS. Surface analysis within AIAS-1 had already shown that copper and zinc form metal iodides while species such as the highly water soluble aluminium triiodide were not detected. Copper iodide was found to be the most immobile and insoluble metal iodide.

The revaporisation of deposited iodine aerosols from the paint surfaces showed to be mainly dominated by the heat degradation of the paint film. Both, heat and irradiation showed to have an effect on the revaporisation. Teknopox Aqua VA paint and its degradation under containment relevant conditions has been studied intensively at Chalmers [6]. An increased revaporisation from the fresh, non-heat treated paint can be explained by the reaction of the iodine of the aerosols with the paint solvents in the paint. Close to the surface revaporisation occurs before the solvents of the inner matrix are affected by the containment conditions. Thus, a higher paint solvent concentration is found in the centre of the paint profile where the iodine species migrate to and possibly are chemically converted. Thus, the paint samples that had been for a long time aged at high temperatures showed the least ability to react and retain iodine from the deposited aerosols. Most paint solvents are less water soluble than the iodine species itself. One of the main paint solvents in the studied paint is texanol ester. Studies at Chalmers in which the paint solvents found in the paint were reacted with iodine and the consumption of iodine was measured using UV/VIS spectroscopy. Irradiating of these solutions caused the formation of volatile alkyl iodides such as methyl, ethyl and isopropyl iodide [19].

The results showed that both copper and the paint films react chemically more with the iodine from CsI deposits.

While the deposits on the metal surfaces washed easily off (without copper), due to the depth profile of paint films with a higher solvent content in the depths of the paint the migration in the paint and the chemical conversion rate in the paint films is much higher. Thus, an additional delayed revaporisation occurs at higher temperatures. Due to the less water soluble organic solvents, chemically converted iodine species remain longer in the paint film. Solvent extraction of the leaching water of paint that had been heat treated and irradiation treated is in form of organic iodides.

The IOx aerosol deposits produced at 120 °C showed an accelerated decomposition in the presence of carbon monoxide. Carbon monoxide will be released during a severe nuclear accident when cable, paint and other plastics present in the containment undergo pyrolysis and radiolysis degradation under the harsh conditions.

7   References

[1]   A. C. Vikis, R. MacFarlane, R., Reaction of iodine with ozone in the gas phase, Journal of Physical Chemistry, 89, 812-815, 1985.

[2]   T. Kärkelä, J. Holm, A. Auvinen, R. Zilliacus, U. Tapper, Experimental study on iodine chemistry (EXSI) – Containment experiments with elemental iodine, VTT-R-00717-09, 2009.

[3]   J. C. Wren, J. M. Ball, G. A. Glowa, The chemistry of iodine in containment, Journal of Nuclear Technology, 129, 297-325, 2000.

[4]   D. R. Lide, CRC Handbook of Chemistry and Physics, 86th edition, CRC Press, Boca Raton (FL), 2005.

[5]   M. W. Chase, NIST-JANAF thermochemical tables for the iodine oxides, Journal of Physical and Chemical Reference Data, 25(5), 1297–1340, 1996.

[6]   S.Tietze, M. Foreman, C. Ekberg, B. van Dongen, Identification of the chemical inventory of different paint film types applied in nuclear facilities, Journal of Radioanalytical and Nuclear Chemistry, 3, 1981-1999, 2013.

[7]   H. Glänneskog, Y. Albinson, J.O. Liljenzin, G. Skarnemark, Apparatus for on-line measurements of iodine species concentrations in aqueous and gaseous phases, Journal of Nuclear Instruments and Methods in Physics Research, 498, 517-521, 2003.

[8]   B. Hamner, B, Vattenfall-Ringhals, Ringhals 1-4, Oskarshamn 1-3, Forsmark 1-3: Varifiering av vattenskrubber – sammanfattning, Technical Report, PR-TEKN RAPP 25/88, 1988.

[9]   B. Murray, A. Haddrell, S. Peppe, J. Davies, J. Reid, D. O'Sullivan, H. Price, R. Kumar, R. Saunders, J. Plane, N. Umo, T. Wilson, Glass formation and unusual hygroscopic growth of iodic acid solution droplets with relevance for iodine mediated particle formation in the marine boundary layer, Atmos. Chem. Phys., 12, 8575–8587, 2012

[10]   S. Sunder, J. C. Wren and A. C. Vikis, Raman Spectra of I_4O_9 Formed by the Reaction of Iodine with Ozone, Journal of Raman Spectroscopy, 16, 6, 424-426, 1985

[11]   J. Bronić, L. Sekovanić, A. Mužic, T. Biljan, J. Kontrec and B. Subotić, Host-Guest Interaction of Iodine with Zeolite A, Acta Chim. Slov., 53, 166–171, 2006.

[12]   J. Mihály, S. Sterkel, H. Ortner, L. Kocsis, L. Hajba, É. Furdyga, J. Minka, FTIR and FT-Raman Spectroscopic Study on Polymer Based High Pressure Digestion Vessels, CROATICA CHEMICA ACTA CCACAA 79, (3), 497-501, 2006.

[13]   J. Chastain, R. C. King Jr (Eds.), Handbook of X-ray Photoelectron Spectroscopy, Physical Electronics, Eden Prairie 1995.

[14]   F. Mercier, V. Moulin, M. J. Guittet, N. Barré, N. Toulhoat, M. Gautier-Soyer, P. Toulhoat, Applications of NAA, PIXE and XPS for the quantification and characterization of the humic substances/iodine associations, Radiochim. Acta 88, 779, 2000.

[15]   F. Mercier, V. Moulin, M. J. Guittet, N. Barré, M. Gautier-Soyer, P. Trocellier, P. Toulhoat, Applications of new surface analysis techniques (NMA and XPS) to humic substances, Org. Geochem., 33, 247, 2002.

[16]   C. D. Wagner, W. M. Riggs, L. E. Davis, J. F. Moulder, Handbook of X-ray Photoelectron Spectroscopy, Perkin-Elmer Corporation (Physical Electronics), 1979.

[17]   D. Briggs, M. P. Seah, Practical Surface Analysis – Auger and X-ray Photoelectron Spectroscopy, Wiley, New York, 1990.

[18]   J. Durig, O. Bonne, W. Breazeale, Raman studies of iodic acid and sodium iodate, J. Phys. Chem., 69, 3886–3892, 1965.

[19]   S. Tietze, M. Foreman, C. Ekberg, Formation of organic iodides from containment paint ingredients caused by gamma irradiation, Journal of Nuclear Science and Technology, In press, 2012.

[20]   F. A. Cotton, Advanced inorganic chemistry, 5 th edition, 538, 1988.

Appendices

Appendix A. Raman spectra of a HIO_3 particle on increasing RH

The Raman spectra of a HIO_3 particle on increasing RH have been studied by Murray et al. [9]. The measured spectra are presented in Figures A1 and A2. The corresponding assignment of bands in the Raman spectra of aqueous HIO_3 is presented in Table A1.
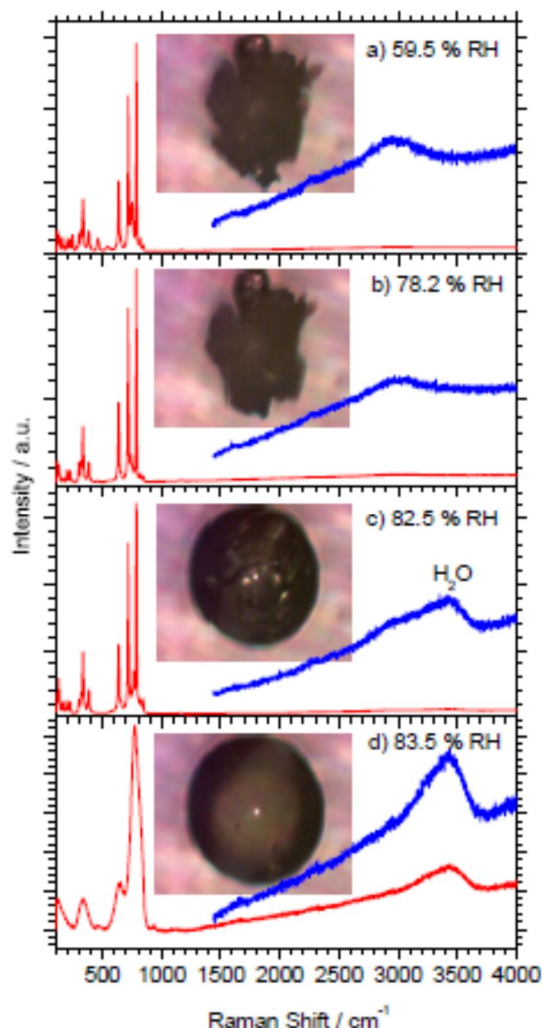
Figure A1. Raman spectra of an initially crystalline HIO_3 particle on increasing RH. The blue spectra are the region above ~1500 cm^{-1} expanded for clarity. Deliquescence occurs around 82.5 % RH (c-d) and is clearly evident in changes in both the image of the droplets and the Raman spectra. The width of the microscope image is 160 μm.

Table A1. Assignment of bands in Raman spectra of aqueous HIO_3 (cm^{-1}).

This Work	12 M Aqueous Solution (Durig et al., 1965)	Description
814	814	
768	771	IO_2 (HO-IO_2) assym. stretch
–	737	
644	638	IO stretch
333	324	IO_2 deformation
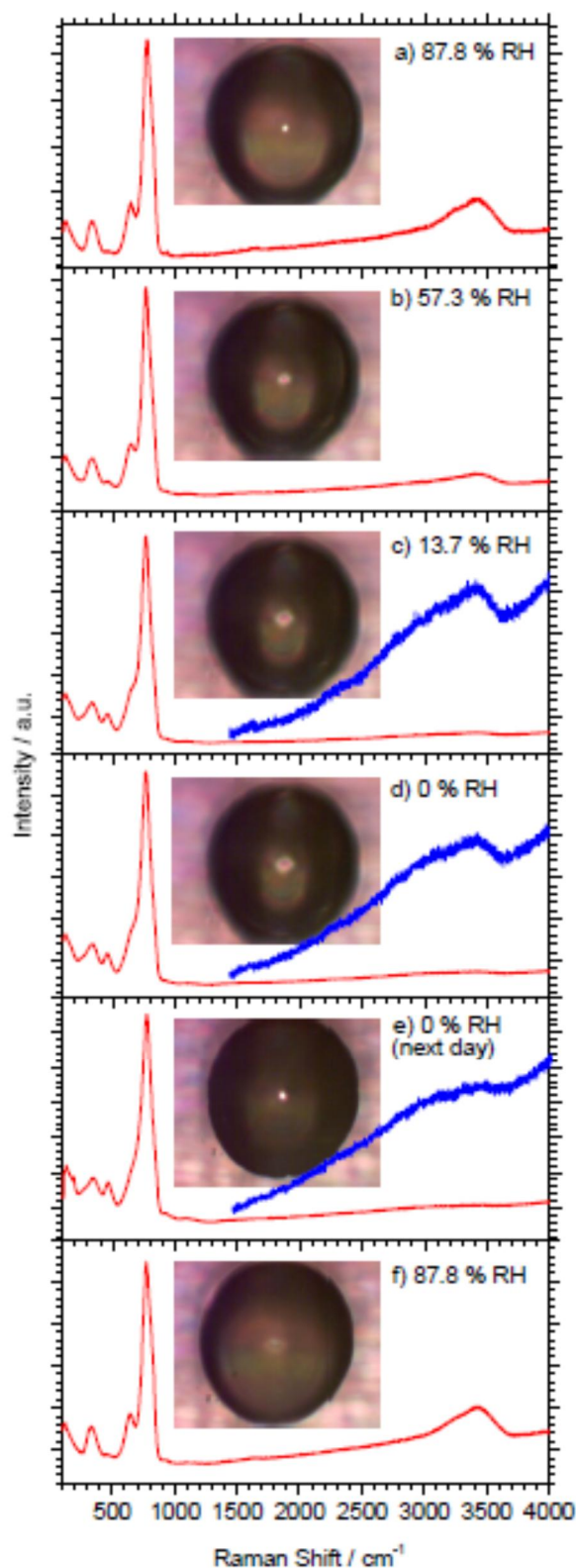
Figure A2. Raman spectra of deliquesced HIO₃ on decreasing RH (a–d) and then increasing RH again on the following day (e–f) after leaving the droplets at 0% RH overnight. The spectra are for the same droplet as in Figure A1, but tests demonstrated that all droplets (~30 droplets) on the slide responded in a similar manner. The OH stretch band associated with water (~3400 cm⁻¹) decreases dramatically on reducing RH, but the droplet does not revert back to its crystalline form. The blue expanded spectra are included only in cases where the OH band is weak. The width of the microscope images is 160 μm.

Appendix B1. The spectral data of the measured Raman spectra

Table B1. The Raman spectral data of IOx particles on a filter (sample 1, 2 and 3) and filter material (sample 4). The particles were produced at 50 °C, 100 °C and 120 °C. The intensity of the peaks is presented as well: s, strong; m, medium, w, weak; v, very; br, broad; sh, shoulder.

IOx particles on filter						Filter	
Sample 1 50 °C		Sample 2 100 °C		Sample 3 120 °C		Sample 4 Filter	
cm^{-1}	Intensity	cm^{-1}	Intensity	cm^{-1}	Intensity	cm^{-1}	Intensity
-	-	3225	vw, br	3225	vw, br	3225	vw, br
3200	vw, br	-	-	-	-	-	-
1377	m	1377	m	1377	m	1377	m
1298	m	1298	m	1298	m	1298	m
1213	m	1213	m	1213	m	1213	m
765	s	765	s	765	s	-	-
743	s, sh	743	s, sh	743	s, sh	-	-
-	-	-	-	-	-	731	s
660	m, br, sh	660	m, br, sh	660	m, br, sh	-	-
-	-	-	-	-	-	581	m
452	vw, br	452	vw, br	452	vw, br	-	-
383	w, br	-	-	-	-	383	m
290	w, br	-	-	-	-	290	m
-	-	-	-	-	-	200	w, br
185	m	-	-	-	-	-	-

Appendix B2. Raman spectrum of a PTFE sample

Mihály et al. [12] have studied the surface corrosion of polytetrafluoroethylene (PTFE) based microwave digestion vessels. The material for the investigated digestion vessels was polytetrafluorethylene modified with 0.2 to 0.5 % perfluorovinyl ether (PTFE-TFM). The addition of small quantities (less than 1 %) of perfluorovinyl ether does not affect the chemical, thermic or electric properties of PTFE. The corrosion process was monitored by reflection Fourier Transform InfraRed (FTIR) and Raman techniques.

Infrared (attenuated total reflection method - ATR) and Raman spectra of the PTFE-TFM wall sample after a corrosion test are shown in Figure B1. The proposed assignments (Table B1) were made on the basis of the general formula of PTFE: $-[-CF_2-CF_2-]n-$. Dominant IR bands at 1299, 1199, 1146, 715–774, 553, 507 cm^{-1} and Raman bands at 1296, 735, 386, 291 and 202 cm^{-1} belong to the different modes of CF_2 groups. Weak IR bands at 2960, 2927, 2853 (CH_2, CH_3 stretching mode) and 1438 cm^{-1} (CH_2, CH_3 deformation) as well as the Raman band around 2900 cm^{-1} (CH_2, CH_3 stretching) belong to surface hydrocarbons formed on the surface of the vessel wall during the corrosion test.
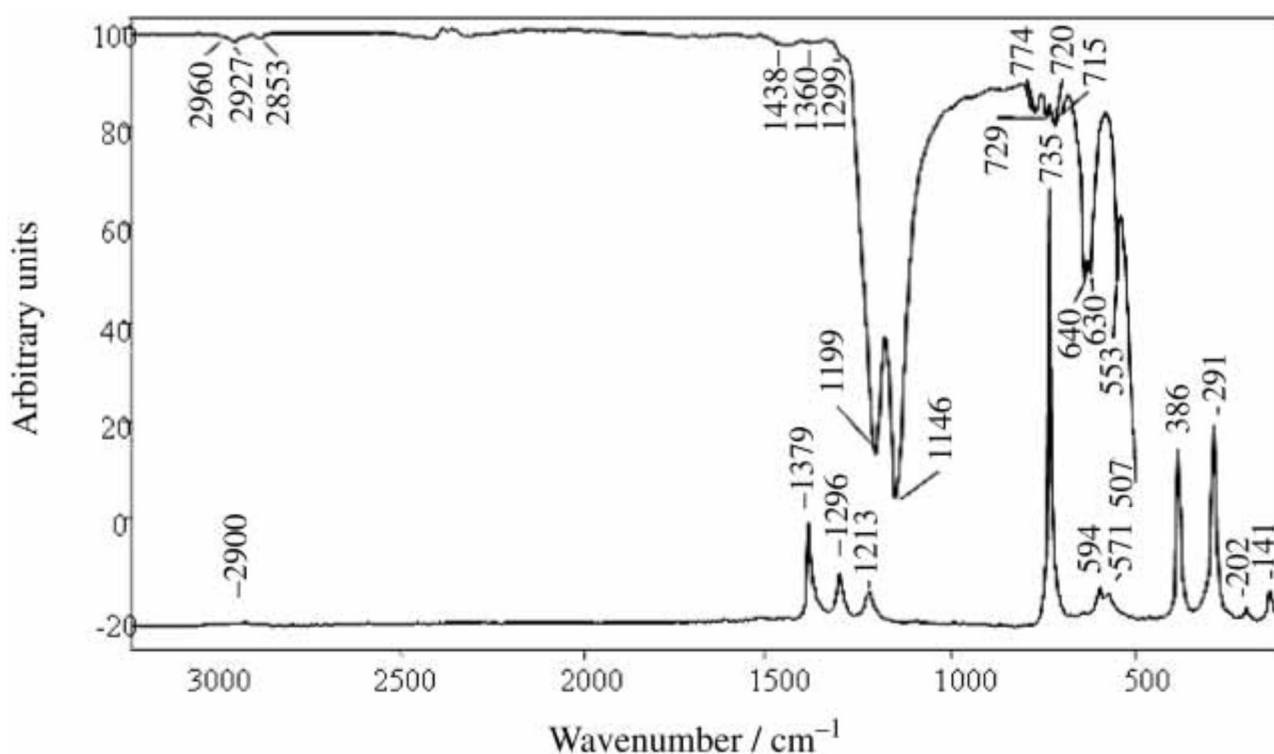
Figure B1. Infrared (upper trace) and Raman (lower trace) spectra of the PTFE vessel wall sample.

Table B1. IR and Raman band assignments of the PTFE vessel wall sample after the corrosion test.

IR bands	Raman bands	Assignment
2960 vvw		
2927 vw	≈2900 vw, b	CH_2, CH_3 stretching[a]
2853 vw		
1458 vw		CH_2, CH_3 deformation[a]
	1379 m	CF stretching
1360 vvw		NO_3^- (nitrate)[a]
1299 vw, sh	1296 m, w	CF_2 asymmetric stretching
	1213 w	CC stretching
1199 vs		CF_2 symmetric stretching
1146 vvs		
	1084 vvw	CF_3 symmetric stretching
	735 vvs	CF_2 symmetric stretching[b]
774 w		
729 w		CF_2 scissoring
720 w		
715 vw, sh		
640 m		CF deformation
630 m		
	594 w	CF_3 symmetric deformation
	571 w	(umbrella)
553 m		CF_2 bending
507 s		
	386 s	CF_2 twisting
	291 s	CF_2 wagging
	202 vw	CF_2 rocking

[a] Marked band assignments belong to species formed on the surface of the vessel wall during 200 digestion cycles.

[b] Assigned to A_1 mode, involving symmetric C–F and C–C stretching modes.[11]

Appendix C1. The binding energies of IOx deposits on metal surfaces measured with XPS.

Steel surface
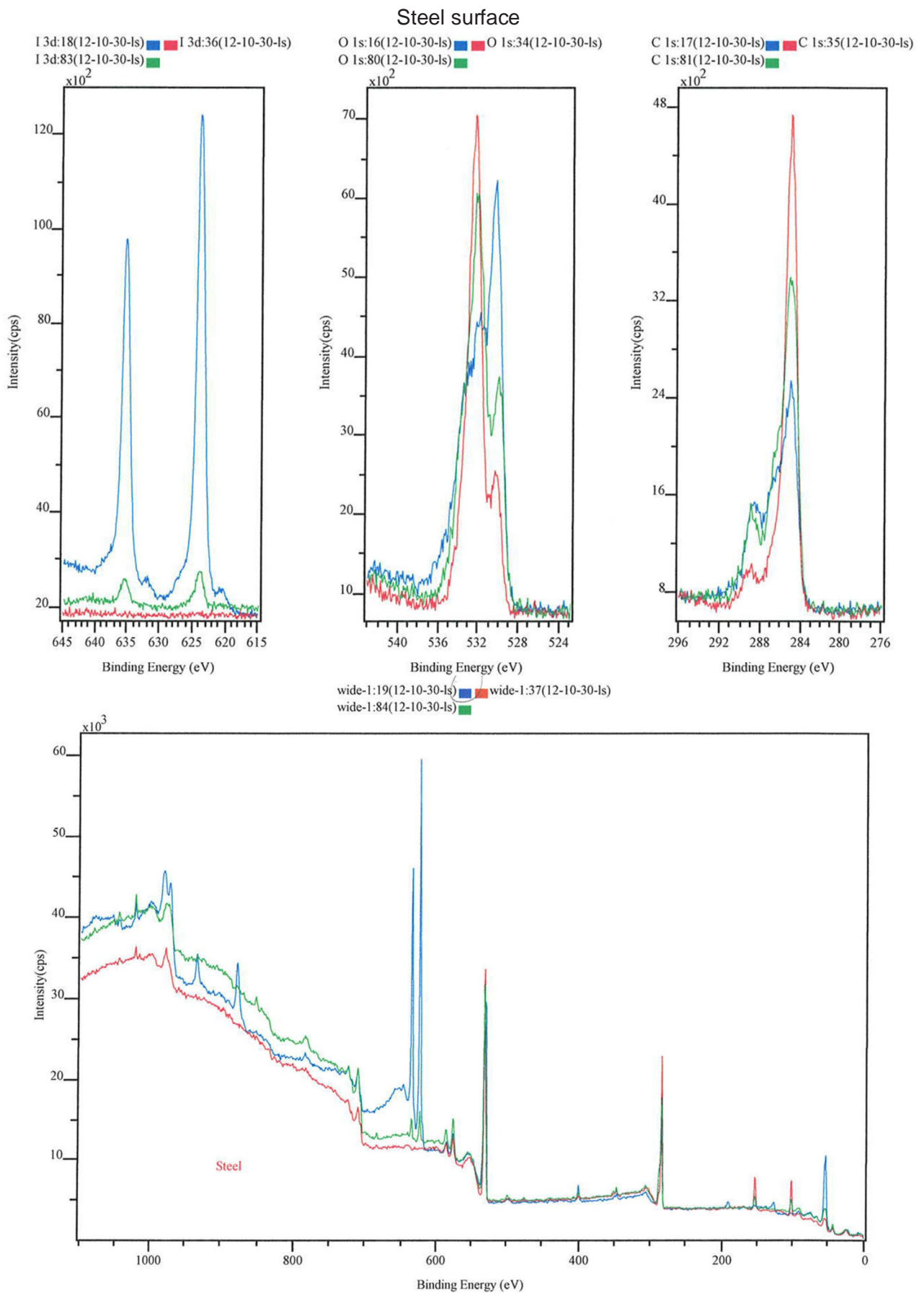
Appendix C2. The binding energies of IOx deposits on metal surfaces measured with XPS.

Aluminium surface
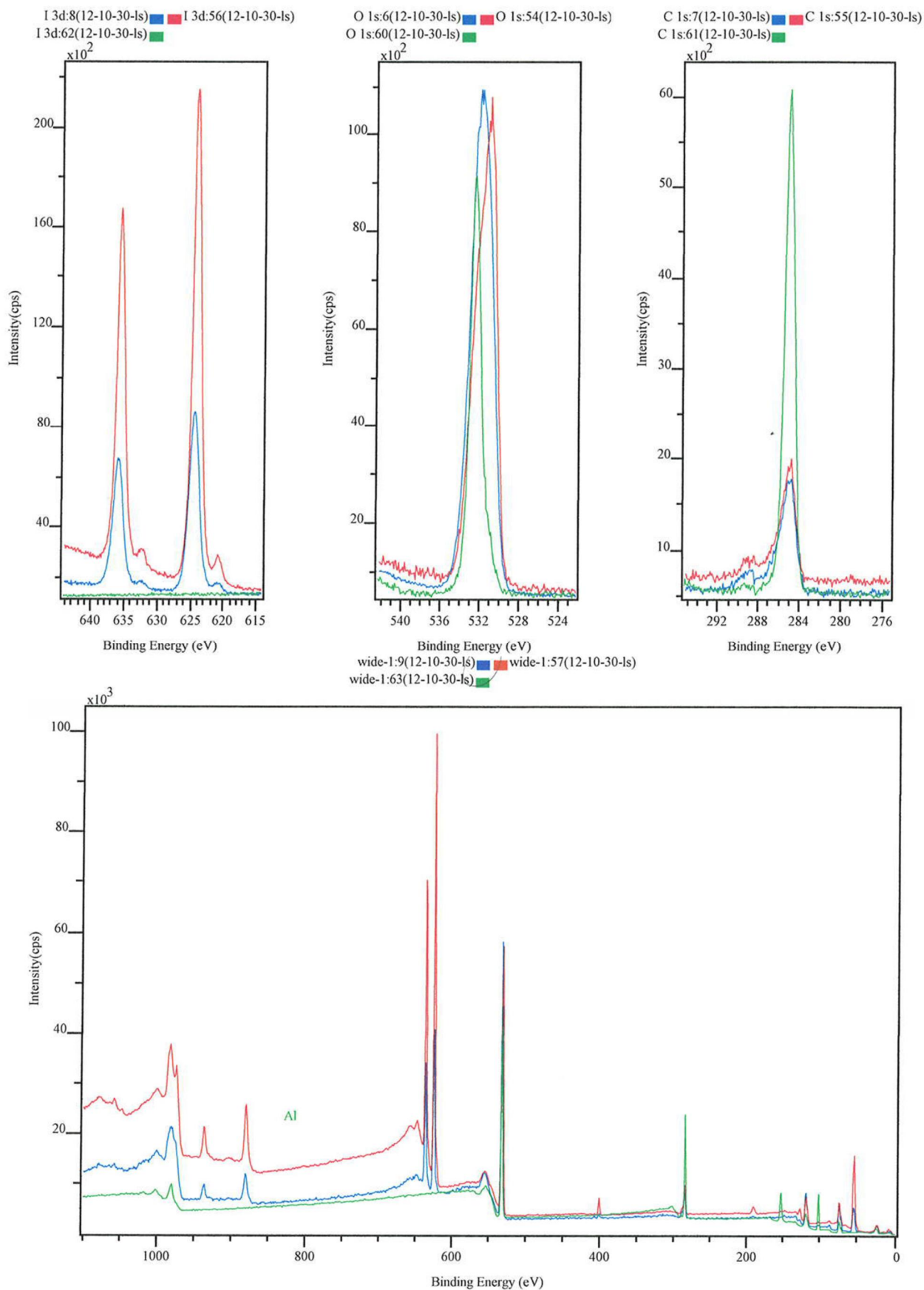
Appendix C3. The binding energies of IOx deposits on metal surfaces measured with XPS.

Copper surface
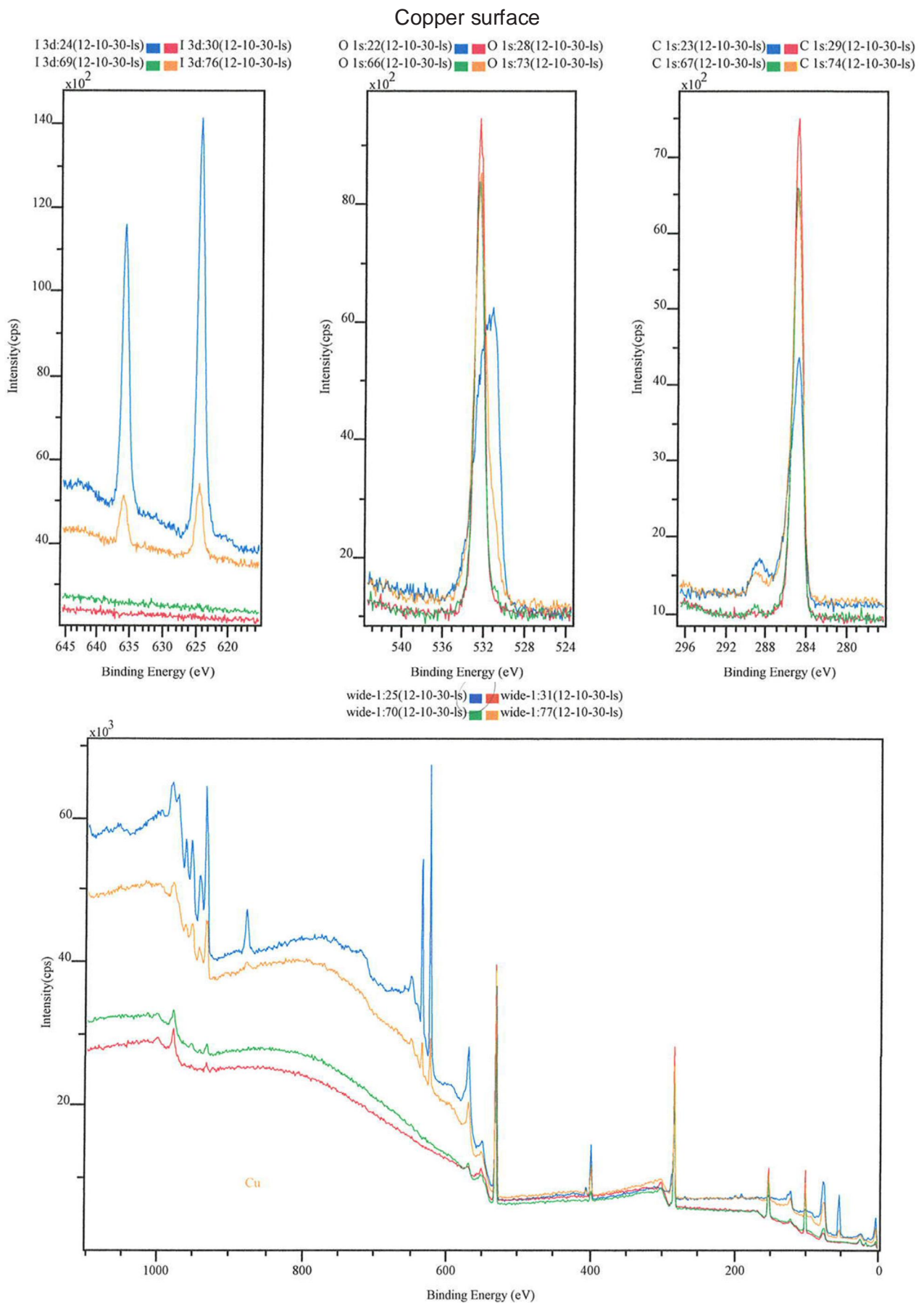
Appendix C4. The binding energies of IOx deposits on metal surfaces measured with XPS.

Zinc surface
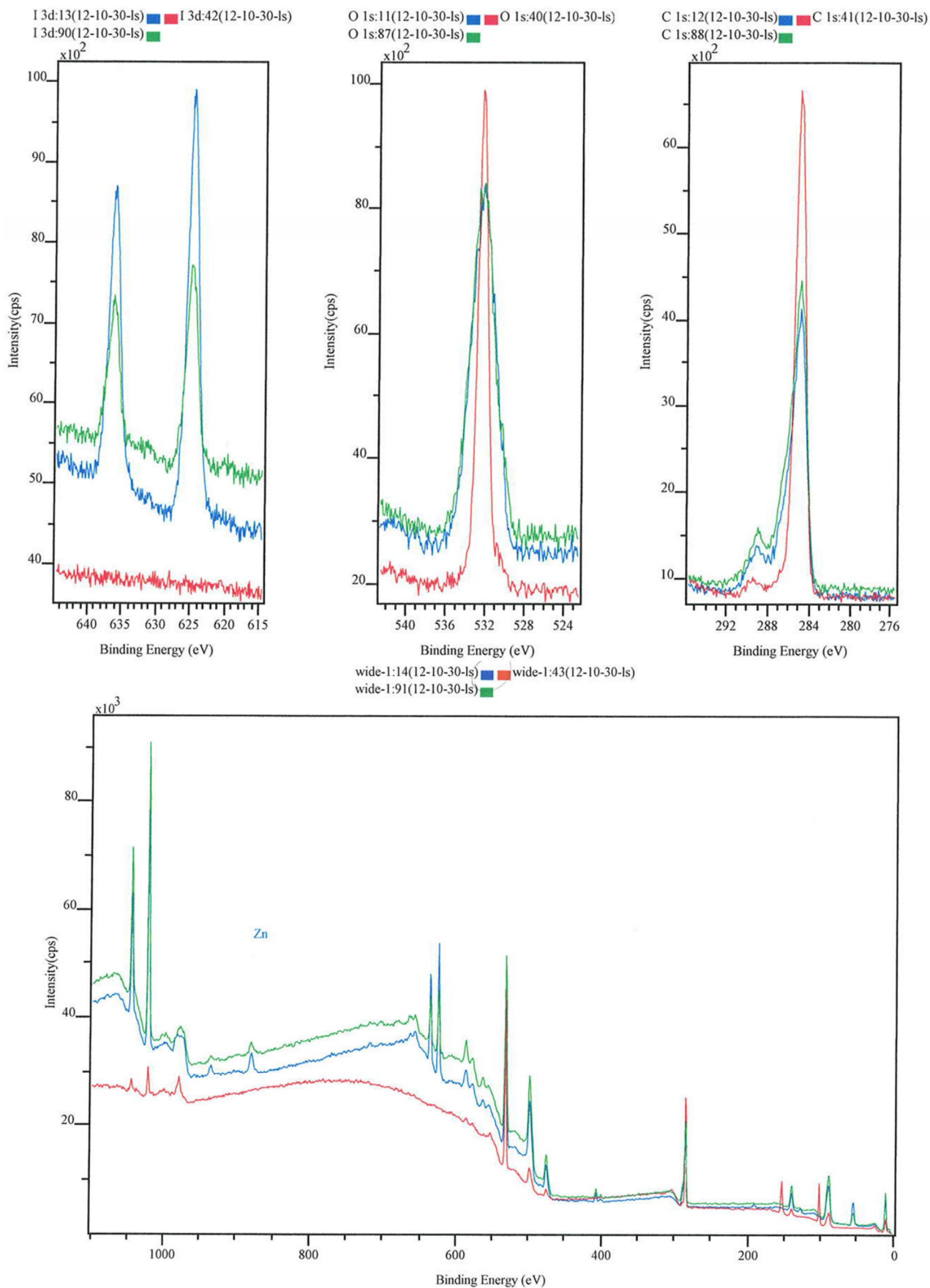
Appendix D. The atomic concentrations of elements on the IOx deposits on metal samples measured with XPS.

Teemu Kärkelä

October 2012
Second XPS investigation on iodine containing surfaces
Measurements dataset: 12-10-30-ls

Samples	location #	O 1s	C 1s	I 3d	N 1s	Si 2p	(metal)				C-C	C-O	C=O	COO
		Atomic Concentrations from wides									C 1s HiRes components			
							Fe	Cr	Zn	Ca				
Steel	1 spot	40.6 %	43.4 %	5.3 %	2.8 %		4.9 %	2.6 %	0.0 %	0.4 %	49.0 %	22.0 %	13.2 %	15.8 %
	3 off spot	35.5 %	48.1 %	0.3 %	1.0 %	3.7 %	7.5 %	3.1 %	0.4 %	0.6 %	60.0 %	21.4 %	5.5 %	13.1 %
	2 no iodine	32.4 %	50.6 %	-	0.6 %	10.0 %	3.5 %	2.1 %	0.4 %	0.5 %	79.3 %	11.2 %	3.7 %	5.8 %
							Cu							
Cu	1 spot	31.0 %	44.2 %	3.6 %	12.6 %		8.7 %				75.5 %	12.3 %	3.3 %	8.9 %
	4 off spot	26.9 %	54.7 %	0.6 %	5.8 %	8.8 %	3.2 %				85.9 %	8.4 %	1.5 %	4.2 %
	2 no iodine	25.0 %	57.2 %	-	0.6 %	16.9 %	0.3 %				97.1 %	2.9 %		
		24.9 %	57.5 %	-	2.4 %	14.9 %	0.3 %				94.3 %	4.6 %		1.1 %
							Al							
Al	2 spot	49.7 %	17.5 %	8.0 %	4.6 %		20.2 %				68.4 %	15.4 %	5.8 %	10.3 %
	1 off spot	53.9 %	17.1 %	3.5 %	1.7 %		23.7 %				69.7 %	15.9 %	3.8 %	10.7 %
	3 no iodine	31.1 %	45.8 %	-		13.2 %	10.0 %				95.0 %	3.9 %	0.1 %	0.9 %
							Zn							
Zn	1 spot	34.6 %	49.2 %	2.8 %	3.8 %		9.5 %				67.5 %	17.5 %	4.8 %	10.2 %
	3 off spot	34.4 %	50.1 %	1.2 %	3.4 %		10.9 %				65.1 %	19.7 %	5.1 %	10.1 %
	2 no iodine	26.9 %	57.9 %	0.1 %		14.0 %	1.1 %				92.1 %	4.9 %	0.9 %	2.2 %

Appendix E1. The binding energies of CsI deposits on metal surfaces measured with XPS.

Steel surface
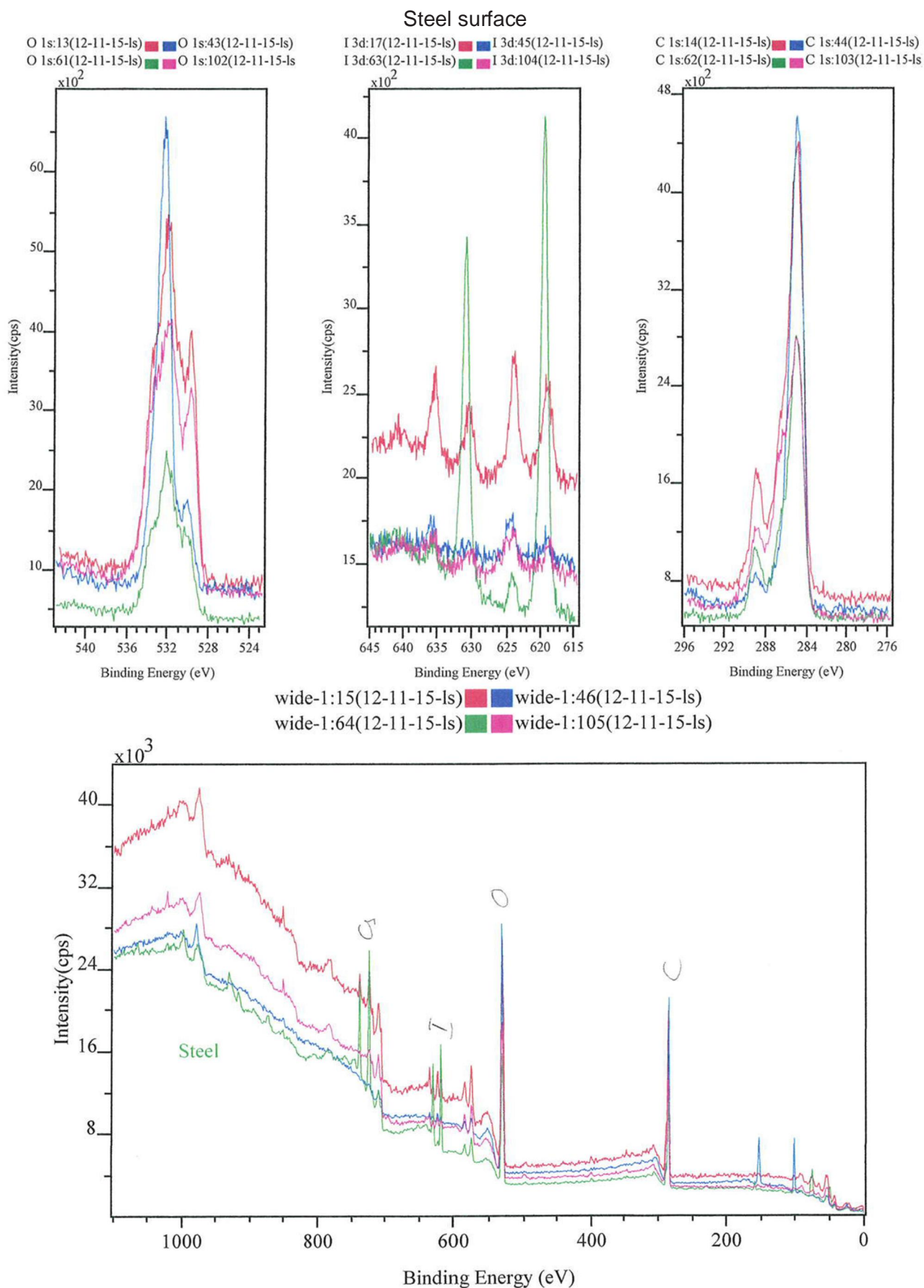
Appendix E2. The binding energies of CsI deposits on metal surfaces measured with XPS.

Aluminium surface

O 1s:26(12-11-15-ls) ■ ■ O 1s:33(12-11-15-ls)
O 1s:76(12-11-15-ls) ■ ■ O 1s:82(12-11-15-ls)
O 1s:88(12-11-15-ls) ■

I 3d:31(12-11-15-ls) ■ ■ I 3d:35(12-11-15-ls)
I 3d:78(12-11-15-ls) ■ ■ I 3d:84(12-11-15-ls)
I 3d:90(12-11-15-ls) ■

C 1s:27(12-11-15-ls) ■ ■ C 1s:34(12-11-15-ls)
C 1s:77(12-11-15-ls) ■ ■ C 1s:83(12-11-15-ls)
C 1s:89(12-11-15-ls) ■

wide-1:28(12-11-15-ls) ■ ■ wide-1:36(12-11-15-ls)
wide-1:79(12-11-15-ls) ■ ■ wide-1:85(12-11-15-ls)
wide-1:91(12-11-15-ls) ■
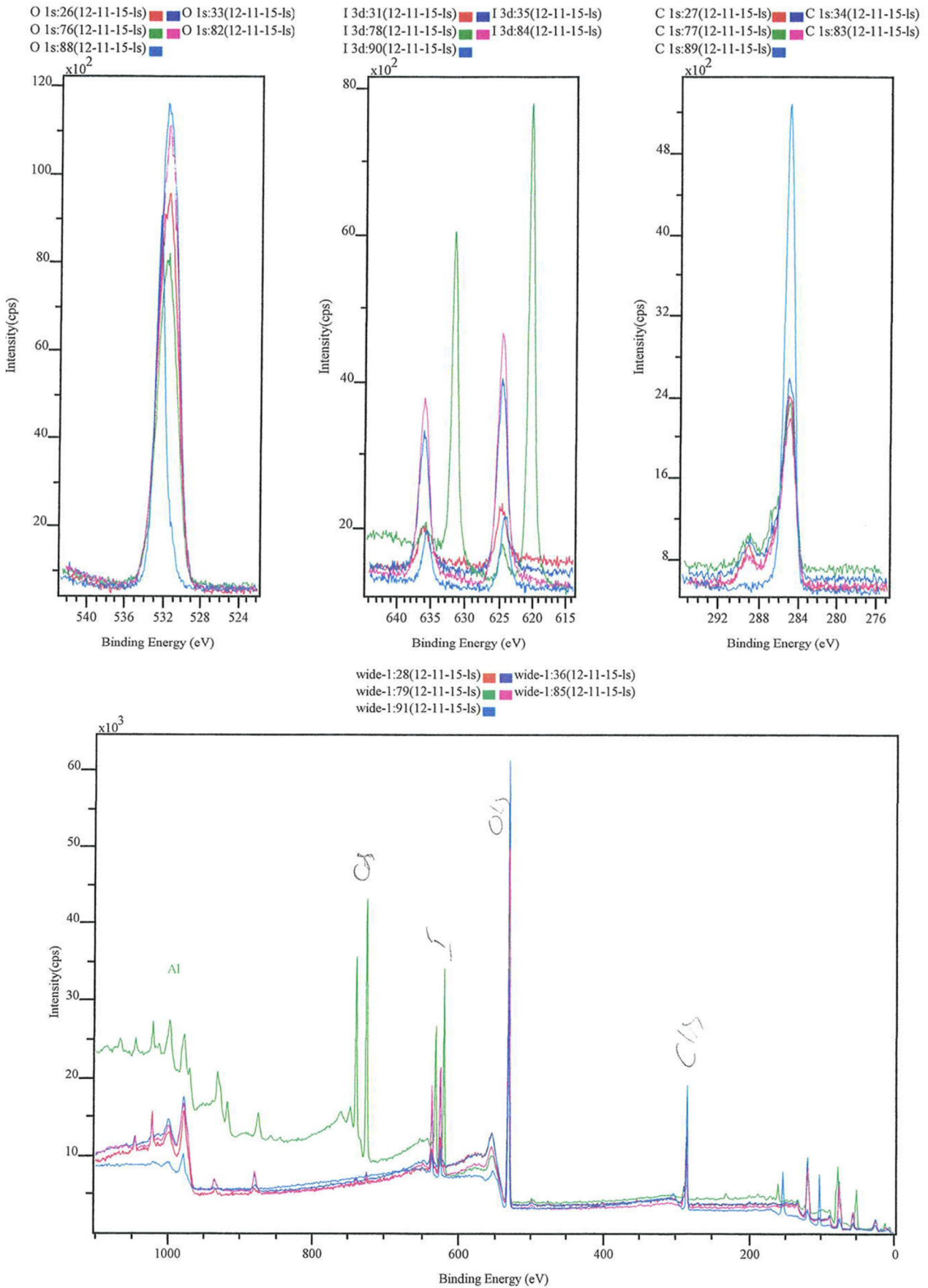
Appendix E3. The binding energies of CsI deposits on metal surfaces measured with XPS.

Copper surface

O 1s:6(12-11-15-ls) O 1s:48(12-11-15-ls)
O 1s:108(12-11-15-ls) O 1s:114(12-11-15-ls

I 3d:11(12-11-15-ls) I 3d:50(12-11-15-ls)
I 3d:110(12-11-15-ls) I 3d:116(12-11-15-ls)

C 1s:7(12-11-15-ls) C 1s:49(12-11-15-ls)
C 1s:109(12-11-15-ls) C 1s:115(12-11-15-ls

wide-1:8(12-11-15-ls) wide-1:51(12-11-15-ls)
wide-1:111(12-11-15-ls) wide-1:117(12-11-15-ls)
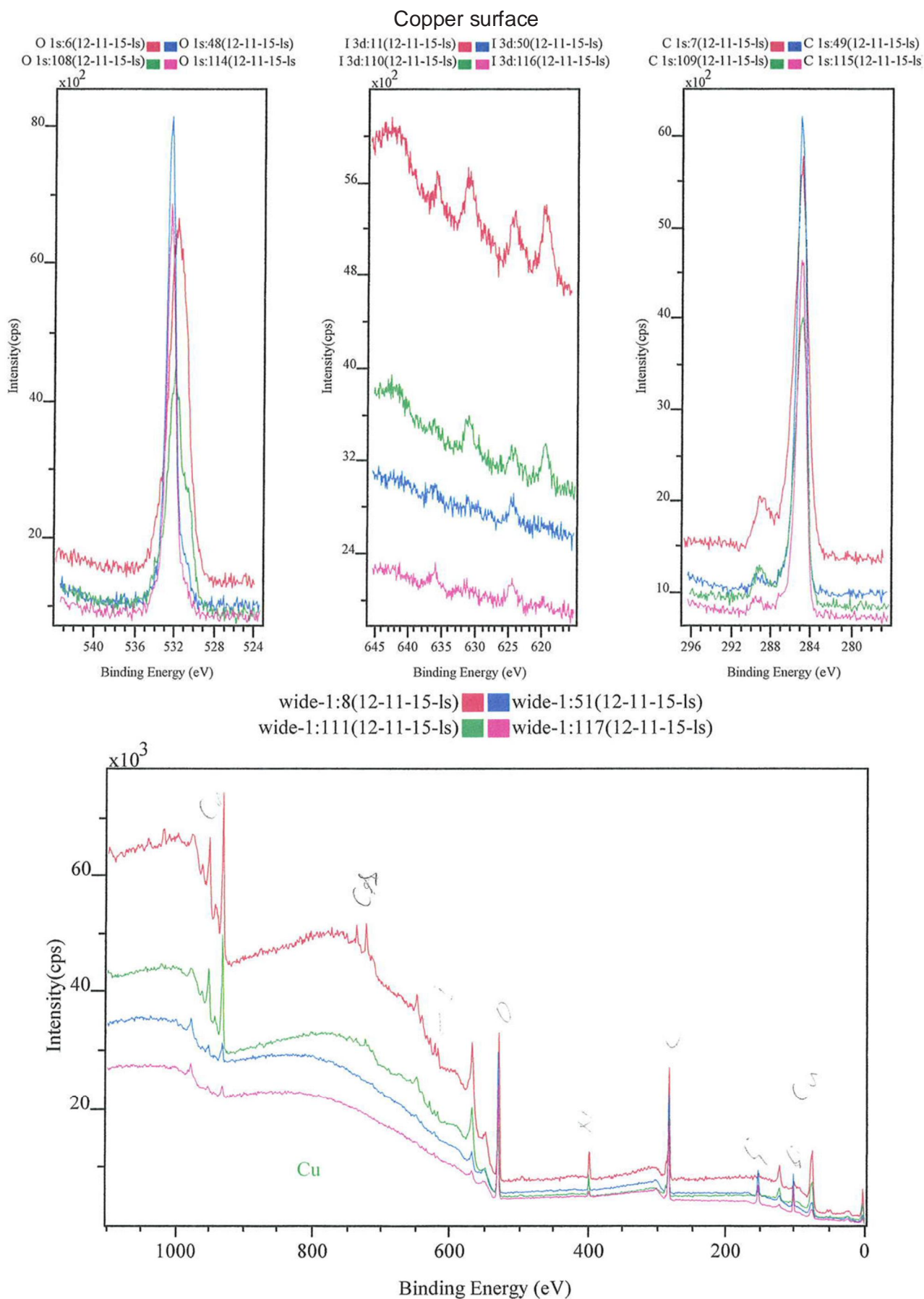
Appendix E4. The binding energies of CsI deposits on metal surfaces measured with XPS.
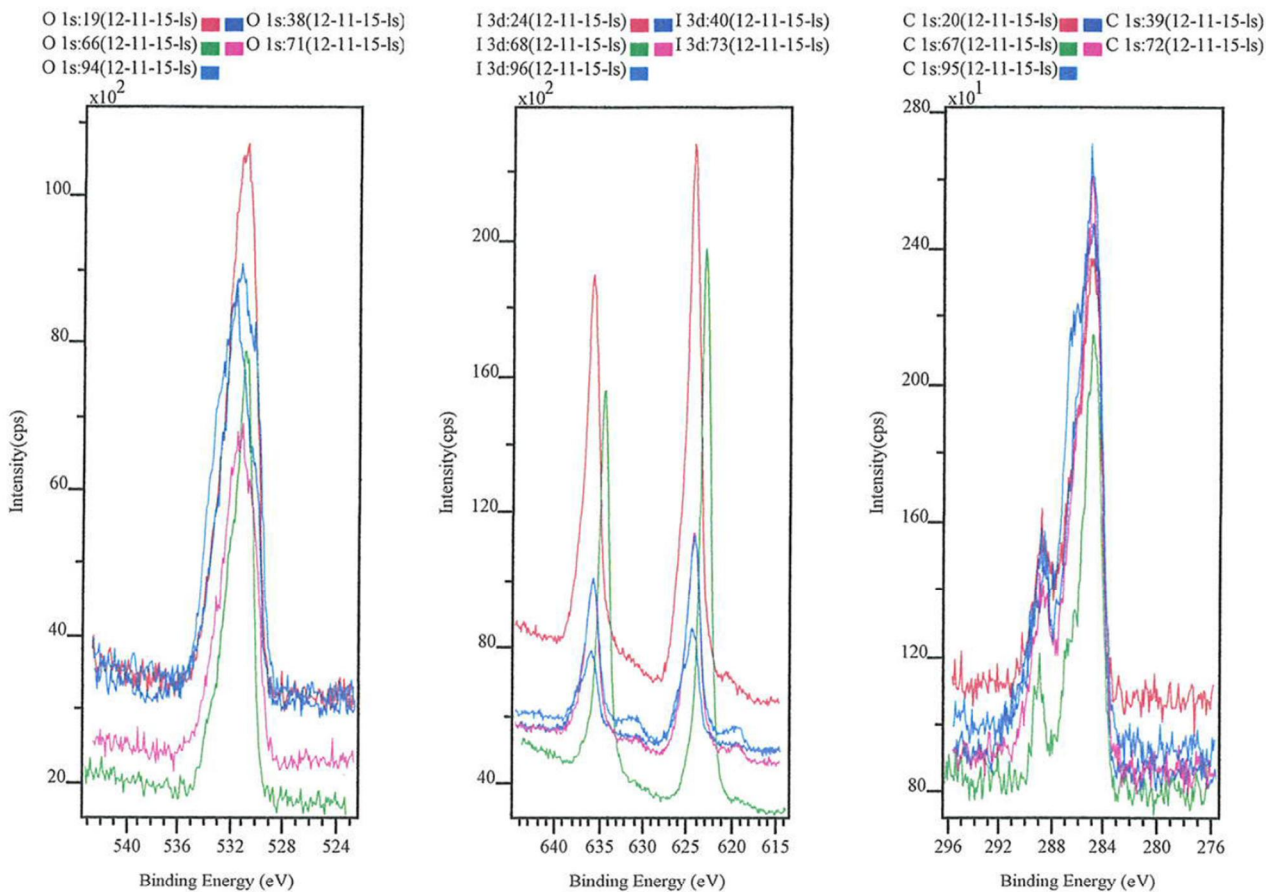
Zinc surface

O 1s:19(12-11-15-ls) ■ O 1s:38(12-11-15-ls) ■
O 1s:66(12-11-15-ls) ■ O 1s:71(12-11-15-ls) ■
O 1s:94(12-11-15-ls) ■

I 3d:24(12-11-15-ls) ■ I 3d:40(12-11-15-ls) ■
I 3d:68(12-11-15-ls) ■ I 3d:73(12-11-15-ls) ■
I 3d:96(12-11-15-ls) ■

C 1s:20(12-11-15-ls) ■ C 1s:39(12-11-15-ls) ■
C 1s:67(12-11-15-ls) ■ C 1s:72(12-11-15-ls) ■
C 1s:95(12-11-15-ls) ■

wide-1:21(12-11-15-ls) ■ wide-1:41(12-11-15-ls) ■
wide-1:69(12-11-15-ls) ■ wide-1:74(12-11-15-ls) ■
wide-1:97(12-11-15-ls) ■
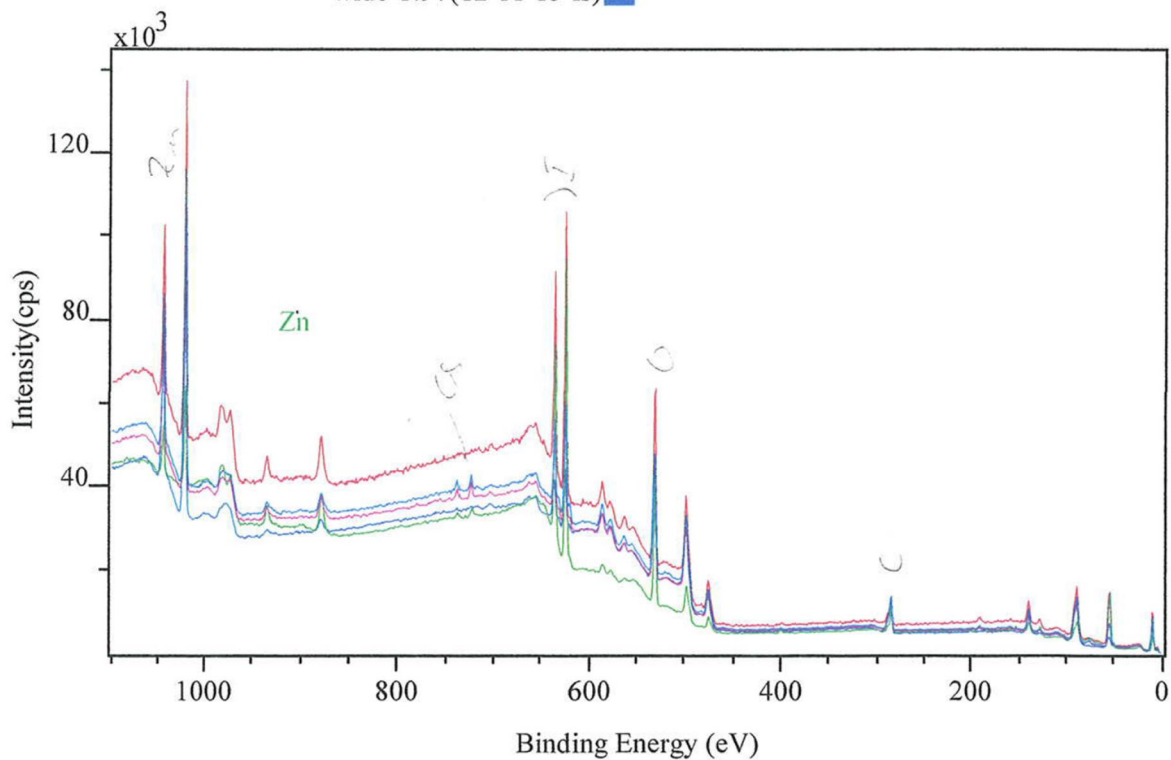
Teemu Kärkelä

Appendix F. The atomic concentrations of elements on the CsI deposits on metal samples measured with XPS.

Samples	location #	O 1s	C 1s	I 3d	N 1s	Cs 3d	Fe / Cu / Al / Zn	Cr	Ni 2p	Si 2p	trace-Cl	trace-Zn	C-C	C-O	C=O	COO
Steel - CsI	opt on I	32.5 %	59.3 %	0.3 %	1.0 %	0.4 %	2.7 %	3.2 %	0.2 %			0.3 %	63.2 %	19.0 %	4.4 %	13.4 %
	offspot	29.1 %	54.6 %	0.1 %	0.6 %	0.1 %	0.8 %	1.1 %	0.2 %	13.3 %		0.1 %	83.9 %	9.5 %	2.0 %	4.6 %
	opt on Cs	30.8 %	58.8 %	1.7 %	1.2 %	2.1 %	2.3 %	2.6 %	0.1 %			0.3 %	64.7 %	18.5 %	3.5 %	13.3 %
	offspot	33.6 %	57.9 %	0.1 %	0.9 %	0.2 %	3.0 %	3.7 %	0.2 %			0.4 %	54.6 %	26.4 %	6.3 %	12.7 %
Cu - CsI	opt on I	25.4 %	56.5 %	0.5 %	6.6 %	0.4 %	7.5 %			3.1 %			78.1 %	10.4 %	2.9 %	8.6 %
	off spot	25.6 %	57.4 %	0.2 %	2.4 %		0.3 %			14.1 %			90.0 %	6.7 %	1.0 %	2.3 %
	opt on Cs	24.4 %	56.9 %	0.2 %	7.6 %	0.1 %	8.0 %			2.8 %			81.0 %	9.8 %	1.9 %	7.4 %
	off spot	26.3 %	57.1 %	0.1 %	2.2 %		0.7 %			13.6 %			88.7 %	6.6 %	1.6 %	3.1 %
Al - CsI	opt on I	47.8 %	25.3 %	0.3 %	0.1 %	0.1 %	25.6 %				0.2 %	0.6 %	71.6 %	13.8 %	3.0 %	11.7 %
	off spot	49.6 %	22.4 %	1.1 %	0.3 %	0.1 %	26.2 %				0.2 %	0.1 %	70.8 %	13.4 %	4.5 %	11.2 %
	opt on Cs	46.3 %	28.5 %	2.7 %	0.3 %	3.5 %	17.6 %				0.4 %	0.7 %	64.8 %	19.8 %	4.6 %	10.8 %
	opt on I	49.3 %	21.7 %	1.7 %	0.3 %	0.2 %	26.8 %				0.1 %	0.1 %	72.2 %	13.5 %	4.5 %	9.8 %
	off spot	29.7 %	47.4 %	0.4 %			7.6 %				14.7 %	0.2 %		95.1 %	3.8 %	0.6 %	0.5 %
Zn - CsI	opt on I	46.9 %	28.4 %	7.7 %	1.5 %		15.5 %						54.3 %	23.3 %	7.2 %	15.3 %
	off spot	41.9 %	38.6 %	2.0 %	0.5 %		17.0 %			0.0 %			47.0 %	30.9 %	9.6 %	12.6 %
	opt on I	48.6 %	35.4 %	10.6 %	0.5 %	0.1 %	4.7 %						67.1 %	19.3 %	1.8 %	11.8 %
	opt on Cs	42.8 %	37.4 %	3.8 %	0.8 %	0.4 %	14.9 %						56.3 %	22.2 %	7.9 %	13.6 %

Note: *Atomic Concentrations from wides* = O 1s, C 1s, I 3d, N 1s, Cs 3d. *Substrate elements* column group: Fe (Steel) / Cu / Al / Zn, plus Cr and Ni 2p for Steel. *Trace elements* = trace-Cl, trace-Zn. *C 1s HiRes components* = C-C, C-O, C=O, COO.

Appendix G1. The binding energies of IOx deposits on paint surfaces measured with XPS.

No treatment

O 1s:77(2013-03-12-ls) ■ O 1s:127(2013-0 I 3d:79(2013-03-12-ls) ■ I 3d:129(2013-03 C 1s:78(2013-03-12-ls) ■ C 1s:128(2013-0
O 1s:132(2013-03-12-ls) ■ 3dw:137(2013-03 ■ C 1s:133(2013-03-12-ls) ■
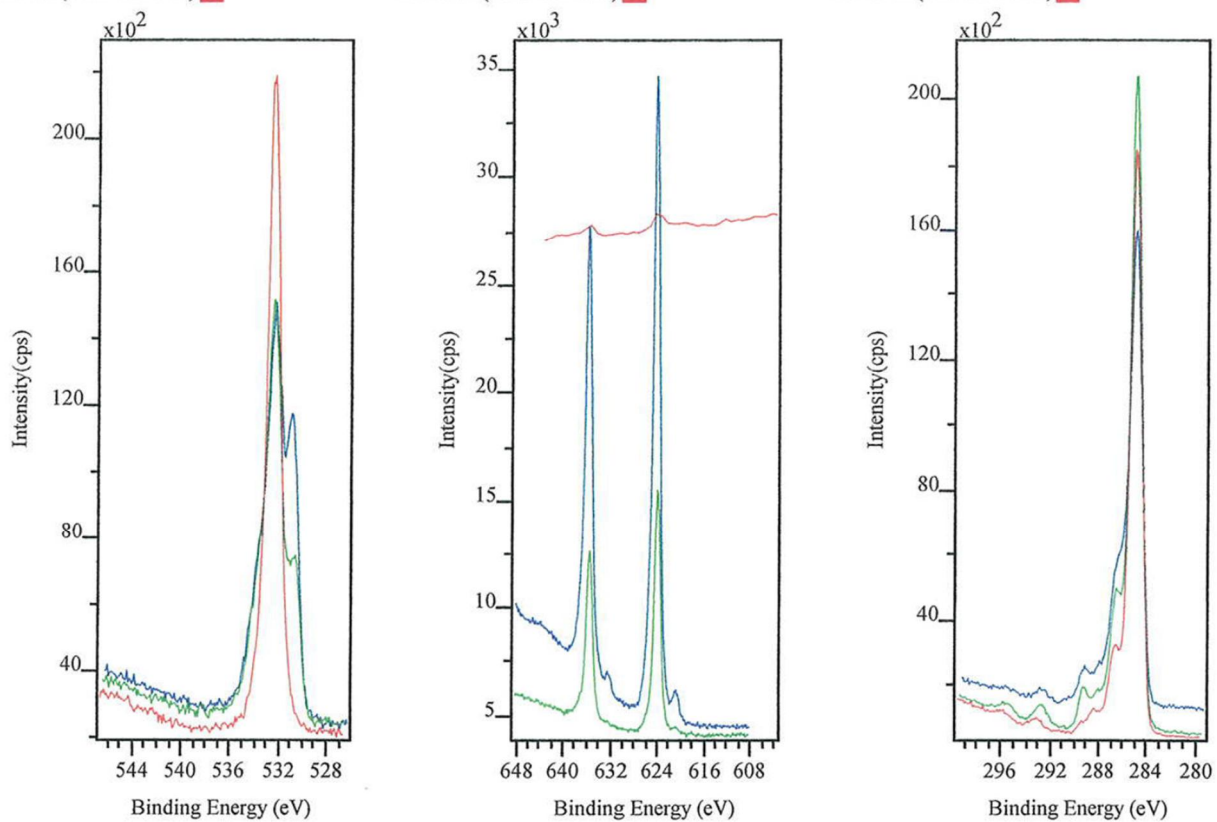
wide:80(2013-03-12-ls) ■ wide:130(2013-03-12-ls)
wide:134(2013-03-12-ls) ■

IOx Non
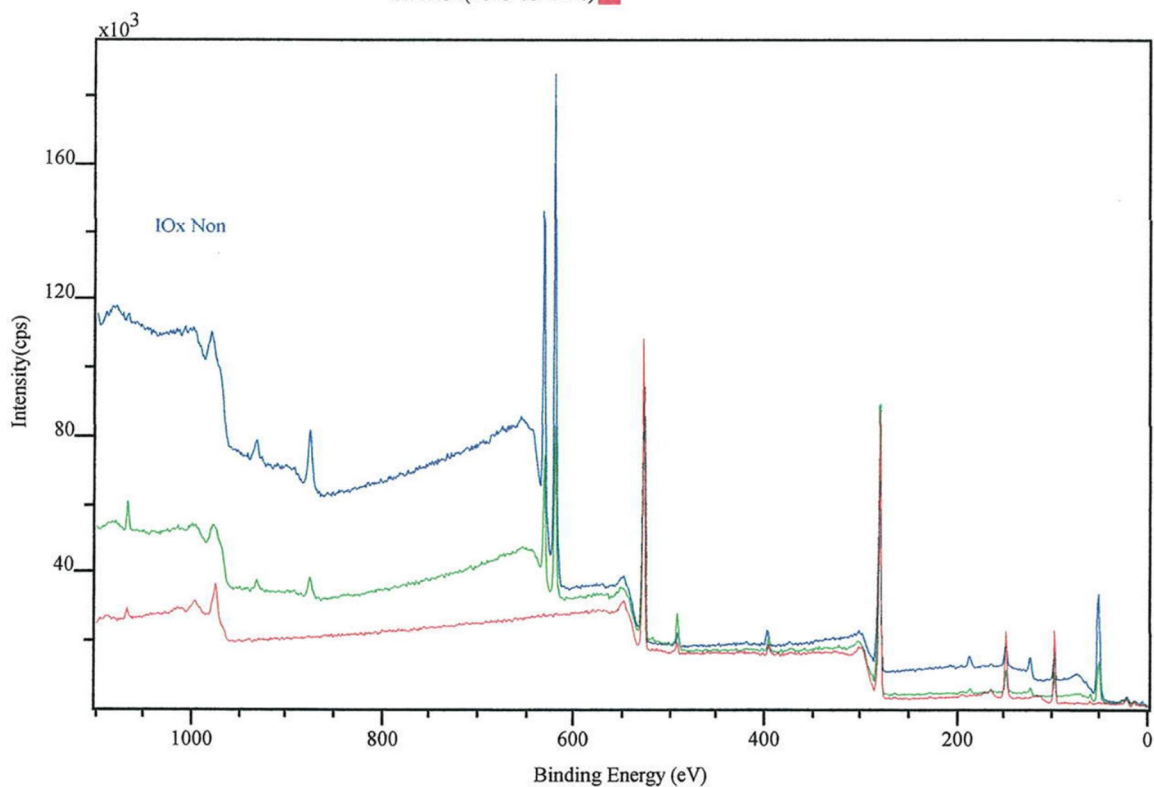
Appendix G2. The binding energies of IOx deposits on paint surfaces measured with XPS.

Heat treatment

O 1s:87(2013-03-12-ls)■■ O 1s:107(2013-0   I 3d:89(2013-03-12-ls)■■ I 3d:109(2013-03   C 1s:88(2013-03-12-ls)■■ C 1s:108(2013-0
O 1s:112(2013-03-12-ls)■   3dw:115(2013-03-12-ls)■   C 1s:113(2013-03-12-ls)■
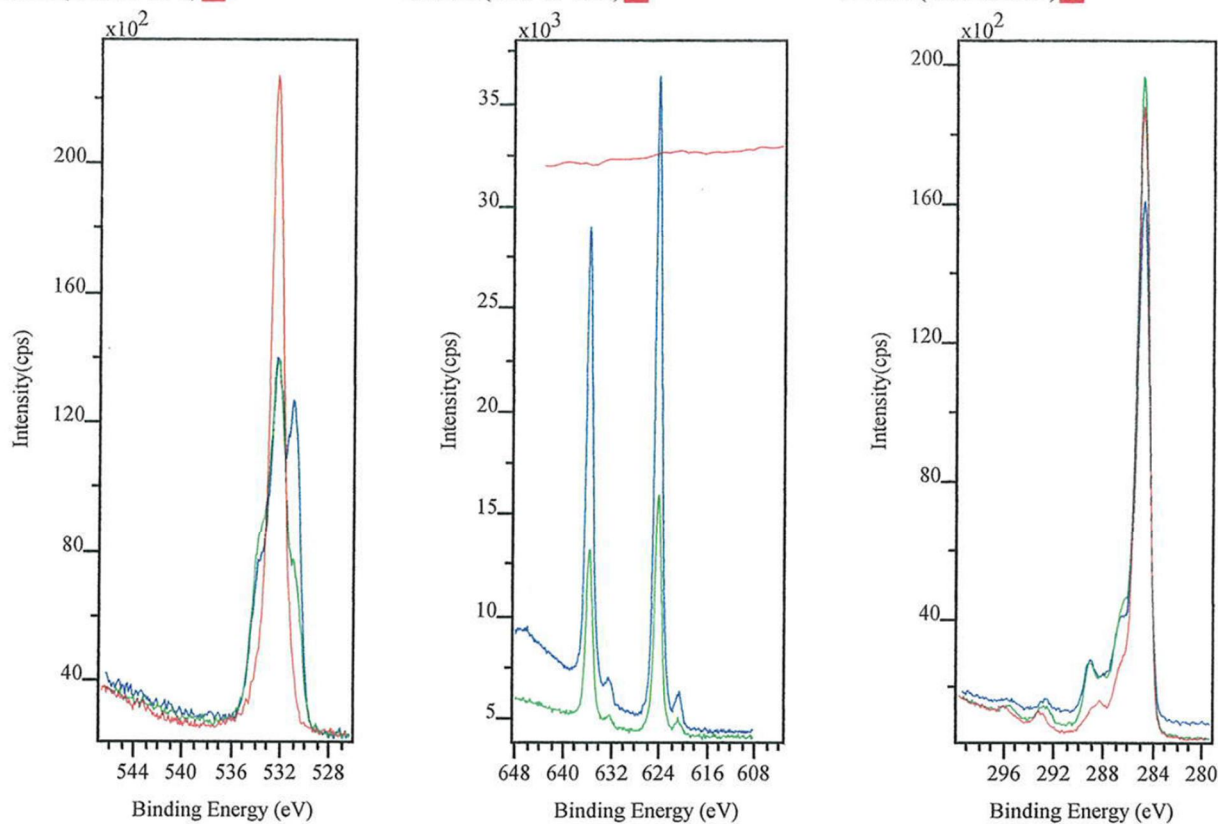
wide:90(2013-03-12-ls)■■ wide:110(2013-03-12-ls)
wide:114(2013-03-12-ls)■
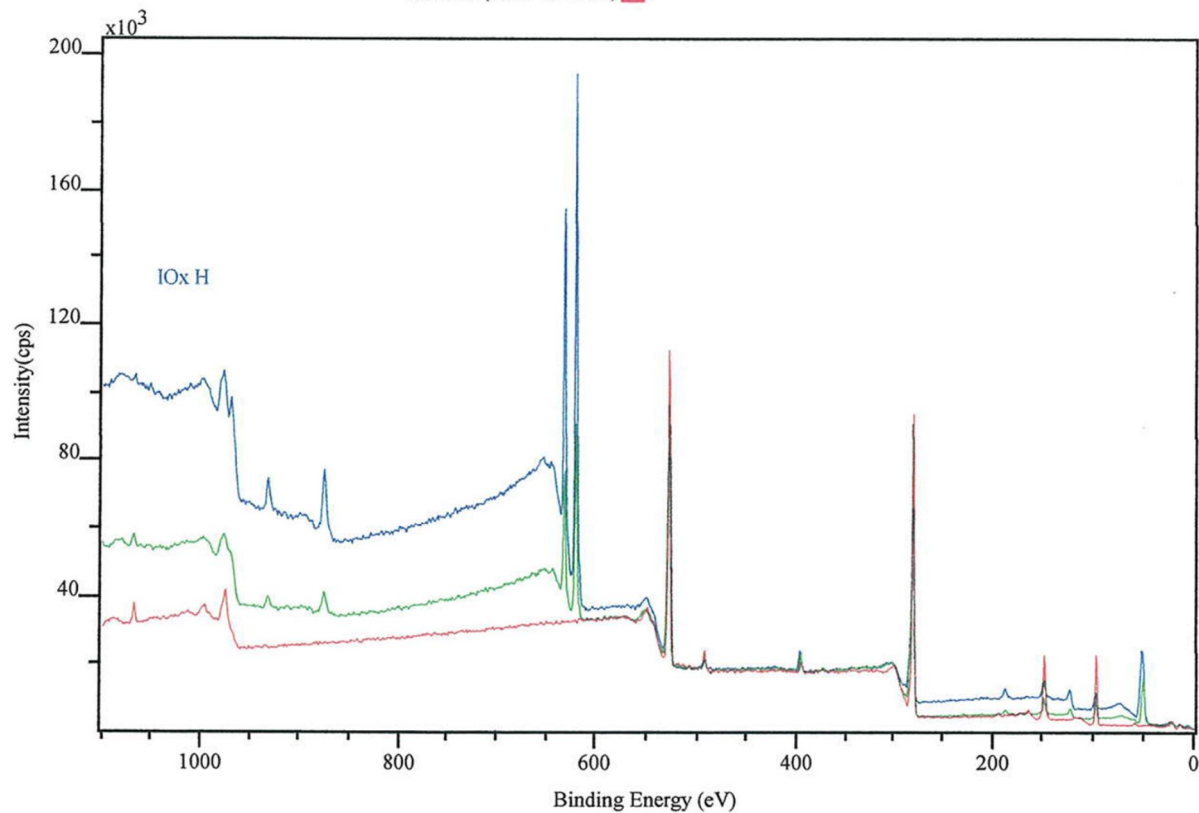
Appendix G3. The binding energies of IOx deposits on paint surfaces measured with XPS.

Short gamma irradiation and heat treatment

O 1s:92(2013-03-12-ls) ■■ ■ O 1s:97(2013-03   I 3d:94(2013-03-12-ls) ■■ ■ I 3d:104(2013-03   C 1s:93(2013-03-12-ls) ■■ ■ C 1s:98(2013-03

O 1s:102(2013-03-12-ls) ■   :3dw:141(2013-03-12-ls) ■   C 1s:103(2013-03-12-ls) ■
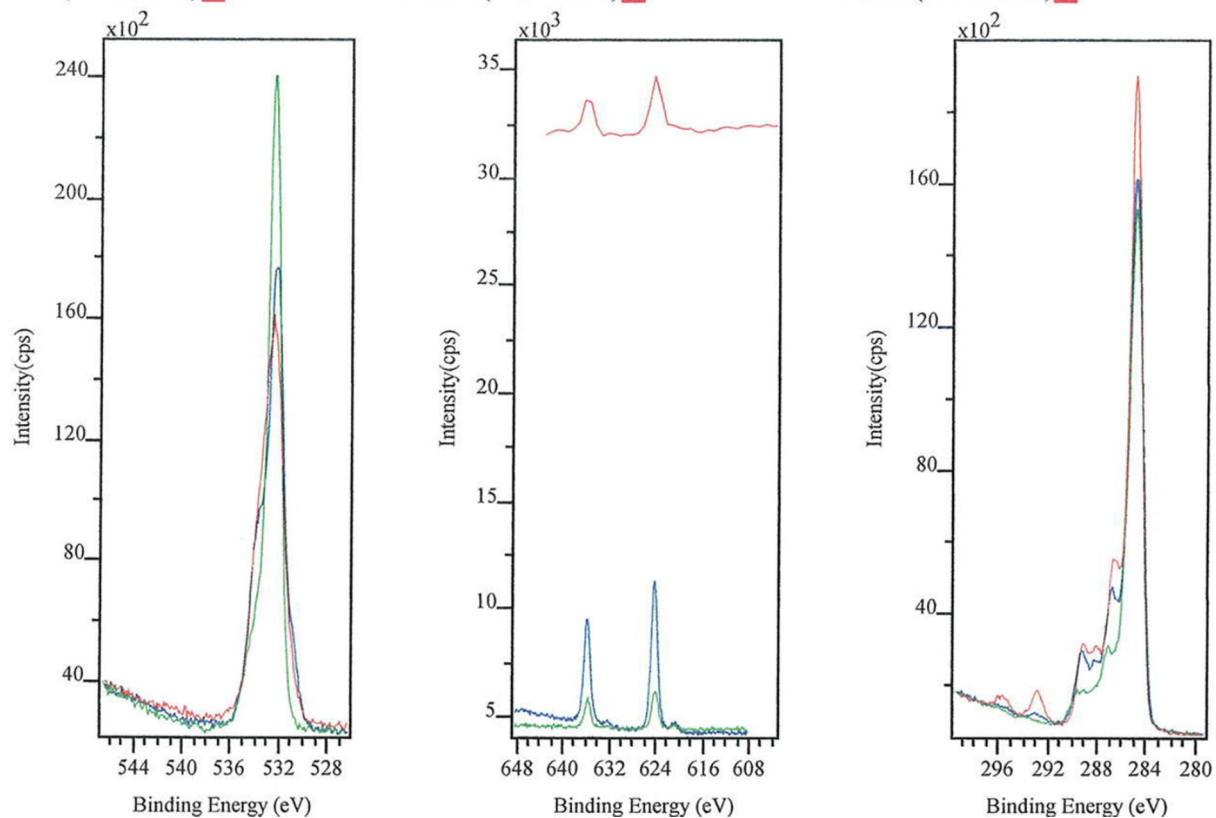
wide:95(2013-03-12-ls) ■■ ■ wide:99(2013-03-12-ls)

wide:105(2013-03-12-ls) ■
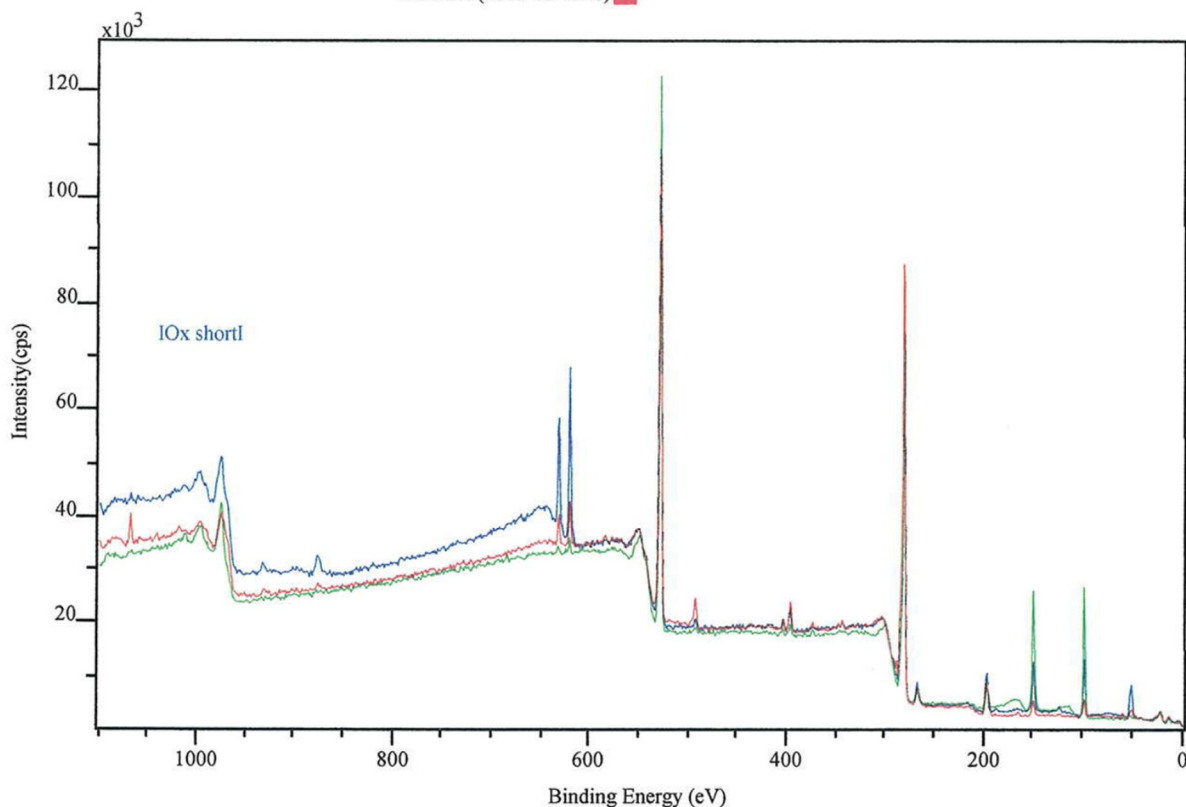
Appendix G4. The binding energies of IOx deposits on paint surfaces measured with XPS.

Long gamma irradiation

O 1s:82(2013-03-12-ls) ■■ O 1s:117(2013-0 I 3d:84(2013-03-12-ls) ■■ I 3d:119(2013-03 C 1s:83(2013-03-12-ls) ■■ C 1s:118(2013-0
O 1s:122(2013-03-12-ls) ■   3dw:139(2013-03-12-ls) ■   C 1s:123(2013-03-12-ls) ■
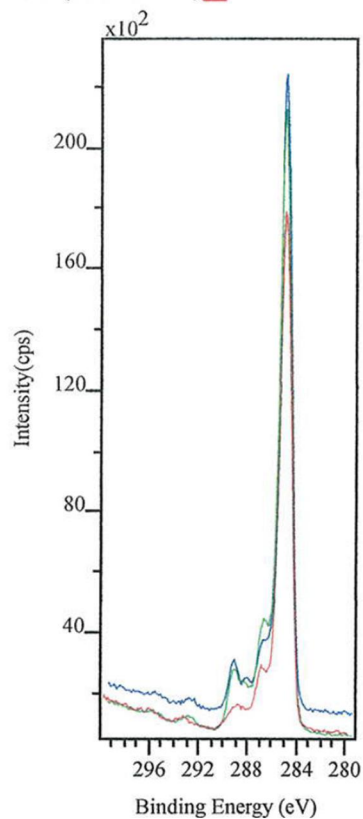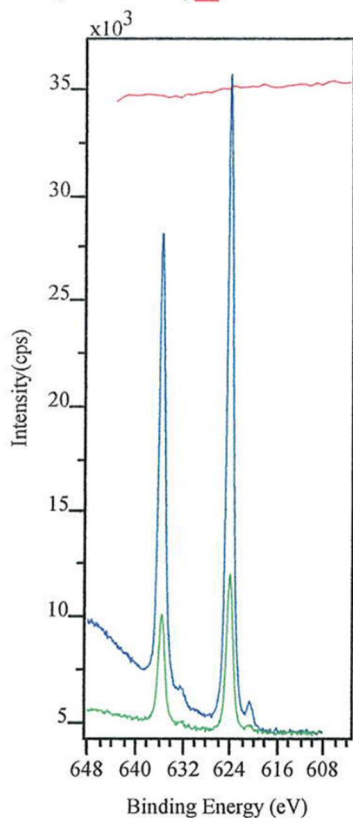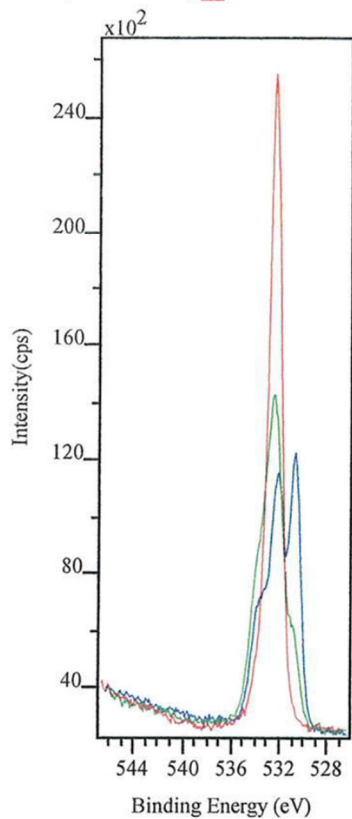
wide:85(2013-03-12-ls) ■■ wide:120(2013-03-12-ls)
wide:124(2013-03-12-ls) ■
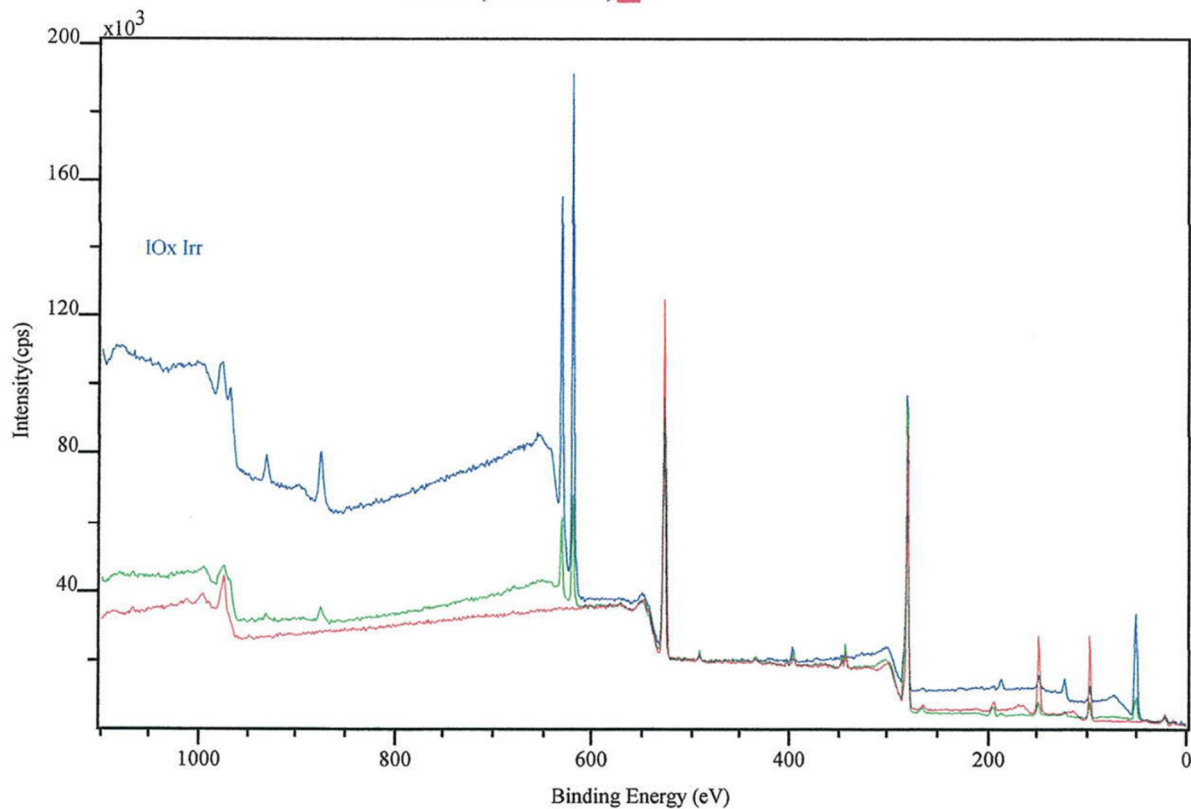
Appendix H. The atomic concentrations of elements on the IOx and CsI deposits on paint samples measured with XPS.

Teemu Kärkelä

March 2013
Another XPS investigation with a spot of iodine particles (CsI or IOx) on paint surface
Measurements dataset: 13-03-12-ls

CsI series	location #	O 1s	C 1s	I 3d	Cs 3d	Si 2p	N 1s	Na 1s	Cl 2p	Ca	K	C-C	C-O	C=O	COO
				Atomic concentrations from wides								C 1s HiRes components			
no treatment	1 spot	15.7 %	78.7 %	0.09 %	0.23 %	2.3 %	1.7 %	0.9 %	0.3 %		trace	79.2 %	13.6 %	4.1 %	3.2 %
(note point order)	3	20.7 %	66.8 %	0.02 %	0.06 %	11.0 %	0.9 %	0.5 %	0.1 %			??			
	2 paint	16.4 %	77.9 %	0.01 %	0.03 %	2.2 %	1.9 %	1.2 %	0.3 %		trace	77.5 %	14.8 %	4.6 %	3.2 %
heat treatment	1 spot	16.2 %	77.7 %	0.24 %	0.33 %	3.3 %	1.1 %	0.6 %	0.1 %	trace	0.4 %	82.7 %	10.4 %	3.4 %	3.5 %
	2	16.7 %	76.1 %	0.02 %	0.00 %	3.9 %	1.3 %	0.7 %	0.2 %	trace	1.2 %	82.1 %	10.7 %	3.7 %	3.5 %
	3 paint	16.1 %	77.4 %	0.02 %	0.00 %	3.0 %	1.3 %	1.1 %	0.2 %	trace	1.1 %	82.1 %	10.5 %	3.6 %	3.9 %
short-irr and heat	1 spot	17.5 %	75.6 %	0.04 %	0.21 %	4.3 %	1.2 %	0.0 %	1.1 %	trace	trace	??			
(note point order)	3	22.8 %	65.8 %	0.02 %	0.08 %	7.1 %	2.2 %	0.2 %	1.9 %	trace	trace	59.2 %	23.6 %	10.9 %	6.3 %
	2 paint	14.9 %	78.5 %	0.02 %	0.01 %	3.6 %	1.5 %	0.1 %	1.3 %	trace	trace	78.9 %	12.5 %	3.7 %	4.9 %
long-irr	1 spot	16.6 %	76.8 %	0.26 %	0.46 %	4.0 %	0.6 %	0.0 %	0.6 %	0.6 %	trace	82.5 %	10.2 %	2.9 %	4.4 %
	2 (?)	14.5 %	79.6 %	0.01 %	0.06 %	3.0 %	1.5 %	0.2 %	0.6 %	0.6 %	trace	??			
	3 (?)	21.5 %	63.8 %	0.04 %	0.00 %	12.0 %	1.2 %	0.3 %	0.8 %	0.3 %	trace	80.4 %	12.7 %	3.3 %	3.7 %
IOx series		**O 1s**	**C 1s**	**I 3d**	**Cs 3d**	**Si 2p**	**N 1s**	**Na 1s**	**Cl 2p**	**Ca**	**K**				
no treatment	1 spot	25.9 %	62.6 %	3.87 %		5.1 %	2.3 %	0.2 %	0.0 %		trace	70.5 %	19.8 %	5.4 %	4.3 %
	2	21.3 %	70.9 %	1.31 %		3.9 %	1.6 %	0.9 %	0.2 %		trace	75.4 %	15.8 %	4.7 %	4.2 %
	3 paint	21.7 %	63.1 %	0.02 %		13.7 %	1.0 %	0.4 %	0.2 %		trace	83.6 %	12.2 %	3.0 %	1.3 %
heat treatment	1 spot	27.9 %	60.6 %	4.23 %		3.6 %	3.4 %	0.3 %	0.1 %		trace	75.0 %	13.9 %	4.9 %	6.2 %
	2	22.1 %	71.1 %	1.48 %		2.7 %	2.1 %	0.5 %	0.0 %		trace	74.6 %	14.0 %	5.4 %	6.1 %
	3 paint	22.3 %	62.5 %	0.01 %		12.9 %	1.4 %	0.7 %	0.3 %		trace	84.1 %	9.8 %	3.9 %	2.3 %
short-irr and heat	1 spot	24.4 %	64.7 %	0.79 %		5.8 %	2.1 %	0.1 %	2.0 %	0.2 %	0.0 %	69.7 %	16.2 %	6.4 %	7.7 %
(note point order)	3	21.7 %	70.2 %	0.21 %		2.0 %	2.6 %	0.5 %	1.9 %	0.2 %	0.7 %	67.8 %	17.4 %	7.8 %	7.1 %
	2 paint	24.6 %	57.7 %	0.05 %		14.7 %	0.9 %	0.0 %	1.3 %	0.0 %	0.6 %	77.8 %	12.5 %	5.4 %	4.3 %
long-irr	1 spot	22.7 %	69.1 %	3.62 %		2.9 %	1.3 %	0.0 %	0.2 %	0.1 %	trace	81.5 %	9.6 %	3.8 %	5.2 %
	2	20.1 %	72.0 %	0.76 %		2.8 %	2.3 %	0.2 %	1.0 %	1.0 %	trace	75.1 %	13.5 %	5.1 %	6.3 %
	3 paint	24.2 %	57.4 %	0.01 %		15.3 %	1.5 %	0.2 %	0.7 %	0.6 %	trace	84.0 %	10.1 %	2.9 %	3.0 %

Appendix I1. The binding energies of CsI deposits on paint surfaces measured with XPS. No treatment

Note : Red spectra badly charged, HiRes data not good

O 1s:6(2013-03-12-ls) ■ ■ O 1s:33(2013-03   I 3d:4 ■ ■ I 3d:36(2013-03·   C 1s:7(2013-03-12-ls) ■ ■ C 1s:34(2013-03
O 1s:63(2013-03-12-ls) ■   I 3d:66(2013-03-12-ls) ■   C 1s:64(2013-03-12-ls) ■
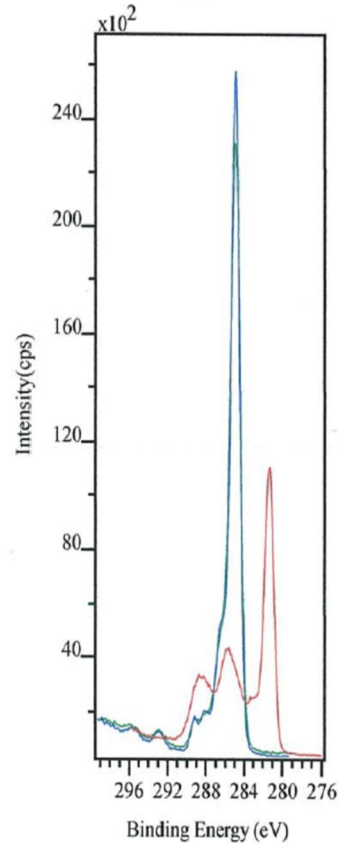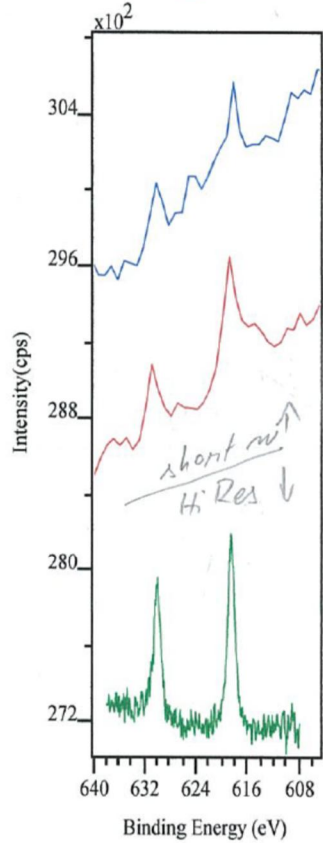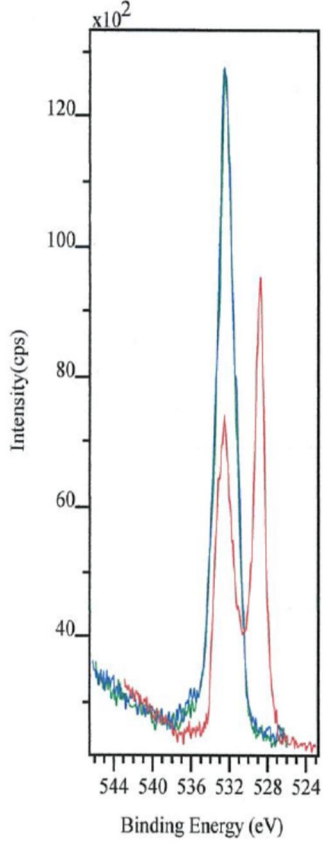
short ~↗
Hi Res ↓

wide:9(2013-03-12-ls) ■ ■ wide:35(2013-03-12-ls)
wide:65(2013-03-12-ls) ■

CsI not treated
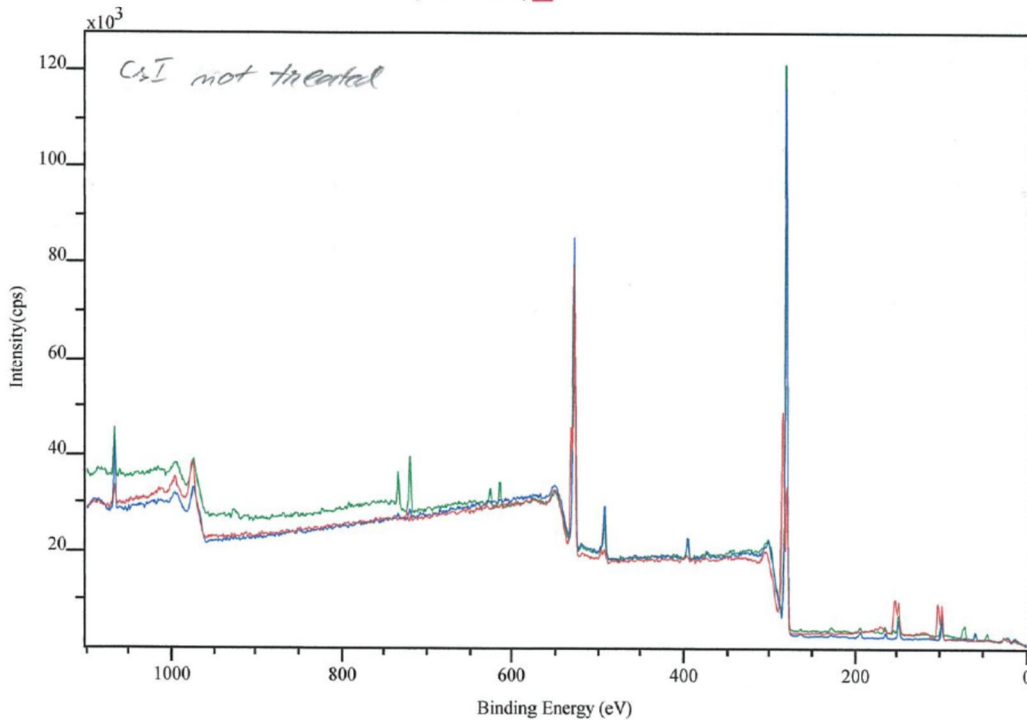
Appendix I2. The binding energies of CsI deposits on paint surfaces measured with XPS.
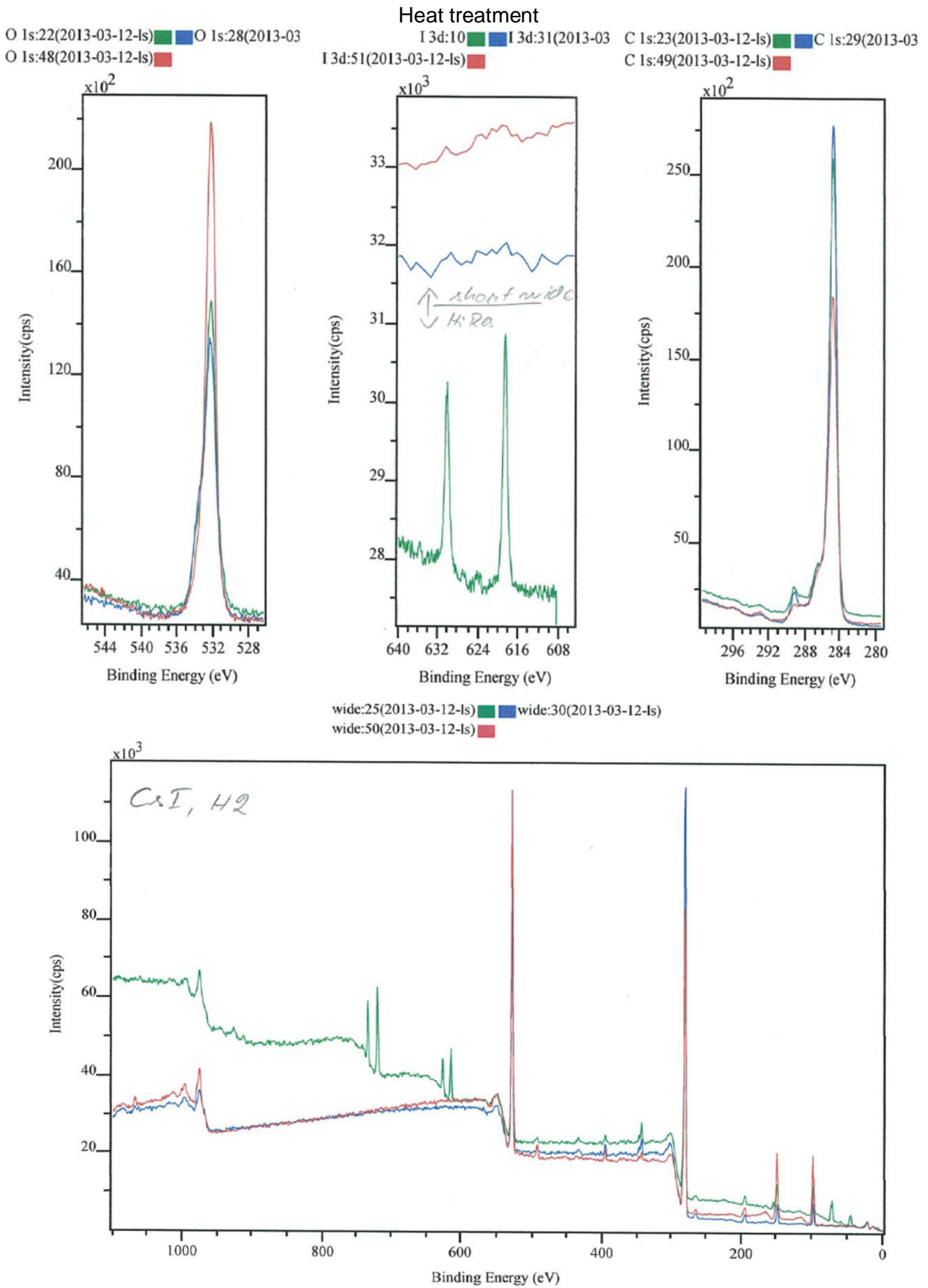
Heat treatment

O 1s:22(2013-03-12-ls) ■ ■ O 1s:28(2013-03   I 3d:10 ■ ■ I 3d:31(2013-03   C 1s:23(2013-03-12-ls) ■ ■ C 1s:29(2013-03
O 1s:48(2013-03-12-ls) ■   I 3d:51(2013-03-12-ls) ■   C 1s:49(2013-03-12-ls) ■

wide:25(2013-03-12-ls) ■ ■ wide:30(2013-03-12-ls)
wide:50(2013-03-12-ls) ■

Appendix I3. The binding energies of CsI deposits on paint surfaces measured with XPS.

Short gamma irradiation and heat treatment

O 1s:17(2013-03-12-ls)■ ■O 1s:43(2013-03
O 1s:53(2013-03-12-ls)■

I 3d:8■ ■I 3d:46(2013-03-
I 3d:56(2013-03-12-ls)■

C 1s:18(2013-03-12-ls)■ ■C 1s:44(2013-03
C 1s:54(2013-03-12-ls)■
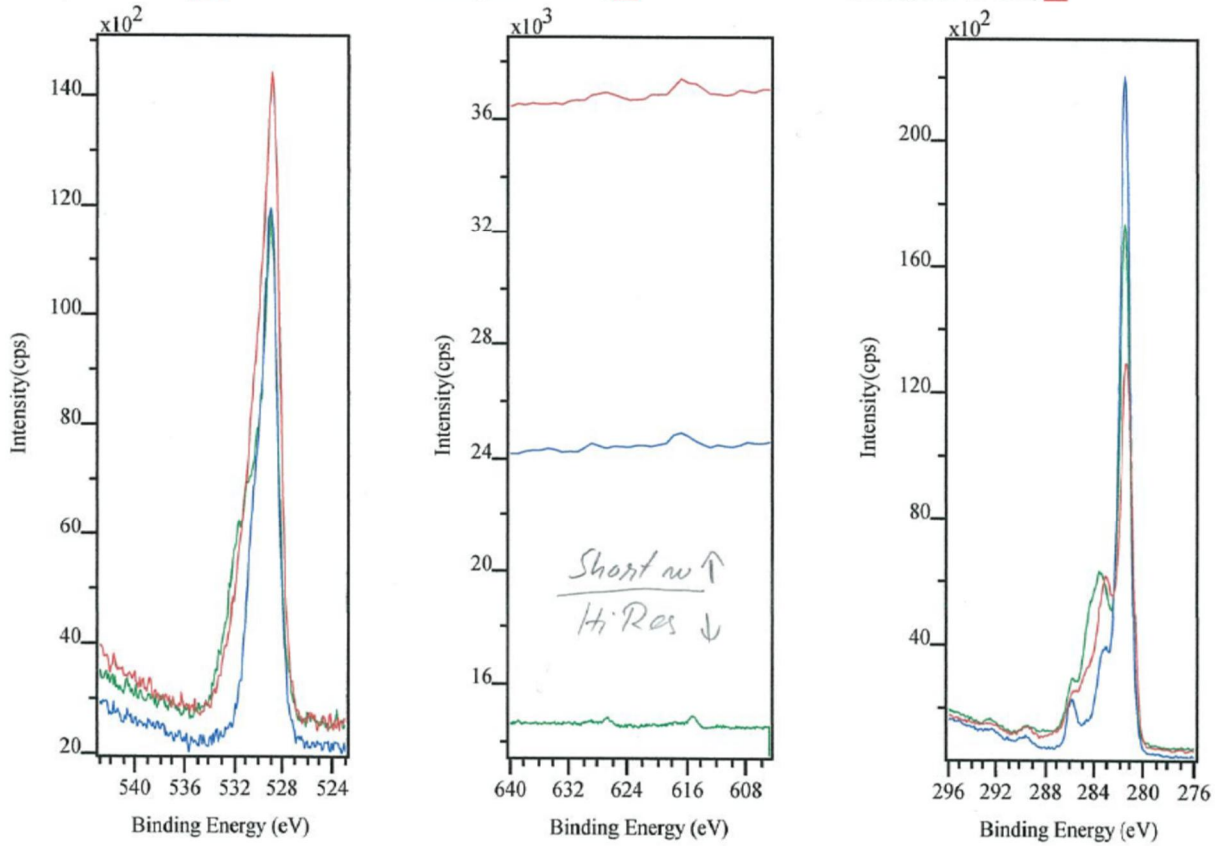
wide:20(2013-03-12-ls)■ ■wide:45(2013-03-12-ls)
wide:55(2013-03-12-ls)■
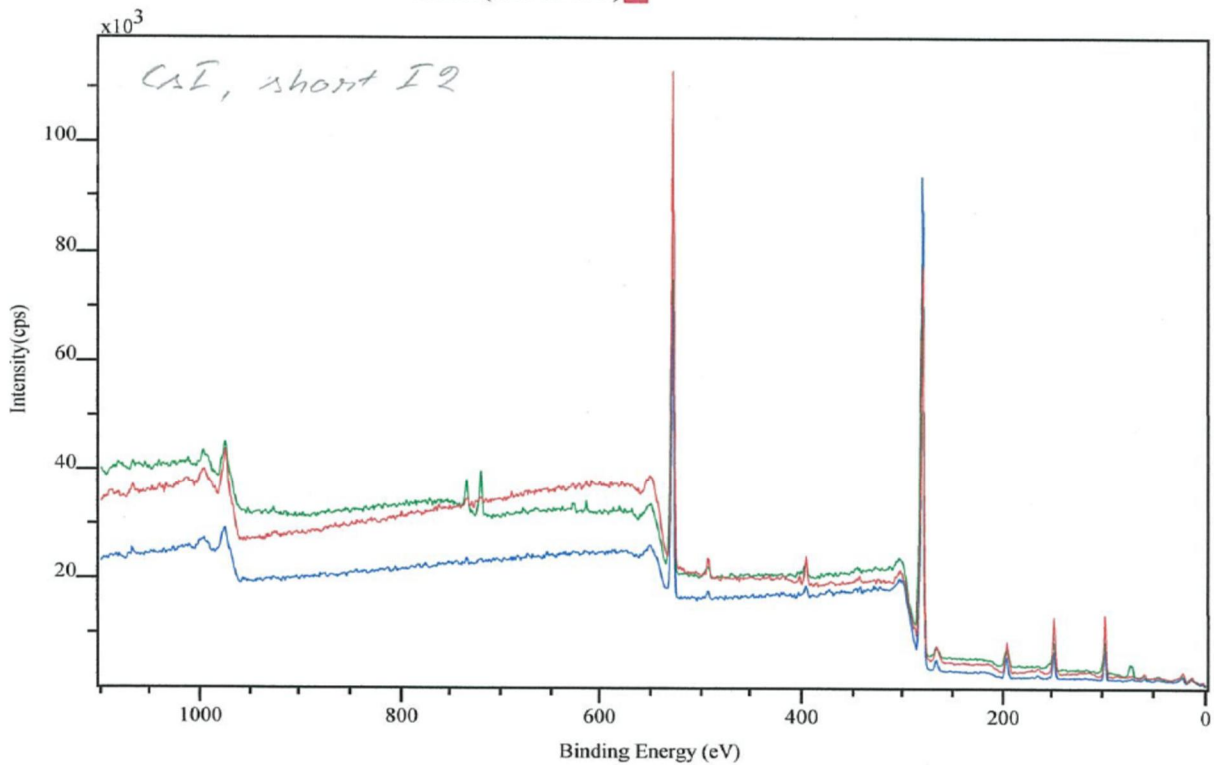
Appendix I3. The binding energies of CsI deposits on paint surfaces measured with XPS.

Long gamma irradiation

O 1s:12(2013-03-12-ls) [green] [blue] O 1s:38(2013-03
O 1s:58(2013-03-12-ls) [red]

I 3d:6 [green] [blue] I 3d:41(2013-03
I 3d:61(2013-03-12-ls) [red]

C 1s:13(2013-03-12-ls) [green] [blue] C 1s:39(2013-03
C 1s:59(2013-03-12-ls) [red]

wide:15(2013-03-12-ls) [green] [blue] wide:40(2013-03-12-ls)
wide:60(2013-03-12-ls) [red]

Title	Adsorption and revaporisation studies of thin iodine oxide and CsI aerosol deposits from containment surface materials in LWRs
Author(s)	S. Tietze[1], M. Foreman[1], C. Ekberg[1] T. Kärkelä[2], A. Auvinen[2], U. Tapper[2], J. Jokiniemi[2,3]
Affiliation(s)	[1]Chalmers University of Technology, SE-41296 Göteborg, Sweden [2]VTT Technical Research Centre of Finland, FI-02044 Espoo, Finland [3]University of Eastern Finland, FI-70211 Kuopio, Finland
ISBN	978-87-7893-360-7
Date	July 2013
Project	NKS-R / AIAS
No. of pages	58 (+ 25 appendices)
No. of tables	9
No. of illustrations	67
No. of references	20

Abstract

During a severe nuclear accident released fission and radiolysis products can react with each other to form new species which might contribute to the volatile source term. Iodine will be released from UO2 fuel mainly in form as CsI aerosol particles and elemental iodine. Elemental iodine can react in gaseous phase with ozone to form solid iodine oxide aerosol particles (IOx).

Within the AIAS-2 (Adsorption of Iodine Aerosols on Surfaces) project the interactions of IOx and CsI aerosols with common containment surface materials was investigated. Common surface materials in Swedish and Finnish LWRs are Teknopox Aqua V A paint films and metal surfaces such as Cu, Zn, Al and SS. Non-radioactive and ^{131}I labelled aerosols were produced from a KI solution and ozone with a new facility designed and built at VTT Technical Research Centre of Finland. CsI aerosols were produced from a CsI solution with the same facility. A monolayer of the aerosols was deposited on the surfaces. The deposits were analysed with microscopic and spectroscopic measurement techniques to identify the chemical form of the deposits on the surfaces to identify if a chemical conversion on the different surface materials had occured.

The revaporisation behaviour of the deposited aerosol particles from the different surface materials was studied under the influence of heat, humidity and gamma irradiation at Chalmers University of Technology, Sweden. Studies on the effects of humidity were performed using the FOMICAG facility, while heat and irradiation experiments were performed in a thermostated heating block and with a gammacell 22 with a dose rate of 14 kGy/h. The revaporisation losses were measured using a HPGe detector. The decomposition effect of the radiolysis product carbon monoxide was tested on IOx aerosols deposited on a glass fibre filter.

Iodine oxide particles were produced at 50 °C, 100 °C and 120 °C and deposited on filter samples in order to study the chemical speciation of the particles. The formation of HIO_3 was verified with Raman analysis regardless of the reaction temperature. Furthermore, elemental iodine was also observed in the measured

Raman spectra. Probably, iodine oxide particles had reacted with air humidity forming iodic acid and elemental iodine.

IOx and CsI particles that were deposited on various sample surfaces were synthesized at 120°C. According to XPS analysis, it seemed that IOx particles were mainly in form of HIO_3 on the metal and on the painted surfaces.

The XPS spectrum of CsI was observed on all metal and painted samples on which CsI particles were deposited. However, the CsI particles seemed to have dissolved at least partially by air humidity. Iodine was observed at areas outside the caesium iodide deposits on metal and on painted surfaces. According to the XPS analyses, iodine was in oxidised form. The measurements indicated that iodine may have reacted with the oxidized metal surfaces to form metal iodates. Only trace amounts of oxidized iodine were detected on the painted surfaces.

An interesting result in the XPS analysis was that a part of the acquired signal from CsI on the painted surfaces seemed to originate deeper from the structure of the paint when it was pre-treated either with heat or gamma irradiation. SEM analysis revealed that heat and gamma irradiation treatment increased the porosity of the paint. Therefore, dissolved CsI may have been transported into the matrix of the paint.

Besides copper the studied metal surfaces underwent slow reactions with the iodine of the aerosol deposits which showed in the high revaporisation rates at room temperature and elevated temperatures. On the copper and paint samples it could be shown that these surfaces react more easily with the iodine from cesium iodide deposits. From the chemically converted metal iodides only copper iodide remained on the surfaces after exposure to hot humid air and as well after immersion in boiling water. Both, non aged and fresh paint films, showed to be very reactive towards the iodine in the aerosol deposits. At lower temperatures (< 50 °C) it showed that the solvent rich paint films showed reduced revaporisation. At high temperatures when the paint starts to significantly degrade the release of iodine from the solvent rich paints increased significantly. The containment conditions or conditions of a severe nuclear accident cause the revaporisation of paint solvents and thus an uneven distribution within the paint film. Near to the surface revaporisation starts and thus an higher paint solvent concentration is found in the center of the paint profile where the iodine species migrate to and possibly are chemically converted. Thus, the paint samples that had been for a long time aged at high temperatures showed the least ability to react and retain iodine from the deposited aerosols. Most paint solvents are less water soluble than the iodine species itself. Thus, elevated temperatures and hot water are required to wash out the iodine in the paint matrix. In all paint films iodine was still detected after 4 weeks immersion in hot water (50 °C).